



UNIVERSIDADE ESTADUAL DE CAMPINAS
Faculdade de Engenharia Química

YESID JAVIER RUEDA ORDÓÑEZ

ANÁLISE DA DECOMPOSIÇÃO TÉRMICA DE PALHA DE CANA-DE-AÇÚCAR
EM ATMOSFERAS INERTE E OXIDANTE MEDIANTE MÉTODOS
TERMOANALÍTICOS

THERMAL DECOMPOSITION ANALYSIS OF SUGARCANE STRAW IN INERT AND
OXIDATIVE ATMOSPHERES THROUGH THERMOANALYTICAL METHODS

CAMPINAS

2016

YESID JAVIER RUEDA ORDÓÑEZ

THERMAL DECOMPOSITION ANALYSIS OF SUGARCANE STRAW IN INERT AND
OXIDATIVE ATMOSPHERES THROUGH THERMOANALYTICAL METHODS

ANÁLISE DA DECOMPOSIÇÃO TÉRMICA DE PALHA DE CANA-DE-AÇÚCAR EM
ATMOSFERAS INERTE E OXIDANTE MEDIANTE MÉTODOS TERMOANALÍTICOS

Tese apresentada à Faculdade de Engenharia Química
da Universidade Estadual de Campinas como parte dos
requisitos exigidos para obtenção do título de Doutor
em Engenharia Química

Thesis presented to the School of Chemical Engineering
of the University of Campinas in partial fulfillment of
the requirements for the degree of Doctor in Chemical
Engineering

Supervisor/Orientador: Profa. Dra. Katia Tannous

Co-supervisor/Co-orientador: Prof. Dr. Edgardo Olivares Gómez

ESTE EXEMPLAR CORRESPONDE À VERSÃO
FINAL TESE DEFENDIDA PELO ALUNO YESID
JAVIER RUEDA ORDÓÑEZ, E ORIENTADA
PELA PROFA. DRA. KATIA TANNOUS

CAMPINAS
2016

Agência(s) de fomento e nº(s) de processo(s): CAPES, 33003017034P8

Ficha catalográfica
Universidade Estadual de Campinas
Biblioteca da Área de Engenharia e Arquitetura
Luciana Pietrosanto Milla - CRB 8/8129

R886t Rueda-Ordóñez, Yesid Javier, 1986-
Thermal decomposition of sugarcane straw in inert and oxidative atmospheres through thermoanalytical methods / Yesid Javier Rueda Ordóñez. – Campinas, SP : [s.n.], 2016.
Orientador: Katia Tannous.
Coorientador: Edgardo Olivares Gomez.
Tese (doutorado) – Universidade Estadual de Campinas, Faculdade de Engenharia Química.
1. Termogravimetria. 2. Cinética. 3. Biomassa. 4. Pirólise. 5. Combustão. I. Tannous, Katia, 1962-. II. Olivares Gomez, Edgardo. III. Universidade Estadual de Campinas. Faculdade de Engenharia Química. IV. Título.

Informações para Biblioteca Digital

Título em outro idioma: Análise da decomposição térmica de palha de cana-de-açúcar em atmosferas inerte e oxidante mediante métodos termoanalíticos

Palavras-chave em inglês:

Thermogravimetry

Kinetics

Biomass

Pyrolysis

Combustion

Área de concentração: Desenvolvimento de Processos Químicos

Titulação: Doutor em Engenharia Química

Banca examinadora:

Katia Tannous [Orientador]

Elizabeth Jordão

Waldir Antonio Bizzo

Eliane Vieira Canettieri

Juan Miguel Mesa Pérez

Data de defesa: 19-07-2016

Programa de Pós-Graduação: Engenharia Química

FOLHA DE APROVAÇÃO

Tese de Doutorado defendida por Yesid Javier Rueda Ordóñez e aprovada em 19 de Julho de 2016 pela banca examinadora constituída pelos doutores:

Profa. Dra. Katia Tannous – FEQ/unicamp - Orientador

Profa. Dra. Eliane Vieira Canettieri – FEG/Unesp

Profa. Dra. Elizabete Jordão – FEQ/Unicamp

Dr. Juan Miguel Mesa Pérez – Bioware Tecnologia

Prof. Dr. Waldir Antonio Bizzo – FEM/Unicamp

Informamos que a Ata da Defesa, assinada pelos membros da Comissão Examinadora, consta no processo de vida acadêmica do aluno.

ACKNOWLEDGMENTS

I would like to express my sincere appreciation to my supervisor professor Katia Tannous for giving me the opportunity to develop this research at the University of Campinas under her mentorship.

I would like also to thank Dr. Edgardo Olivares Gómez as joint supervisor of this research and Dr. Antônio Carlos Luz Lisboa to give us the opportunity to use the laboratory facilities.

I also appreciate the help and assistance of the undergraduate student, Luisa Azevedo Higuchi and colleagues of our research group.

I also acknowledge the Coordination for the Improvement of Higher Education Personnel (CAPES) for my scholarship.

I would like to express my gratitude to my parents for their support and encouragement during the period of my time in Brazil.

And finally, I would like to thank my wife and our son for their unconditional support, patience, and company through these years in Brazil. I wish to dedicate this work to all of them.

RESUMO

Este trabalho teve por objetivo o estudo cinético da decomposição térmica da palha de cana-de-açúcar (*Saccharum officinarum* Linnaeus) em atmosferas inerte e oxidante. O diâmetro médio das partículas foi de 0,510 mm obtido entre as peneiras padrão Tyler de número 28 e 35. As características térmicas (base seca) foram obtidas mediante análise imediata conforme: teores de material volátil=86,6% (ASTM E872–82), de cinzas=3,8% (ASTM E1755–01) e de carbono fixo=9,6% por diferença; o poder calorífico superior de 18,6 MJ/kg foi obtido mediante bomba calorimétrica. A característica química foi determinada através de um analisador elementar obtendo-se os teores mássicos de carbono=42,8%, hidrogênio=6,2%, nitrogênio=0,3% e o oxigênio=46,9% por diferença em base seca e livre de cinzas. A determinação dos teores de hemicelulose=33% e celulose=40% foi feita mediante a técnica ANKOM A200 baseada no método de Van Soest. O teor de lignina=22% foi determinado aplicando o método de Klason baseado em hidrólise ácida. Os experimentos de decomposição térmica foram realizados em um analisador termogravimétrico (TG) e o fluxo de calor foi medido em um calorímetro diferencial de varredura (DSC), usando nitrogênio e ar sintético como meio reativo. Estas análises foram realizadas utilizando quatro taxas de aquecimento (1,25; 2,5; 5 e 10 °C/min) em nitrogênio e três (2,5; 5 e 10 °C/min) em ar sintético aplicando massas em torno de 3 mg. A análise cinética realizada para as duas atmosferas abrangeu três esquemas de reações: reação global, reações consecutivas, e reações paralelas. A modelagem cinética através do esquema de reação global foi realizada aplicando os métodos isoconversionais de Friedman (nitrogênio) e Vyazovkin (ar sintético). Em atmosfera inerte, obteve-se energia de ativação de 149,7 kJ/mol, fator pré-exponencial de $1,82 \times 10^9 \text{ s}^{-1}$ e modelo de reação de difusão bidimensional. No entanto, em atmosfera oxidante não foi possível modelar a reação através deste esquema de reação. Analisando reações globais de primeira ordem através de modelos de ajuste e considerando 805 cenários diferentes, obtiveram-se correlações entre fator pré-exponencial e energia de ativação, correlacionando a taxa de aquecimento, temperatura e taxa de conversão no pico. O esquema de três reações consecutivas descreveu muito bem os dados experimentais, aplicando reações de primeira ordem obtendo-se energias de ativação de 133, 198 e 56 kJ/mol, e 200, 300 e 100 kJ/mol em atmosfera inerte e oxidante, respectivamente. Os fatores pre-exponenciais de 2×10^9 , 5×10^3 , e 5 s^{-1} foram obtidos em atmosfera inerte e 2×10^{16} , 3×10^{28} , e $5 \times 10^4 \text{ s}^{-1}$ em oxidante. A aplicação do esquema de reações paralelas e independentes foi realizada avaliando três

reações de primeira ordem em atmosfera inerte e seis em atmosfera oxidante. Os resultados experimentais e teóricos mostraram uma boa concordância, obtendo-se energias de ativação de 142, 212, e 40 kJ/mol em atmosfera inerte e 176, 313, 150, 80, 150, e 100 kJ/mol em oxidante. Os fatores pre-exponenciais obtidos foram em atmosfera inerte 1×10^{10} , 8×10^{14} , e $0,3 \text{ s}^{-1}$, e em oxidante 1×10^{14} , 1×10^{25} , 2×10^{10} , 5×10^3 , 1×10^8 , e $1 \times 10^4 \text{ s}^{-1}$. Finalmente, o calor de reação em atmosfera inerte foi endotérmico, requerendo energia máxima de 1 MJ/kg em 350 °C, e em atmosfera oxidante foi completamente exotérmico liberando até 8 MJ/kg.

ABSTRACT

The aim of this work was the kinetic study of the thermal decomposition of sugarcane straw (*Saccharum officinarum* Linnaeus) in inert and oxidative atmospheres. The mean diameter of particles was 0.510 mm obtained between the Tyler standard sieves number 28 and 35. The thermal characteristics (dry base) were determined through proximate analysis according to: volatile matter content = 86.6% (ASTM E872-82), ash content=3.8% (ASTM E1755-01) and fixed carbon content =9.6% by difference; the higher heating value of 18.6 MJ/kg was obtained using a bomb calorimeter. The chemical characteristics were determined through an elemental analyzer, obtaining in dry and ash free basis carbon=42.8%-m, hydrogen=6.2%-m, nitrogen=0.3%-m and oxygen=46.9%-m by difference. The sample chemical composition was hemicellulose=33% and cellulose=40% determined by the application of the ANKOM A200 technique, based on the Van Soest's method. The lignin content=22% was obtained applying the Klason's method based on acid hydrolysis. The thermal decomposition experiments were carried out in a thermogravimetric analyzer (TG) and the heat flux was measured in a differential scanning calorimeter (DSC), using nitrogen and synthetic air atmospheres, respectively. These analyses were carried out using four heating rates (1.25, 2.5, 5, and 10 °C/min) in nitrogen, and three (2.5, 5, and 10 °C/min) in synthetic air applying sample mass around 3 mg. The kinetic analysis in both atmospheres covered three reaction schemes: global reaction, consecutive reactions, and parallel reactions. In the global reaction analysis were applied the isoconversional methods of Friedman (nitrogen) and Vyazovkin (synthetic air). In inert atmosphere, was obtained activation energy of 149.7 kJ/mol, pre-exponential factor of $1,82 \times 10^9 \text{ s}^{-1}$, and reaction model of bi-dimensional diffusion. However, in oxidative atmosphere, it was not possible to modeling the reaction through this reaction scheme. Analyzing first order global reactions through fitting models and considering 805 different scenarios, were obtained correlations between pre-exponential factor and activation energy, correlating the heating rate, peak temperature, and peak conversion rate. The three consecutive first order reactions scheme represented the experimental data obtaining activation energies of 133, 198, and 56 kJ/mol in inert atmosphere, and 200, 300, and 100 kJ/mol in oxidative atmosphere. The pre-exponential factors correspondent were 2×10^9 , 5×10^3 , and 5 s^{-1} in inert atmosphere and 2×10^{16} , 3×10^{28} , and $5 \times 10^4 \text{ s}^{-1}$ were oxidative atmosphere. The kinetic modeling through the independent parallel reactions scheme was carried out evaluating three and six first order reactions in inert and oxidative atmosphere,

respectively. The experimental and theoretical results showed a good agreement obtaining activation energies of 142, 212, and 40 kJ/mol in inert atmosphere, and 176, 313, 150, 80, 150, and 100 kJ/mol in oxidative atmosphere. The pre-exponential factors were 1×10^{10} , 8×10^{14} , and $0,3 \text{ s}^{-1}$ in inert atmosphere and 1×10^{14} , 1×10^{25} , 2×10^{10} , 5×10^3 , 1×10^8 , and $1 \times 10^4 \text{ s}^{-1}$ in oxidative atmosphere. Finally, the heat of reaction in inert atmosphere was endothermic requiring maximum energy of 1 MJ/kg at 350°C, and in oxidative atmosphere, it was completely exothermic releasing 8 MJ/kg.

LIST OF FIGURES

Figure 2.1. Heat and mass transfer of a biomass particle submitted to pyrolysis	28
Figure 2.2. Independent parallel reactions scheme.....	48
Figure 2.3. Logarithm of pre-exponential factor as a function of the activation energy of the main components of lignocellulosic biomass obtained by several researchers.....	50
Figure 3.1. (a) Flowchart exemplifying the data selection for the application of heating isoconversional methods. (b) Conversion as a function of temperature for several rates. (c) Data organization for each heating rate	62
Figure 3.2. Flowchart of the determination of the activation energy through isoconversional methods. (a) Ozawa-Flinn-Wall, (b) Coats-Redfern modified, and (c) Friedman methods.....	63
Figure 3.3. Schematic of normalized mass as a function of temperature in inert gas. (a) Two consecutive reactions scheme. (b) Three consecutive reactions scheme.....	68
Figure 4.1. (a) Normalized mass and (b) normalized DTG as a function of temperature	77
Figure 4.2. (a) TG and (b) DTG curves of thermal decomposition of sugarcane straw in synthetic air and nitrogen	80
Figure 4.3. (a) Derivative of conversion with respect to temperature and (b) Activation energy, as a function of conversion	82
Figure 4.4. Theoretical and experimental master plots for the thermal decomposition of sugarcane straw at the heating rates of (x)1.25°C/min, (◊)2.5°C/min, (Δ)5°C/min, (o)10°C/min as a function of conversion.....	84
Figure 4.5. Linearization of the conversion rate equation as a function of the inverse of absolute temperature.....	85
Figure 4.6. Conversion curves as a function of temperature. Modeled data as solid lines, and experimental data in symbols	86
Figure 4.7. Activation energy as a function of conversion for the two stages, oxidative pyrolysis and combustion	88
Figure 4.8. Results of the conversion rate simulation. (a) Effect of the pre-exponential factor at 10 °C/min, and (b) Effect of the heating rate (β) using $\log A = 10 \log s^{-1}$	90
Figure 4.9. Diagrams obtained using the proposed correlations for a heating rate (β) of 5°C/min. (a) Peak conversion rate as a function of peak temperature and (b) activation energy as a function of peak temperature.....	92
Figure 4.10. Analysis of the behavior of each parameter with the increasing of heating rate, from 1 °C/min to 50 °C/min. Empirical parameters (a) y_0 , (b) y_1 , (c) x_2 , (d) x_3 , (e) y_2 , and (f) y_3	93
Figure 4.11. Model validation, heating rate of 10 °C/min and $\log A = 10 \log s^{-1}$. Simulated curve as solid line and curve obtained with correlation in symbols (o)	95

Figure 4.12. (a) Conversion and (b) conversion rate as a function of temperature at 10 °C/min in inert atmosphere applying two consecutives reactions. Experimental data in symbol (O), model in solid line	98
Figure 4.13. (a) and (d) Conversion; (b) and (e) Conversion rate, and (c) and (f) Concentration as a function of temperature in inert atmosphere. (a), (b), and (c) data at 1.25 °C/min. (d), (e), and (f) data at 2.5 °C/min	101
Figure 4.14. (a) and (d) Conversion; (b) and (e) Conversion rate, and (c) and (f) Concentration as a function of temperature in inert atmosphere. (a), (b), and (c) data at 5 °C/min. (d), (e), and (f) data at 10 °C/min	102
Figure 4.15. (a) and (d) Conversion; (b) and (e) Conversion rate, and (c) and (f) Concentration as a function of temperature in oxidative atmosphere. (a), (b), and (c) data at 2.5 °C/min. (d), (e), and (f) data at 5 °C/min.....	104
Figure 4.16. (a) Conversion; (b) Conversion rate, and (c) Concentration as a function of temperature at 10 °C/min in oxidative atmosphere	105
Figure 4.17. Conversion rate curves as a function of temperature for different heating rates. Experimental data in symbol (o), IPRS model as a solid line and pseudo-components as dotted lines.....	108
Figure 4.18. Independent parallel reaction scheme for biomass smoldering reaction	110
Figure 4.19. Conversion rate as a function of temperature obtained with the independent parallel reaction scheme. The capital letters HC, C, and L are related to hemicellulose, cellulose, and lignin, respectively. The symbol (*) represent combustion reaction.....	113
Figure 4.20. Experimental heat measurements obtained with DSC of the thermal decomposition of sugarcane straw in atmosphere of (a) Nitrogen, and (b) Synthetic air	116
Figure 4.21. Heat of reaction as a function of temperature for the thermal decomposition of sugarcane straw in atmosphere of (a) Nitrogen, and (b) Synthetic air	118
Figure C.1. Configuration of SOLVER tool in excel for minimization of equation (3.11) ...	146
Figure D.1. Flowchart of the application of the consecutive reactions scheme	147
Figure E.1. Flowchart of the application of the independent parallel reactions scheme	155

LIST OF TABLES

Table 2.1. Main features of integral and differential methods	37
Table 2.2. Activation energy of several biomasses obtained by isoconversional methods.....	41
Table 2.3. Integral and differential form of several reaction models for solid-state kinetics (adapted from Vyazovkin et al., 2011)	44
Table 2.4. Recent kinetics biomass studies considering TG conditions, modeling and parameters.....	53
Table 4.1. Proximate and ultimate analyses and heating values of sugarcane straw	75
Table 4.2. Chemical composition of sugarcane straw and sugarcane bagasse.....	76
Table 4.3. Kinetic parameters of sugarcane straw in inert atmosphere for a global reaction...	87
Table 4.4. Empirical parameters for the correlations proposed at several heating rates	94
Table 4.5. Parameters of the consecutive reactions scheme in nitrogen	99
Table 4.6. Parameters of the consecutive reactions scheme in synthetic air	99
Table 4.7. Empirical parameters for the correlations proposed to obtain the kinetic parameters of sugarcane straw by independent parallel reactions scheme	107
Table 4.8. Kinetic parameters of sugarcane straw.....	108
Table 4.9. Kinetic parameters of smoldering reaction of sugarcane straw.....	111
Table 4.10. Summary of the results of the kinetic analysis in nitrogen	114
Table 4.11. Summary of the results of the kinetic analysis in synthetic air	115
Table A.1. Experimental TG/DTG data normalization procedure	138
Table A.2. Procedure to obtain experimental conversion and conversion rate from normalized mass and normalized DTG	139
Table C.1. Experimental conversion, temperature and conversion rate.....	140
Table C.2. Selection of data for application of isoconversional methods	140
Table C.3. Experimental data applied in the method of Friedman and procedure of determination of activation energy	141
Table C.4. Experimental data applied in the method of Ozawa-Flynn-Wall	142
Table C.5. Procedure of determination of activation energy through the method of Ozawa-Flynn-Wall.....	143
Table C.6. Experimental data used in the method of Vyazovkin.....	143
Table C.7. Procedure of determination of $x=E/RT$	144
Table C.8. Procedure of solution of equation (3.10a)	145
Table C.9. Procedure of solution of equation (3.10b)	145

Table C.10. Procedure of solution of equation (3.10c)	145
Table C.11. Procedure of solution of the temperature integral $I(E\alpha, T\alpha)=(E\alpha/R)[p(x)]$	146
Table C.12. Procedure of solution of the minimization correlation for determination of activation energy.....	146
Table D.1. Initial kinetic parameters for the three reactions analyzed.....	149
Table D.2. Initial conditions of time, temperature, and concentration and their increasing ..	149
Table D.3. Procedure for solution of the parameter K_1 presented in equation (3.45)	150
Table D.4. Procedure for solution of the parameter K_2 presented in equation (3.46)	150
Table D.5. Procedure for solution of the parameter K_3 presented in equation (3.47)	150
Table D.6. Procedure for solution of the parameter K_4 presented in equation (3.48)	150
Table D.7. Procedure of determination of the concentration rate of [A] in equation (3.17)..	151
Table D.8. Procedure of determination of the concentration rate of [B] in equation (3.18) .	151
Table D.9. Procedure of determination of the concentration rate of [C] in equation (3.19) .	151
Table D.10. Procedure of determination of the concentration rate of [D] in equation (3.20)	151
Table D.11. Procedure of determination of the theoretical normalized mass, W	152
Table D.12. Procedure of determination of the normalized DTG, dW/dt	152
Table D.13. Procedure of determination of theoretical conversion.....	152
Table D.14. Procedure of determination of theoretical conversion rate.....	153
Table D.15. Procedure of application of the least squares method	153
Table D.16. Procedure of determination of the average deviation (AD).....	154
Table E.1. Initial kinetic parameters for an example of three independent parallel reactions scheme	157
Table E.2. Initial conditions of time, temperature, and conversion.....	157
Table E.3. Procedure for solution of the parameter K_1 presented in equation (3.45).....	158
Table E.4. Procedure for solution of the parameter K_2 presented in equation (3.46).....	158
Table E.5. Procedure for solution of the parameter K_3 presented in equation (3.47).....	158
Table E.6. Procedure for solution of the parameter K_4 presented in equation (3.48).....	158
Table E.7. Procedure of determination of the conversion rate	158
Table E.8. Procedure of determination of the final conversion rate.....	159
Table F.1. Procedure for the determination of the heat capacity of sample and char	160
Table F.2. Procedure for the determination of heat flux required for heating the biomass sample (Q_S).....	161
Table F.3. Procedure of determination of the heat flux of reaction, Q_R	161

NOMENCLATURE

a	Stoichiometric coefficient	[-]
A	Pre-exponential factor	[s ⁻¹]
AD	Average deviation	[%]
c_p	Heat capacity	[J/kg°C]
$c_{p,c}$	Char heat capacity	[J/kg°C]
$c_{p,s}$	Sample heat capacity	[J/kg°C]
E	Activation energy	[kJ/mol]
F	Volatilized fraction	[-]
HHV	Higher heating rate	[MJ/kg]
H_R	Global heat of reaction	[kJ/kg]
k	Arrhenius constant	[-]
LHV	Lower heating rate	[MJ/kg]
m	Mass measured by TG	[mg]
m_0	Initial mass measured by TG	[mg]
m_f	Final mass measured by TG	[mg]
m_t	Mass measured by TG at a given temperature/time	[mg]
n	Reaction order	[-]
N	Number of experimental data	[-]
OF	Objective function	[-]
$p(x)$	Approximate solution of temperature integral	[-]
Q_{DSC}	Heat flux	[J/s]
Q_R	Heat of reaction	[J/s]
Q_S	Heat required to heat up the sample	[J/s]
R	Universal gas constant	[kJ/molK]
RSS	Least squares method	[-]
t	Time	[s]
T	Temperature	[°C]
T_{max}	Maximum temperature	[°C]
T_p	Peak temperature	[°C]
W	Normalized mass at a given temperature/time	[-]

W_0	Initial normalized mass	[-]
W_f	Final normalized mass	[-]
x	E/RT	[-]

Greek Letters

α	Conversion	[-]
$d\alpha/dt$	Conversion rate	[s ⁻¹]
β	Heating rate	[°C/min]

Abbreviations and Acronyms

C	Cellulose
CRM	Coats-Redfern modified method
CRS	Consecutive reactions scheme
DAEM	Distributed activation energy model
DL	Dry leaves
DMA	Dynamical mechanical analysis
DSC	Differential scanning calorimetry
DTA	Differential thermal analysis
DTG	First derivative of the thermogravimetry
FD	Friedman method
GL	Green leaves
GRS	Global reaction scheme
HC	Hemicellulose
ICTAC	International confederation for thermal analysis committee
IPRS	Independent parallel reactions scheme
KAS	Kissinger-Akahira-Sunose method
KS	Kissinger method
L	Lignin
LaProM	Laboratory of Particle Technology and Multiphase Processes
OFW	Ozawa-Flynn-Wall method

T	Tops of sugarcane plants
TG	Thermogravimetric analysis
VZ	Vyazovkin method

SUMMARY

Chapter 1 - Introduction	19
1.1 Objectives	20
Chapter 2 – Literature Review.....	22
2.1 Biomass.....	22
2.1.1 Biomass composition	23
2.2 Sugarcane straw	24
2.3 Analysis of the Biomass Thermal Decomposition.....	25
2.3.1 Thermal decomposition in inert atmosphere (pyrolysis)	27
2.3.2 Thermal decomposition in oxidative atmosphere (combustion).....	30
2.4 Kinetic Modeling of Biomass Thermal Decomposition	33
2.4.1 Isoconversional methods (Model-free methods).....	35
2.4.2 Reaction model and master-plots application	42
2.4.3 Consecutive reactions scheme.....	45
2.4.4 Independent parallel reactions scheme.....	47
2.4.5 Distributed activation energy models.....	51
Chapter 3 – Materials and Methods.....	56
3.1 Biomass Analyzed	56
3.1.1 Sample characterization	56
3.2 Experimental Set-up.....	57
3.2.1 Thermogravimetric analyzer	57
3.2.2 Differential scanning calorimetric analyzer	58
3.3 Data analysis	58
3.4 Isoconversional methods.....	59
3.4.1 Method of friedman.....	60
3.4.2 Method of Vyazovkin	60
3.4.3 Application of isoconversional methods.....	61
3.4.4 Reaction model determination	64
3.4.5 Pre-exponential factor determination.....	65
3.5 Consecutive Reactions Scheme	65
3.6 Independent Parallel Reactions Scheme	68
3.7 Heat of Reaction	71
Chapter 4 – Results and Discussion	74

4.1 Biomass Characterization	74
4.2 Thermal Decomposition Analysis in Inert Atmosphere	76
4.2.1 Dehydration.....	77
4.2.2 Devolatilization.....	77
4.2.3 Carbonization	78
4.3 Thermal Decomposition Analysis in oxidative atmosphere	79
4.4 Isoconversional Method Results in Inert Atmosphere.....	81
4.4.1 Reaction model and pre-exponential factor determination	83
4.4.2 Evaluation of the kinetic parameters.....	86
4.5 Isoconversional Method Results in Oxidative Atmosphere.....	87
4.6 Analysis and Considerations on Model Fitting.....	88
4.6.1 Application of the correlations in complex reaction schemes	96
4.7 Results of the Consecutive Reactions Scheme in Inert and Oxidative Atmospheres	97
4.8 Results of the Independent Parallel Reactions Scheme in Inert Atmosphere	106
4.9 Results of the Independent Parallel Reactions Scheme in Oxidative Atmosphere.....	109
4.10 Summary of the Kinetic Analysis of the Thermal Decomposition of Sugarcane Straw	114
4.11 Heat of Reaction in Nitrogen and Synthetic Air Atmospheres.....	116
Conclusions	119
References	121
Future Research Directions	135
Publications Related to the Thesis.....	136
Appendix A – Lower heating value calculations.....	137
Appendix B – Preparation of TG/DTG data for thermal and kinetic analyses.....	138
Appendix C – Application of isoconversional methods.....	140
Appendix D – Application of the consecutive reactions scheme	147
Appendix E – Application of the independent parallel reactions scheme.....	155
Appendix F – Determination of the heat of reaction	160
Annexe A – Permission of the publisher IGI Global	137
Annexe B – Permission of the publisher Elsevier B.V.....	138

CHAPTER 1

INTRODUCTION

The sugarcane straw is composed by dry leaves, green leaves and tops of the sugarcane plant. Each ton of stalks corresponds to 140 kg of dry residues. Part of the sugarcane is mechanically harvested and the straw is left on the ground, and other great part is burned before the harvesting of sugarcane in order to reduce the cost of this operation.

São Paulo and Minas Gerais states in Brazil are the major producers of sugarcane with around two thirds of the whole production in the country. These states are committed for the total removal of burning process in the farms until 2018. This process has been controlled by the Brazilian government by law No. 11241 (September 19th, 2002) to promote the gradual reduction of sugarcane burning until 2031. Due to the high generation of this agricultural residue in ethanol production, it turns necessary to find one or more energetic applications for sugarcane straw. Combustion, gasification or pyrolysis processes could be some possibilities.

Pyrolysis is a thermochemical process that involves the heating of materials in the absence of oxidizing agents. The heating process can use isothermal or constant heating rate conditions to reach a maximum pyrolysis temperature. The nature of the products depends on different variables, including temperature, heating rate, condensation temperature, and particle size. Pyrolysis is one of the most important ways to transform biomass into value added products (e.g., bio-char, bio-oil, fuels, synthesis gas, and chemicals) with several industrial applications.

In order to design industrial reactors, as well as to obtain important empirical parameters for process modeling and controlling, the kinetics involved in biomass pyrolysis should be well understood. This not only allows the estimation of kinetic parameters, but also the simulations beyond the temperature range. Experimentally, thermogravimetric analysis (TG) is the procedure commonly applied to study the pyrolysis kinetics.

Another thermal analysis technique is the differential scanning calorimetry (DSC), which is widely applied in the measurement of the heat of reaction involved in the thermal decomposition of biomass. Nevertheless, this technique could be also applied for kinetic

analysis, providing similar results than the obtained by thermogravimetry. However, TG is considered more accurate, and therefore, more reliable, since the experimental data obtained by this technique is directly related to the sample behavior, which in DSC does not occurs. Normally, in biomass pyrolysis the reactions involved are endothermic with an exothermic stage above 450 °C related to lignin decomposition.

The Laboratory of Particle Technology and Multiphase Processes (LaProM) coordinated by Prof. Dra. Katia Tannous has been working in different domains considering storage and transportation of solids, fluidized beds, and recently chemical reactors applying different types of biomasses and its particularities. Taking into account this history of research, in this thesis was covered several topics regarding physical, chemical and thermal characterization, thermal behavior, and reaction kinetics of sugarcane straw as raw material por thermal conversion processes such as pyrolysis and combustion.

This work presents an overview of the different approaches for heterogeneous kinetics in solid state with special attention in the thermal decomposition of biomass, in order to obtain reliable simulations and understand how the reactions occur in this process.

1.1. General Objectives

The aim of this investigation was the study of the thermal decomposition reaction kinetics of sugarcane straw (*Saccharum officinarum* Linnaeus) in inert and oxidative atmospheres.

1.1.1. Specific Objectives

- Presentation of the theoretical fundamentals of the kinetic modeling of biomass thermal decomposition;
- Determination of the physical, chemical, and thermal properties of sugarcane straw in order to investigate the viability of this biomass as a source for thermal conversion processes;

- Analysis of the thermal decomposition of sugarcane straw by dynamic thermogravimetric (TG) in nitrogen and synthetic air atmospheres;
- Estimation of the activation energy through the isoconversional kinetic methods of Friedman (differential) and Vyazovkin (integral), assuming a scheme of global reaction;
- Proposal of a new analysis procedure to obtain the kinetic parameters of lignocellulosic biomass pyrolysis assuming first order reactions;
- Analysis of the thermal decomposition of sugarcane straw considering a scheme of consecutive reactions in nitrogen and synthetic air atmospheres;
- Analysis of the thermal decomposition of sugarcane straw considering a scheme of independent parallel reactions s in nitrogen and synthetic air atmospheres;
- Determination of the heat of reaction and analysis of the thermal decomposition reaction of sugarcane straw in nitrogen and synthetic air atmospheres by direct scanning calorimetry (DSC).

CHAPTER 2

LITERATURE REVIEW

The main goal of this chapter is to present the theoretical fundamentals of the kinetic modeling of biomass thermal decomposition, discussing its complexities in the application of the different kinetic schemes, i.e., global reaction, consecutive reactions, independent parallel reactions, and reaction with distributed activation energy.

2.1. Biomass

The balance between carbon dioxide emissions and fixation presented by photosynthesizing biomasses, as well as the great availability (especially regarding agricultural residues), have shown the great potential of biomass in becoming a widespread source of fuels and chemicals (Abbasi & Abbasi, 2010).

Biomass is a generic term that refers to every organic non-fossilized animal, vegetable or microbiological raw materials that can be converted into chemicals and fuels (Vassilev, Baxter, Andersen, & Vassileva, 2010). Special focus has been given to vegetable and microbiological biomasses, or simply *phytomass* (Abbasi & Abbasi, 2010). This kind of biomass is represented by an abundant and diverse spectrum comprising: food crops-to-energy (e.g., sugarcane, corn, and soybean); hydrocarbon-rich plants (e.g., latex-bearing species such as *Plumeria alba*); agricultural (e.g., straws, shells, and endocarps), forestry (e.g., leaf litter, and sawmill waste) and food wastes (e.g., biomass components of municipal solid waste); and, energetic fast-growing crops and woody species (e.g., poplar, pine, and switchgrass).

Due to its composition, phytomass is usually referred as a lignocellulosic material. Lignocellulosic biomasses are mainly composed by hemicellulose, cellulose, and lignin as well as smaller amounts of extractives (e.g., essential and fatty oils, terpenes, phenolic compounds, and resins), moisture, and inorganic matter (White, Catallo, & Legendre, 2011). Vassilev et al. (2010) pointed out that great variability has been observed in lignocellulosic biomass composition, depending on a diversity of factors such as: type of biomass, plant species, part of the plant, growing conditions, age, transport and storage conditions, and harvesting time.

Biomass is the main renewable raw material to be used in sustainable bio-refineries, integrating processes for the production of food, biofuels, chemicals, biomaterials, electricity, and heat. Biomass structure can be decomposed using technologies such as pyrolysis and gasification to generate a variety of value-added products (Kajaste, 2014; Menon & Rao, 2012; Pippo, Luengo, Alberteris, Garzone, & Cornacchia, 2011).

The conversion of biomass generates different energetic products, such as ethanol, biodiesel, biogases, bio-oil, and biochar, depending on the conversion technique applied. These products can be directly burned, or used in engines, turbines, and fuel cells to obtain electricity, heat, and power (Basu, 2010). There are mainly three ways to convert biomass into fuels, the thermochemical, biochemical, and mechanical routes. Among these, the thermochemical route presents some advantages over the others, such as lower pollutants emission, faster reaction times, and lower generation of by-products (Demirbas & Balat, 2007).

2.1.1. Biomass composition

As aforementioned, biomass presents a complex and variable composition. In this context, Vassilev, Baxter, Andersen, Vassileva, and Morgan (2012) presented an overview of organic and inorganic composition of 93 biomasses including wood and woody biomass, herbaceous and agricultural biomass, animal, and contaminated biomass. A great diversity has been observed in the fractional composition of biomass pseudo-components. For example, the mean weight percentages of woody biomass pseudo-components on a dry ash-free basis were 34.5%, 39.5%, and 26.0% for hemicellulose, cellulose, and lignin, respectively, while for shells and husks these percentages change to 27.4%, 40.0%, and 32.6%, respectively.

The hemicelluloses are natural highly branched polymers composed by several monomeric polysaccharides such as xylose, mannose (prevalent in hardwoods), glucose, galactose, arabinose (prevalent in softwoods), and other polysaccharides (Lanzetta & Di Blasi, 1998) with a random and amorphous structure (Vassilev et al., 2012). The hemicellulose binds non-covalently to the cellulose microfibrils and is thermally less stable than cellulose. It undergoes dehydration at temperatures below 280 °C, forming anhydride fragments, water soluble acids, char, gases, and water. At higher temperatures, it depolymerizes yielding volatile organics, levoglucosan and other anhydrohexoses,

levoglucosenones, and furans (Van de Velden et al., 2010).

Celluloses are natural polymers formed by anhydroglucose units connected by glycosidic bonds. It is the main component of the plant cell wall and its decomposition is the mostly investigated and well understood (Van de Velden et al., 2010). The long linear chains formed in this polymer are bond to one another by a network of hydrogen bonds (Vassilev et al., 2012), what makes cellulose thermally more stable than hemicellulose. At temperatures below 350 °C it goes through dehydration where the water content and volatiles are released, and there is a large decrease in the degree of polymerization (Van de Velden et al., 2010). Between 300 – 450 °C the depolymerization to levoglucosan and other primary anhydrosugars is dominant, while the fragmentation takes place at around 600 °C, forming hydroxy-acetaldehyde, 5-hydroxymethyl-furfural, methanol, acetaldehyde, and carbon monoxide and dioxide as the main products (Ranzi et al., 2008; Van de Velden et al., 2010).

Lignins are three-dimensional, highly branched, polyphenolic polymers, formed by three main phenylpropane units, namely p-coumaril, coniferyl, and sinapyl. It is an amorphous cross-linked resin that forms an irregular array of hydrogen bonds. Lignin thermal decomposition occurs in a broad temperature range, as a result of its high thermal stability. It is mostly responsible for char and volatiles of low molecular mass formation (Liu, Zhong, Wang, & Luo, 2011; Várhegyi, Antal, Jakab, & Szabó, 1997). At temperatures lower than 500 °C dehydration is dominant and a diversity of products is released, while higher temperatures lead to the formation of a variety of lignite monomers such as catechols, vanillins, and aromatic carbohydrates. Above 700 °C these monomers are decomposed and released to the vapor phase (Van de Velden et al., 2010).

2.2. Sugarcane straw

Annually, Brazil produced and processed more than 650 million metric tons of sugarcane in 2014/2015 crop, which corresponds to a production of 34 million tons of sugar and 30 million cubic meters of ethanol (Brazilian Sugarcane Industry Association -UNICA). The sugarcane straw is composed by dry leaves, green leaves and tops of the sugarcane plant. Each ton of stalks corresponds to 140 kg of dry residues. Part of the sugarcane is mechanically harvested and the straw is left on the ground, and other great part is burned before the harvesting of sugarcane in order to reduce the cost of this operation (Leal et al.,

2013). The states of São Paulo and Minas Gerais in Brazil, which are the major producers of sugarcane (around two thirds of the production) are committed for the total removal of burning process until 2018 (Leal et al., 2013). This process has been controlled by the Brazilian government by law No. 11241 (September 19th, 2002) to promote the gradual reduction of the sugarcane burning until 2031. Due to the high generation of this agricultural residue in the ethanol production, it turns necessary to find one or more energetic applications for sugarcane straw, e.g., combustion, gasification, or pyrolysis could be some possibilities.

In the last few years, there has been a growing interest in sugarcane straw, and some studies have been conducted on pyrolysis application. Moraes et al. (2012) analyzed the chemical composition of volatile compounds produced during the sugarcane straw pyrolysis, identifying more than 120 compounds, mainly oxygenated ones (acids, aldehydes, alcohols, phenols, ethers, and ketones). Mesa-Pérez et al. (2013) investigated the pyrolysis in a bubbling fluidized bed reactor, obtaining maximum yields of bio-oil and bio-char of 35.5 wt% and 48.2 wt%, respectively, at a temperature of 470°C. These authors make a great contribution to the field, exhibiting the importance and viability of sugarcane straw as an energetic source.

2.3. Analysis of the Biomass Thermal Decomposition

The study of kinetics involved in biomass thermal decomposition is relevant, firstly, because the complex interdependence between kinetic and transport phenomena makes the kinetic modeling an indispensable step to pyrolysis practical use (Mettler et al., 2012). Secondly, because it provides means to: simulate complete conversion-time curves, control and optimize the process parameters (Sbirrazzuoli, Vincent, Mija, & Guigo, 2009), and design industrial reactors.

Experimentally, the kinetic analysis of biomass thermal decomposition is associated with thermo-analytical data from differential scanning calorimetry (DSC), dynamical mechanical analysis (DMA), thermogravimetric analysis (TG) and its first derivative (DTG) (Sbirrazzuoli et al., 2009) or differential thermal analysis (DTA) (White et al., 2011). According to White et al. (2011) the use of TG is the most common procedure in studies of solid-phase thermal decomposition, being specially and widely applied in the study of biomass pyrolysis.

In TG measurements, the remaining mass at a specific heating rate is registered as a function of time or temperature, while DTG provides the reaction rate (White et al., 2011). There are two kinds of TG, isothermal and non-isothermal. In the first one, a constant specific temperature is used in the analysis, while in the second the temperature is gradually increased by a linear heating rate. Both techniques have been employed in pyrolysis kinetic modeling (Vyazovkin et al., 2011).

Nevertheless, all experimental techniques present some limitations. In TG, as well as other techniques such as DSC, DMA and DTA, the limitations arise from effects caused by intra- and inter-particle transport phenomena. The intra-particle heat and mass transfer effects are mainly influenced by the particle diameter, sample mass and heating program.

The diameter affects the particles internally, since large particles tend to develop a temperature gradient with external temperatures higher than the center temperature. It was observed that for particle diameters higher than 0.5 mm, the established temperature profile induces the generation of composition gradients, due to different reactions velocities in different temperatures (Nascimento, 2012).

The inter-particle heat and mass limitations strongly depend on the sample mass used in the analysis. In TG experiments, the sample is inserted in, generally, a metallic pan forming a packed bed with small dimensions (Becidan, Várhegyi, Hustad, & Skreiberg, 2007). Therefore, if high amounts of mass are used, temperature profiles can also be formed in this small dimension bed, where the particles of the external layer will be at a higher temperature than those at the center of the sample bed, also inducing the development of a composition gradient. In order to avoid this kind of experimental limitations, the literature recommends the use of sample mass lower than 10 mg. Although, depending on the biomass density, which is greatly variable, previous mass influence studies must be performed in order to obtain the least variable decomposition profile (Nascimento, 2012).

Another parameter that affects the decomposition by thermogravimetry is the heating rate. If heating rates faster than 20 °C/min are used, the reacting time will be shortened in such a manner that some of the reactions steps will fail to be registered by the equipment, diminishing the experimental reliability (Rueda-Ordóñez, Olivares-Gómez, & Tannous, 2013). Lisboa and Watkinson (1999) investigated the influence of the particle diameter

(<0.074 mm and <0.250 mm), gas flow rate (62-300 mL/min), and sample mass (5.81-20.9 mg) on the pyrolysis of oil shale by thermogravimetry, using heating rates of 50 °C/min and 70 °C/min. The authors observed that is possible to avoid the thermal lag effects using particle diameter, gas flow rate, and sample mass lower than 0.25 mm, 100 mL/min, and 20 mg, respectively. However, as the biomass compositional and physicochemical properties are variable, one is advised to perform a set of preliminary experiments in order to define the best conditions, and having Lisboa and Watkinson's values as a reference.

2.3.1. Biomass thermal decomposition in inert atmosphere (pyrolysis)

Pyrolysis is considered promising in obtaining biofuels because it can convert solid biomass into easily transportable liquids (with a higher energy density) in a rapid and efficient manner (Mettler, Vlachos, & Dauenhauer, 2012). This reaction involves the thermal decomposition of biomass in an inert atmosphere (Figure 2.1), e.g., nitrogen (N₂), argon (Ar), and helium (He), using either isothermal or non-isothermal heating programs to reach temperatures of about 600°C. Nonetheless, according to Basu (2010), the non-condensable gases mixed with air could be used as semi-inert atmosphere, reducing the processing cost. Also, some researchers (Senneca, Chirone & Salatino, 2004; Lautenberger & Fernandez-Pello, 2009; Amutio et al., 2012; Mesa-Pérez et al., 2013) have studied the viability of burning part of biomass in a reactor in order to obtain the heat of pyrolysis and use the combustion gases as inert atmosphere. This process is known as oxidative pyrolysis.

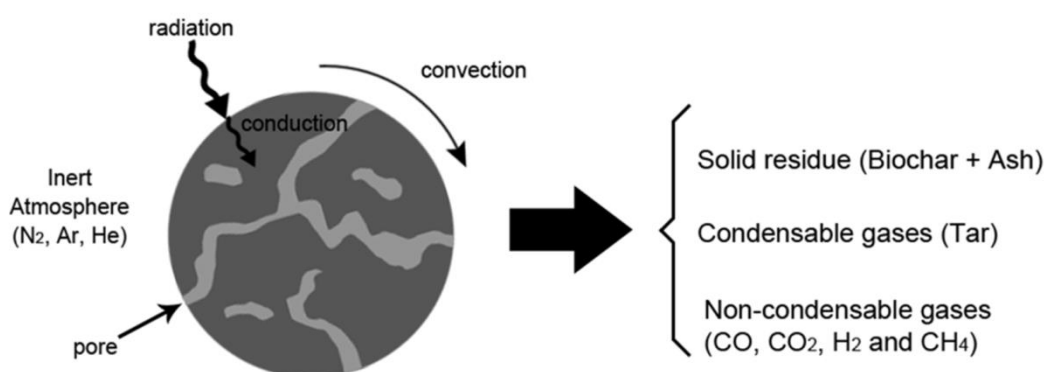


Figure 2.1. Heat and mass transfer of a biomass particle submitted to pyrolysis

Figure 2.1 describes the heat transfer mechanisms of a biomass particle subjected to pyrolysis. The main products are solid residues and gas. Some of the gases are readily condensed while the remaining gas is mainly constituted by carbon monoxide (CO) and dioxide (CO₂), hydrogen (H₂), and methane (CH₄).

In general, the first step in the thermal decomposition of a biomass particle is the drying, which can reach temperatures up to 150 °C. The second step is the torrefaction process, occurring between 150 – 300 °C, where the thermal stage corresponds to the biomass exothermic decomposition and formation of low molecular weight gases (CO and CO₂). The final step takes place between 300 – 600 °C, where a high amount of volatiles is released as condensable gases (vapors and precursors of the liquid fraction), non-condensable gases, and char (Basu, 2010).

According to Mettler et al. (2012), the main difficulties involved in pyrolysis are the complex and multi-scale nature of biomass feedstock, and also to obtain a mathematical model that describes, firstly, the reaction kinetics, and secondly, heat, mass, and momentum phenomena.

As a consequence of biomass complex composition and heterogeneity, its kinetic behavior under pyrolysis is difficult to describe (Van de Velden, Baeyens, Brems, Janssens, & Dewil, 2010). The kinetic modeling of biomass pyrolysis aims to obtain equations that represent the behavior of biomasses in a wide range of experimental conditions, providing a deeper insight into the reactions occurring during pyrolysis, and revealing similarities and differences among biomasses (Várhegyi, Antal, Jakab, & Szabó, 1997)

As lignocellulosic biomass is mainly composed by a complex mixture of hemicellulose, cellulose, and lignin, its behaviour under pyrolysis is influenced by the contents of each pseudo-component (Van de Velden et al., 2010). To date, most devolatilization schemes consider that the different volatiles released during biomass pyrolysis are related to the three main components separately. The sum of these individual devolatilization rates, weighted according to their initially present percentage in the unreacted biomass, gives the total devolatilization process rate (White et al., 2011). Therefore, the study of the individual pseudo-components thermal degradation and kinetics under pyrolysis provides ways of

understanding the expected reaction pathway in biomass degradation (Várhegyi, Antal Jr., Szekely, & Szabó, 1989).

In a review published by Di Blasi (2008) considering a wide number of studies on wood and biomass pyrolysis, the author observed that the mean temperature range for low heating rates in which hemicellulose, cellulose, and lignin present the higher decomposition rates were 225 – 325 °C, 325 – 375 °C, and 250 – 500 °C, respectively. Di Blasi also stated that during thermal conversion, as the heating rate increases, the temperature range of the components degradation becomes narrower.

In biomass decomposition, as even with the use of slow heating rates (< 20 °C/min), hemicellulose and cellulose decompose at a very close temperature range, there is still an overlapping of their degradation zones and usually two distinct peaks cannot be clearly observed in the derivative of the TGA curve (DTG). In these curves, hemicellulose usually represents a shoulder in the cellulose peak, which occurs at approximately 350 °C. Due to the aforementioned complexities, lignin presents a wide and flat DTG peak, overlapped by the cellulose and hemicellulose peaks, reaching also low (< 10%) and high (> 80%) conversions (Parthasarathy & Narayanan, 2014).

In order to understand the thermal decomposition of biomass main pseudo-components various authors studied the pyrolysis of commercially available forms of hemicellulose, cellulose, and lignin, and also of different biomasses regarding the effects of each component (Anca-Couce, Berger, & Zobel, 2014; Branca & Di Blasi, 2013; Orfão, Antunes, & Figueiredo, 1999; Várhegyi et al., 1989; Várhegyi et al., 1997; White et al., 2011). A wide spectrum of models, biomasses and experimental conditions were applied, resulting in a scatter of the estimated kinetic parameters.

White et al. (2011) reviewed the pyrolysis of different nutshells and presented a case study based on sugar cane bagasse slow and fast pyrolysis, under oxidative and non-oxidative media. Most researches used a three-step parallel reaction model considering first-order mechanisms for a variety of heating rates, particle sizes, temperature range, and sample masses. In slow pyrolysis under inert atmosphere, the values of activation energy (E) for the hemicellulose, cellulose, and lignin ranged between 105.0 – 253.5 kJ/mol, 194.0 – 250.0 kJ/mol, and 26.0 – 60.0 kJ/mol, respectively. The values of log of pre-exponential factor (A)

for the hemicellulose, cellulose, and lignin ranged between $15.43 - 17.71 \text{ s}^{-1}$, $7.43 - 18.0 \text{ s}^{-1}$, and $0.78 - 2.58 \text{ s}^{-1}$, respectively.

Anca-Couce et al. (2014) reviewed the pyrolysis of twelve lignocellulosic biomasses (e.g., pine wood, eucalyptus, pine barks, cotton, beech wood, olive husks, hazelnut shells, and corn-cobs), and estimated the kinetic parameters of other four (three beech woods and one pine wood) with a three-step parallel reaction scheme. The researchers have observed that, considering the reviewed and estimated values, the E for cellulose presents the narrowest observed range (190 – 250 kJ/mol). Hemicellulose normally presents lower values of E (75 – 220 kJ/mol) than cellulose, while the values for lignin are fairly low (25 – 200 kJ/mol) and usually do not exceed 100 kJ/mol. These values show there is a lack of consistency among different estimations for the pyrolysis kinetic parameters of biomass pseudo-components.

2.3.2. Biomass thermal decomposition in oxidative atmosphere (combustion)

Alternative and clean energies are composed mainly by solar, wind, and lignocellulosic biomass-based processes, i.e., pyrolysis, combustion, and gasification. The combustion of lignocellulosic biomass is an interesting process to obtain high quantities of energy released as heat. Therefore, the research about combustion of sugarcane straw is considered priority since there is the possibility of mixture with bagasse for burning in the existing boilers (Leal et al., 2013).

The smoldering reaction is a slow and flameless combustion self-sustained through the heat released by the oxidation of the solid fuel, which its reaction kinetics have been analyzed through thermogravimetry (TG) (He, Yi & Zha, 2009; Anca-Couce et al., 2012; Cancellieri et al., 2012; Huang & Rein, 2014; Huang, Rein & Chen, 2015; Huang & Rein, 2016). TG is the technique commonly used to study the thermal decomposition kinetics of biomass carried out under nitrogen, argon, synthetic air and oxygen atmospheres.

Órfão et al. (1999) compared the thermal decomposition of xylan, cellulose, and lignin in nitrogen and synthetic air atmospheres through TG analysis. The authors observed in oxidative atmosphere that the decomposition temperature range of cellulose and xylan were lower than in nitrogen, but for lignin remained unaltered. Also, they observed that the reaction rate in synthetic air for hemicellulose and cellulose was slightly higher than in inert

atmosphere, but for lignin was three times higher. This behavior is due to the exothermic reactions presented in the oxidative thermal decomposition of these biomass components, since the heat released promotes the increasing of the sample temperature, and therefore a faster decomposition. Also, at this stage, the volatilized products interact with the remaining solid (reactant) generating oxidation reactions, which increase the reaction rate and decrease the reaction temperature range (Amutio et al., 2012). The authors also proposed two stages in smoldering of xylan and cellulose: the first stage was related to the oxidative pyrolysis or volatile release from samples, and the second stage to the combustion of the remaining carbonaceous solid.

The combustion reaction kinetics is often studied by two approaches, isoconversional methods (one-step reaction) and independent parallel reactions scheme. Ramajo-Escalera et al. (2006) applied the Vyazovkin isoconversional method (Vyazovkin, 1997) to analyze the combustion kinetics of sugarcane bagasse, obtaining activation energies of 76.1 ± 1.7 kJ/mol for conversion between 2 and 5%, 333.3 ± 15.0 kJ/mol for conversion of 15–60%, and 220.1 ± 4.0 kJ/mol for the conversion range of 70–95%.

Besides that, the independent parallel reactions scheme is widely accepted, and in literature could be found modeling with three up to six reactions. Therefore, the more reactions considered the better the fitting with experimental data. According to Vyazovkin et al. (2011) from Committee of the International Confederation for Thermal Analysis (ICTAC), the kinetic analysis using parallel reactions should apply as a first guess the activation energy obtained by isoconversional methods, in order to improve the fitting.

The differential scanning calorimetry (DSC) has been used to measure the heat of reaction, which could be endothermic, exothermic, or both depending on the process and raw material. For biomass pyrolysis the heat of reaction involved is endothermic (Ramajo-Escalera et al., 2006; He et al., 2006; He et al., 2009; Van de Velden et al., 2010; Shen et al., 2015) with an exothermic stage above 400 °C concerning to the lignin decomposition (Rath et al., 2003). The heat required for pyrolysis reaction varies from 200 kJ/kg to 600 kJ/kg depending on the biomass type. For biomass combustion process the reactions are exothermic above 150 °C (i.e., after drying process), and the heat released can be from 6 MJ/kg to 15 MJ/kg (He et al., 2009; Anca-Couce et al., 2012; Leroy-Cancellieri et al., 2014).

2.4. Kinetic Modelling of Biomass Thermal Decomposition

In the first attempt to understand biomass thermal behavior and kinetics, were considered the classical mathematical methods developed in the 1960's. They assumed that the thermal decomposition could be well described by a single-step reaction (Coats & Redfern, 1965; Flynn & Wall, 1966; Horowitz & Metzger, 1963; Kissinger, 1957).

Firstly, the TG data need to be converted to normalized mass, W , using equation (2.1), where m and m_0 are the mass at a time t , and the initial mass, respectively.

$$W = \frac{m}{m_0} \quad (2.1)$$

Afterward, the DTG curves determined by numerical differentiation have to be also normalized (dW/dt) using equation (2.2).

$$\frac{dW}{dt} = \frac{dm}{dt} \frac{1}{m_0} \quad (2.2)$$

For the kinetic analysis, it is necessary to select the main volatile release range from the normalized mass data. Then, using equation (2.3), were converted in conversion, α , in which W_0 , W , and W_f are the normalized mass at the beginning, at a time t , and at the end of the main volatile release, respectively. The conversion, α , is a dimensionless measurement of the amount of reactants that has been converted into products. Also, the experimental conversion rate $(d\alpha/dt)_{exp}$ is given by equation (2.4).

$$\alpha_{exp} = \frac{W_0 - W}{W_0 - W_f} \quad (2.3)$$

$$\left(\frac{d\alpha}{dt}\right)_{exp} = -\frac{dW}{dt} \frac{1}{(W_0 - W_f)} \quad (2.4)$$

The theoretical conversion rate $(d\alpha/dt)_{theoretical}$ is given by equation (2.5), in which E is the activation energy, A is the pre-exponential factor, R is the universal gas constant (8.314 J/mol K), and T is the absolute temperature.

$$\left(\frac{d\alpha}{dt}\right)_{theoretical} = [f(\alpha)]A \left[\exp\left(\frac{-E}{RT}\right) \right] \quad (2.5)$$

In solid-state kinetics the Arrhenius parameters (A , and E) arise from an analogy with the representation of homogeneous kinetics (gas phase processes) by the collision theory of reaction rates. From this statements, the activation energy (E) is the energetic barrier to be overcome in order to start a chemical reaction, i.e., reactants be converted in products. The pre-exponential factor or frequency factor is defined as the frequency of molecular collision during the reaction (Brown, Dollimore, & Galwey, 1980).

Nonetheless, in solid-state reactions (heterogeneous kinetics) the reactant species are not free-moving (are immobilized) and colliding among them as predicted by the collision theory, they are interacting at a narrow interface between two crystalline phases (Brown et al., 1980). Then, the frequency factor concept is not more conceivable to represent reactions in solid-state and it must be seen as a specific constant related to a specific reaction (Brown et al., 1980; White et al., 2011). Moreover, according to Vyazovkin et al. (2011) and White et al. (2011) in solid-state kinetics this parameter can be assumed as a fitting parameter, i.e., a mathematical constant without physical meaning.

Also, according to Brown et al. (1980) and Upadhyay (2007) the activation energy in solid-state reactions has no significance, except in some rare cases, having more empirical than theoretical meaning. Also, due to the imperfections in the crystal, the reactivity of solids vary, which produce the variation in activation energy with the evolution of the reaction. In the case of solids formed by several components, i.e., wood and biomass, the variation of activation energy with the reaction evolution can be related to the reaction of each component (White et al., 2011; Vyazovkin et al., 2011; Anca-Couce et al., 2014).

2.4.1. Isoconversional methods (Model-free methods)

In solid-state kinetics, many models have been proposed being generally classified based on the graphical shape of their curves of α versus time (t) or $(d\alpha/dt)$ versus α , and on their mechanistic assumptions. It should also be noted that as biomass thermal decomposition usually proceeds via a complex arrangement of reactions, where each one of these reactions have its own activation energy, it is common the use of an average, apparent activation energy to describe the overall process (White et al., 2011).

Model-free methods refer to equations in which a reaction mechanism assumption is not necessary to obtain E . Although no assumptions are needed to perform a complete kinetic analysis, the definition of some reaction model is mandatory to estimate the pre-exponential factor. Among these, there are the isoconversional methods, which can be mainly divided into two categories, integral and differential (Flynn & Wall, 1966).

Depending on the mathematical resolution applied to equation (2.5), differential or integral methods arise. When differential methods are applied, the direct use of classical numerical methods generates an approximated solution within the mathematical method and experimental errors. Since there is no analytical solution to the integrated form of equation (2.5), integral methods are based on approximations given by different authors to the temperature integral.

As no assumption is made over the kinetic models, differential isoconversional methods are prone to be more accurate than integral methods. However, this accuracy is diminished by difficulties on the baseline experimental definition and when there is a dependence of E on heating rates. Thus, differential methods cannot be considered necessarily more precise than integral methods, and kinetic modeling with both methods is advised (Vyazovkin et al., 2011).

Integral Methods

According to Sbirrazzuoli et al. (2009), when non-isothermal analysis is employed, the process temperature is controlled by a constant heating rate, β , which is represented by the variation of temperature with time, $\beta=dT/dt$. The conversion rate can be formulated as derivative of conversion with respect to the temperature (Doyle, 1961) through equation (2.6).

$$\frac{d\alpha}{dt} = \left(\frac{d\alpha}{dT}\right) \left(\frac{dT}{dt}\right) = \left(\frac{d\alpha}{dT}\right) \left(\frac{dT}{dt}\right) = \left(\frac{d\alpha}{dT}\right) \beta \quad (2.6)$$

Equation (2.7) is obtained by modification of equation 2.5 introducing the heating rate effect, $\beta=dT/dt$ of equation (2.6).

$$\frac{d\alpha}{dT} = [f(\alpha)] \left(\frac{A}{\beta}\right) \left[\exp\left(\frac{-E}{RT}\right)\right] \quad (2.7)$$

The integral approach assumes that the apparent activation energy (E) remains constant throughout the entire reaction, and that no reactions occur at low temperatures. Therefore, a value of zero is assumed for the initial conversion, related to an initial temperature. Additionally, as no reaction is observed for low values of temperature, the lower integration limit for this variable is also zero. The integration of equation (2.7), from these initial parameters up to a specific conversion temperature, T_α , related to conversion α , gives the equation (2.8).

$$g(\alpha) = \int_0^\alpha \frac{d\alpha}{f(\alpha)} = \left(\frac{A}{\beta}\right) \int_0^{T_\alpha} \left[\exp\left(\frac{-E}{RT}\right)\right] dT \quad (2.8)$$

In equation (2.8) $g(\alpha)$ is an integral function of the conversion, dependent on the reaction mechanism. The right side is the temperature integral, which the solution is represented by the function $p(x)$ (White, et al., 2011; Sanchez, Otero, Gómez, & Morán, 2009), defined in equation (2.9), where $x=E/RT$:

$$g(\alpha) = \left(\frac{AE}{\beta R}\right) \left[\frac{-\exp(x)}{x} - \int_x^\infty \left(\frac{\exp(-x)}{x^2}\right) dx\right] = \left(\frac{AE}{\beta R}\right) p(x) \quad (2.9)$$

Depending on the approximate solution for the $p(x)$ function, different integral methods have been developed over the years. Table 2.1 shows a summary of the integral and differential isoconversional methods.

Table 2.1. Main features of integral and differential methods

Model	Graphic representation	Activation energy (E)	Reference
$\ln[g(\alpha)] = \ln \left\{ \left(\frac{AR}{\beta E} \right) \left[\left(\frac{0,386}{T_{max}} \right)^{\left(\frac{E}{RT_{max}} \right)} (T_{max} + 1) \right] \right\} + \left[\frac{E}{R(T_{max} + 1)} \right] \ln T$	(2.10) $\ln[g(\alpha)]$ vs $\ln(T)$	mR	Van Krevelen et al. (1951)
$\ln \left[\frac{g(\alpha)}{T^2} \right] = \ln \left[\left(\frac{AR}{\beta E} \right) \left(1 - \frac{2RT}{E} \right) \right] - \left(\frac{E}{RT} \right)$	(2.11) $\ln[g(\alpha)/T^2]$ vs $1/T$	mR	Coats and Redfern (1965)
$\log(\beta) = \left[\log \left(\frac{AE}{R} \right) - \log[g(\alpha)] - 2.315 \right] - 0.4567 \left(\frac{E}{RT} \right)$	(2.12) $\log_{10}(\beta)$ vs $1/T$	$mR/0.4567$	Ozawa (1965) Flynn and Wall (1966)
$\ln \left[\frac{\beta}{T^2} \right] = \ln \left[\left(\frac{AR}{g(\alpha)E} \right) \left(1 - \frac{2RT}{E} \right) \right] - \left(\frac{E}{RT} \right)$	(2.13) $\ln(\beta/T^2)$ vs $1/T$	mR	Braun et al. (1991)
$\ln \left[\frac{\beta}{T_m^2} \right] = \ln \left[\left(\frac{AR}{f'(\alpha)E} \right) \right] - \left(\frac{E}{RT_m} \right)$	(2.14) $\ln(\beta/T_{m,i}^2)$ vs $1/T_{m,i}$	mR	Kissinger (1957)
$\ln \left(\frac{d\alpha}{dt} \right) = \ln(A) + \ln[f(\alpha)] - \frac{E}{RT}$	(2.15) $\ln[(d\alpha/dt)_{\alpha,i}]$ vs $1/T_{\alpha,i}$	mR	Friedman (1964)

One of the first works dealing with an approximation for the temperature integral in equation (2.8) was presented by Van Krevelen, et al. (1951), in which a simple mathematical arrangement, presented in equation (2.16), was proposed, where T_{max} is the peak temperature in the conversion rate curve.

$$\exp\left(\frac{-E}{RT}\right) = \left[\exp\left(\frac{-T_{max}}{T}\right)\right]^{\left(\frac{E}{RT_{max}}\right)} \approx \left[0.368\left(\frac{T}{T_{max}}\right)\right]^{\left(\frac{E}{RT_{max}}\right)} \quad (2.16)$$

The kinetic model developed by Van Krevelen et al. (1951) is presented in equation (2.10), Table 2.1. Flynn and Wall (1966) tested this model comparing it with theoretical curves, in which the kinetic parameters were known, and concluded that the method should be limited to cases with a previously defined reaction model.

Coats and Redfern (1965) proposed a solution of the $p(x)$ function based on an asymptotic expansion shown in equation (2.17), and the model proposed by them is presented in equation (2.11), Table 2.1. The authors observed that analyzing up to the second term of the expansion, acceptable results were obtained.

$$p(x) = \left[\frac{\exp(x)}{x^2}\right] \left(1 + \frac{2!}{x} + \frac{3!}{x^2} + \frac{4!}{x^3} + \dots + \frac{n!}{x^{n-1}}\right) \quad (2.17)$$

The definition of a $g(\alpha)$ function in equation (2.8) is mandatory to apply the Coats and Redfern method, and its use is uncommon in the literature. Flynn and Wall (1966) compared the results obtained through this method with theoretical curves and concluded that it is only applicable for conversions lower than 0.3.

Nevertheless, some recent studies (Tonbul, 2008, Lu, Song, & Lin, 2009) used this method to evaluate the combustion and pyrolysis kinetic parameters. Ebrahimi-Kahrizsangi and Abbasi (2008) used simulated TGA curves for different kind of reactions and compared with results obtained by this method, concluding that it is not accurate, and generates great deviation from the real values.

The Ozawa-Flynn-Wall (OFW) method was proposed independently by Ozawa (1965) and Flynn and Wall (1966), and derived based in equation (2.18), proposed by Doyle (1961).

$$\log_{10}[p(x)]=a+bx \quad (2.18)$$

The values a and b are constants determined by linear interpolation, for example, $a=-2.315$ and $b=-0.4567$ for $20 \leq x \leq 60$. The OFW method is presented in equation (2.12), Table 2.1. In this method application, it is necessary to use at least three different heating rates in the thermogravimetric analysis, and it is considered more reliable than the methods of Van Krevelen, and Coats and Redfern (Flynn & Wall, 1966).

According to White et al. (2011), OFW method introduces error, overestimating E . However, it is commonly used due to its easy application. Some recent works (e.g., Anca-Couce et al., 2014, Ceylan & Topçu, 2014; Ye, Li, Chen, Zhang, & Xu, 2010) employed this method to determine E of different biomasses in TGA experiments under nitrogen atmosphere.

Braun, Burnham, Reynolds and Clarkson (1991) used the asymptotic expansion previously presented by Coats and Redfern (1965), proposing a method that uses different heating rates to obtain E . This method is known as the modified Coats and Redfern (MCR) method. In addition, in the literature, the same mathematical relation is commonly referred as Kissinger-Akahira-Sunose (KAS) method.

The use of MCR in biomass analysis is very common, and the activation energies are lower than those determined by the Ozawa-Flynn-Wall method. Equation (2.12), Table 2.1, presents this method and its linearization form. White et al. (2011) point out that it can overestimate the kinetic values when applied in biomass investigations.

Other approaches have been proposed over the years and, with the computational advances, more accurate procedures emerged. Even so, these proposals, such as the methods of Starink (1996), Vyazovkin (1997), and Tang, Liu, Zhang and Wang (2003) have been sparsely found in the literature.

Differential Methods

Differential isoconversional methods are not dependent on approximations for the temperature integral and, therefore, kinetic parameters can be straight calculated. Vyazovkin

et al. (2011) point out that caution must be taken when using differential models, since its use introduces imprecision into the measured data, and also inaccuracy, when the data are smoothed. Moreover, when the activation energy (E) shows a clear dependency on the heating rate or on the conversion, the use of differential methods should be avoided (Sbirrazzuoli et al., 2009).

The most common differential method is the Friedman (FD) model (Friedman, 1964), shown in equation (2.15), Table 2.1. In this model, the reaction mechanism, $f(\alpha)$, was considered independent of temperature and dependent only on the remaining mass. In this model α represents each different conversions chosen to perform the calculations. For a non-isothermal linear condition, the index i in equation (2.15) identifies a specific heating rate (Sbirrazzuoli et al., 2009).

Another differential method widely used was developed by Kissinger (1956). This method was based on the derivative of equation (2.5), shown in equation (2.19a), in which the right hand term is zero representative of maximum reaction rate.

$$\frac{d}{dt} \left(\frac{d\alpha}{dt} \right) = - \left(\frac{d\alpha}{dt} \right)_p [f'(\alpha)_p] + f(\alpha)_p \frac{E}{RT_p^2} \frac{dT}{dt} = 0 \quad (2.19a)$$

Then, the subscript p represents the values at the peak or maximum conversion rate, $f(\alpha)$ and $f'(\alpha)$ are the reaction model and its derivative, respectively. In equation (2.19b) the peak conversion rate $(d\alpha/dt)_p$ was substituted by its definition presented in equation (2.5), $(d\alpha/dt)_p = f(\alpha)_p A \exp(-E/RT)$.

$$-f(\alpha)_p A \exp\left(\frac{-E}{RT_p}\right) [f'(\alpha)_p] + f(\alpha)_p \frac{E}{RT_p^2} \beta = 0 \quad (2.19b)$$

After that, it was eliminated the peak reaction model, $f(\alpha)_p$, since it is part of both sides of the summation and the equation is equal to zero, and then obtained equation (2.19c).

$$\frac{E}{RT_p^2} \beta = A \exp\left(\frac{-E}{RT_p}\right) [f'(\alpha)_p] \quad (2.19c)$$

The relation β/T_p^2 was isolated in the left side of the equation in order to obtain equation (2.19d).

$$\frac{\beta}{T_p^2} = [f'(\alpha)_p] \frac{R}{E} A \exp\left(\frac{-E}{RT_p}\right) \quad (2.19d)$$

Finally, from equation (2.19b) the Kissinger method was obtained by linearization, and presented in equation (2.14), Table 2.1.

As this method produces only a single set of kinetic parameters, it may not display the general tendency of E for complex kinetics since only one point from DTG data (peak) is considered (Yao, Wu, Lei, Guo, & Xu, 2008). This fact implies that the adequate determination of E can only be accomplished for single-step kinetics.

Table 2.2. Activation energy of several biomasses obtained by isoconversional methods

Reference	Biomass	Activation energy (kJ/mol)			
		FD ^a	FWO ^b	CRM ^c	VZ ^d
Yao et al. (2008)	Bagasse	168.5	169.5	168.7	-
	Bamboo	164.1	162.8	161.9	-
	Cotton stalk	165.3	169.9	169.1	-
	Hemp	180.9	177.9	177.7	-
	Jute	183.1	184.2	184.3	-
	Kenaf	169.8	170.3	169.6	-
	Rice husk	168.2	167.4	166.5	-
	Rice straw	197.6	195.9	196.9	-
	Wood-maple	156.0	155.8	154.3	-
	Wood-pine	161.5	161.8	160.4	-
Ounas et al. (2011)	Sugarcane bagasse	-	199.5	210.0	-
	Olive residue	-	178.3	188.5	-
Mishra and Bhaskar (2014)	Rice straw	195.0	179.4	178.4	179.6
Poletto et al. (2010)	Pine wood	-	158.0	-	-
	Eucalyptus wood	-	155.5	-	-
Slopiecka et al. (2012)	Poplar wood	-	158.6	157.3	-
Anca-Couce et al. (2014)	Beech wood	-	-	183.7	-
	Pine wood	-	-	143.6	-
Ceylan and Topçu (2014)	Hazelnut husk	-	131.1	127.8	-
Baroni et al. (2015)	<i>Tucumã</i> endocarp	160.5	147.3	144.6	145.0
Rueda-Ordóñez et al. (2015)	Brazil nut woody shell	144.5	145.7	142.7	-

^aFriedman method, ^bFlynn-Wall-Ozawa method, ^cCoats-Redfern modified method, ^dVyazovkin method

Table 2.2 presents the activation energy obtained by different isoconversional methods for biomasses (Friedman, Flynn-Wall-Ozawa, Coats-Redfern modified, and Vyazovkin methods), classified in fiber (Yao et al., 2008; Ounas, Aboulkas, El harfi, Bacaoui, and Yaacoubi, 2011; Mishra & Bhaskar, 2014), wood (Poletto, Dettenborn, Pistor, Zeni, & Zattera, 2010; Słopiecka, Bartocci, & Fantozzi, 2012; Anca-Couce, Berger, and Zobel, 2014), and woody shell residues (Ceylan & Topçu, 2014; Baroni, Tannous, Rueda-Ordóñez, & Tinoco-Navarro, 2015; Rueda-Ordóñez, Baroni, Tinoco-Navarro, & Tannous, 2015). Yao et al. (2008) determined the activation energy for ten different species of fibers, considering a general trend, remains around 168 kJ/mol, with the exception of hemp, jute, and rice straw, which presented values, 180.9 kJ/mol, 183.1 kJ/mol, and 197.6 kJ/mol, respectively. According to the authors, the higher is activation energy, the higher is the biomass stability comparative to the others fibers.

Ounas et al. (2011) studied the thermal decomposition of sugarcane bagasse and olive residue from Morocco. The authors divided the kinetic results into two conversion sections from 0.00 to 0.50 and 0.50 to 0.80 concerning the hemicellulose and cellulose reactions, respectively. The activation energies for hemicellulose were between 168-180 kJ/mol and 153-162 kJ/mol, and for cellulose were between 168-180 kJ/mol and 153-162 kJ/mol, for sugarcane bagasse and olive residue, respectively.

The woody residues showed in Table 2.2, pine (Poletto et al., 2010; Anca-Couce et al., 2014), eucalyptus (Poletto et al., 2010), and poplar (Słopiecka et al., 2012), presented activation energy around of 155 kJ/mol, lower than the reported for fibers. The woody shell residues such as hazelnut husk (Ceylan & Topçu, 2014), Tucumã endocarp (Baroni et al., 2015), and Brazil nut woody shell (Rueda-Ordóñez et al., 2015) presented the lowest activation energy compared with the fibrous and woody biomasses, around 140 kJ/mol. Thus, summarizing the data presented in Table 4.1, the activation energies of biomass thermal decomposition in inert atmosphere using isoconversional methods remained between 150 kJ/mol and 200 kJ/mol.

2.4.2. Reaction model determination and master-plots application

During thermal decomposition, physical and chemical phenomena occur simultaneously, but usually, only one of these steps controls the overall kinetics (Vyazovkin

et al., 2011). Therefore, the form of the reaction model function should be suitable for this controlling step.

Several different functions for the reaction model of solid-state kinetics can be found elsewhere (Aboulkas & El Harfi, 2008; Lua & Su, 2006; Vlaev, Markovska, & Lyubchev, 2003; Vyazovkin et al., 2011). These functions present one of the four kinds of possible kinetic curve patterns (linear, accelerating, sigmoidal, and decelerating) (Vyazovkin et al., 2011), and can represent chemical reaction, random nucleation and nuclei growth, phase boundary reaction or diffusion phenomena (Vlaev et al., 2003).

According to White et al. (2011) when kinetic analysis is applied to biomass decomposition, reaction-order models are frequently used, due to their simplicity and closeness to relations that are valid for homogeneous kinetics. This consideration is valid for biomass thermal decomposition when non-isothermal data is analyzed since sigmoidal patterns, arise from the variation of temperature and degree of conversion (Vyazovkin et al., 2011). The reaction model is determined following the recommendations provided by the International Confederation of Thermal Analysis and Calorimetry (ICTAC). According to Vyazovkin et al. (2011) the use of master plots is the correct way to determine the reaction model showed in Table 2.3.

However, since its conception raised from the same definition of the isoconversional methods, the master plots emerged from the definition of the integrated solution of the conversion rate equation (equation 2.5).

In equation (2.9), the unknown pre-exponential factor is directly affected by the reaction model, $g(\alpha)$, and therefore, it is necessary to eliminate its influence. Thus, it is selected a conversion reference point ($\alpha=0.5$), and performed the ratio $g(\alpha)/g(0.5)$ as presented in equation (2.20), which represents the theoretical master plots. Also, the experimental master plots could be obtained from the ratio $p(x)/p(0.5)$.

$$g(\alpha) = \frac{AE}{\beta R} p(x) \quad (2.9)$$

$$\frac{g(\alpha)}{g(0.5)} = \frac{\frac{E_a A}{\beta R} p(x)}{\frac{E_a A}{\beta R} p(x_{0.5})} = \frac{p(x)}{p(x_{0.5})} \quad (2.20)$$

Table 2.3. Integral and differential form of several reaction models for solid-state kinetics
(adapted from Vyazovkin et al., 2011)

Reaction model	Code	$f(\alpha)^a$	$g(\alpha)^b$
Power law	P1	$4\alpha^{3/4}$	$\alpha^{1/4}$
Power law	P2	$3\alpha^{2/3}$	$\alpha^{1/3}$
Power law	P3	$2\alpha^{1/2}$	$\alpha^{1/2}$
Power law	P4	$2/3\alpha^{-1/2}$	$\alpha^{3/2}$
Phase-boundary Controlled reaction (contracting area)	R2	$2(1-\alpha)^{1/2}$	$[1-(1-\alpha)^{1/2}]$
Phase-boundary Controlled reaction (contracting volume)	R3	$3(1-\alpha)^{2/3}$	$[1-(1-\alpha)^{1/3}]$
Avrami Erofe'ev (m=2)	A2	$2(1-\alpha)[- \ln(1-\alpha)]^{1/2}$	$[- \ln(1-\alpha)]^{1/2}$
Avrami Erofe'ev (m=3)	A3	$3(1-\alpha)[- \ln(1-\alpha)]^{2/3}$	$[- \ln(1-\alpha)]^{1/3}$
Avrami Erofe'ev (m=4)	A4	$4(1-\alpha)[- \ln(1-\alpha)]^{3/4}$	$[- \ln(1-\alpha)]^{1/4}$
First order	F1	$(1-\alpha)$	$- \ln(1-\alpha)$
n th order	Fn	$(1-\alpha)^n$	$[1-(1-\alpha)^{(1-n)}]^{(1-n)}$
One-dimensional Diffusion	D1	$1/2\alpha$	α^2
Two-dimensional Diffusion	D2	$[- \ln(1-\alpha)]^{-1}$	$(1-\alpha)\ln(1-\alpha)+\alpha$
Valensi-Carter equation Three-dimensional Diffusion	D3	$(3/2)(1-\alpha)^{2/3}[1-(1-\alpha)^{1/3}]^{-1}$	$[1-(1-\alpha)^{1/3}]^2$
Jander equation Three-dimensional Diffusion	D4	$(3/2)[(1-\alpha)^{-1/3}-1]^{-1}$	$(1-2\alpha/3)-(1-\alpha)^{2/3}$
Ginstling-Brounshtein			

^aDifferential form, ^bIntegrated form

In order to obtain the reaction model which better describes the thermal decomposition reaction, the theoretical and experimental master plots are plotted as a function of conversion. Then, the model which better represents the experimental data at the different heating rates evaluated (at least three < 20 °C/min) is considered the suitable for the reaction description.

The solution of $p(x)$ function in equation (2.20) is recommended to be performed applying the 8th degree rational approximation developed by Pérez-Maqueda and Criado (2000), and presented in equation (2.21). The activation energy used to solve the $x=E/RT$ in

equation (2.21) is the average of the set of activation energies provided by the isoconversional method applied.

$$p(x) = \left(\frac{\exp(-x)}{x} \right) \left(\frac{x^7 + 70x^6 + 1886x^5 + 24920x^4 + \dots}{x^8 + 72x^7 + 2024x^6 + 28560x^5 + 216720x^4 + \dots} \right. \\ \left. \frac{\dots + 170136x^3 + 577584x^2 + 844560x + 357120}{\dots + 880320x^3 + 1794240x^2 + 1572480x + 403200} \right) \quad (2.21)$$

Pre-exponential factor determination

The pre-exponential factor determination is carried out as a forward step, with the knowledge of the reaction model, $f(\alpha)$. Therewith, rearranging equation (2.5) and plotting the values of $\ln[(d\alpha/dt)/f(\alpha)]$ as a function of $1/T$, it is obtained a straight line, in which the intercept represents $\ln A$, and with the slope is determined the final activation energy. This activation energy should not differ more than 10% from the values provided by the isoconversional method (Janković, 2008).

$$\ln \left[\frac{\left(\frac{d\alpha}{dt} \right)}{f(\alpha)} \right] = \ln A - \frac{E}{RT} \quad (2.22)$$

2.4.3. Consecutive reactions scheme

Fitting models are the most popular methods applied in solid–state kinetics investigations, mainly in non-isothermal experiments. Nonlinear least squares method is commonly used to fit biomass thermogravimetric and theoretical data, and to evaluate the Arrhenius parameters (White et al., 2011). Several numerical methods (e.g., Euler and Runge-Kutta) are frequently used to solve the conversion rate equation.

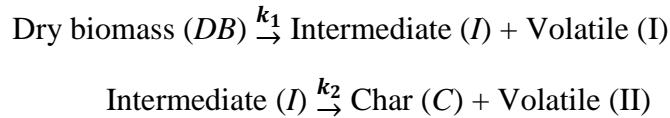
The kinetic parameters estimated are those which minimize the objective function (OF) given in equation (2.23). According to Órfão et al. (1999) the fit between the experimental and theoretical data can be determined by equation (2.24), in which N is the number of data points and $(d\alpha/dt)_{\max}$ is the highest experimental conversion rate. The best fit is obtained when the sum of the weighted squares of the residuals is at minimum, i.e., a value closer to zero,

presenting a smaller random error. The authors also stated that for a 95% confidence interval, a fit of 5% indicates there was a good agreement.

$$OF = \sum_{i=0}^N \left[\left(\frac{d\alpha}{dt} \right)_{i,exp} - \left(\frac{d\alpha}{dt} \right)_{i,calc} \right]^2 \quad (2.23)$$

$$Fit(\%) = \left[\frac{\sqrt{\frac{OF}{N}}}{\left(\frac{d\alpha}{dt} \right)_{e,max}} \right] 100 \quad (2.24)$$

In the analysis of biomass thermal decomposition is commonly applied a two-step consecutive reactions scheme (Guo & Lua, 2001; Chen et al., 2006; Luangkiattikhun et al., 2008; Weerachanchai et al., 2010) according to:



The application of the consecutive reactions scheme, for description of the thermal decomposition of biomass, is often done in terms of concentration instead of conversion as shown by Weerachanchai et al. (2010). Concentration is an amount of a species, element, substance, or reactant in a mixture, which could be measured in mass, volume, or percentage. Conversion is a dimensionless measurement (minimum 0 and maximum 1) of the reactant amount being readily converted in a determined product. The kinetic analysis through concentration facilitates the construction of the mathematical expression for the representative reactions, since they are interdependent, specially the intermediate reactant/product. In the kinetic analysis through conversion the intermediate reaction is difficult to analyze, because the intermediate product is rapidly formed while is also slowly decomposed, differently of the initial or final reactions, which are not dependent on any other reactions.

Based on these aspects, Weerachanchai et al. (2010) presented the mathematical expression of a scheme of two consecutive reactions represented by equations (2.25), (2.26), and (2.27). This scheme is commonly applied in the thermal decomposition of biomass, in

which $[DB]$, $[I]$, and $[C]$ are the concentrations of dry biomass, intermediate, and char, respectively.

$$\frac{d[DB]}{dt} = -(A_1) \left[\exp\left(\frac{-E_1}{RT}\right) \right] [DB] \quad (2.25)$$

$$\frac{d[I]}{dt} = (A_1) \left[\exp\left(\frac{-E_1}{RT}\right) \right] [DB] - (A_2) \left[\exp\left(\frac{-E_2}{RT}\right) \right] [I] \quad (2.26)$$

$$\frac{d[C]}{dt} = (A_2) \left[\exp\left(\frac{-E_2}{RT}\right) \right] [I] \quad (2.27)$$

The concentration rate of dry biomass (DB) is represented by equation (2.25), in which its thermal decomposition produces the intermediate product (I), and the negative signal in the right side represents the formation of I from DB . Equation (2.26) represents the concentration rate of the intermediate (I), in which the first right side term represents the formation of the intermediate from DB , and the second represents the formation of char (C) from the intermediate. The concentration rate of char (C) is described by equation (2.27), in which the intermediate is the unique precursor of the final carbonaceous residue.

2.4.4. Independent parallel reactions scheme

Considering the complexity of reactions that occur during biomass decomposition, researchers observed that is not possible to describe the entire phenomenon with a single reaction (Cai, Wu, Liu, & Huber, 2013; Grønli, Gábor & Di Blasi, 2002).

The independent parallel reactions scheme (IPRS) assumes that each component reacts independently of the others in a certain temperature range, and the summation of the individual conversion rates represents the whole biomass kinetic behavior. The components normally are hemicellulose, cellulose, and lignin. The IPRS (Figure 2.2) also considers that there are no secondary reactions between the gaseous products (v_i) and the char (S_i) formed (Cai et al., 2013). However, few studies also take into account a higher number of reactions, such as the work of Becidan et al. (2007) who evaluated the fitting quality of different

reaction orders and number of reactions, concluding that a four-reaction approach generates more accurate parameters.

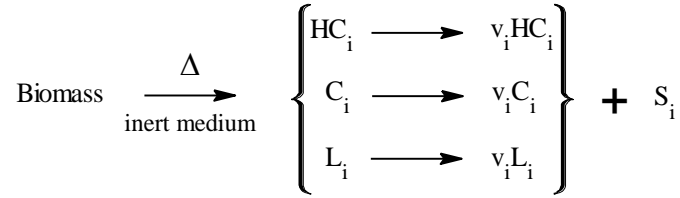


Figure 2.2. Independent parallel reactions scheme

The independent parallel reactions scheme is given by equation (2.28), in which F is the volatilized fraction related to each reaction, n is the number of reactions assumed ($i= 1, 2, 3, \dots, n$). The conversion rate $(d\alpha/dt)_i$ for each reaction is given by equation (2.5), and the differential reaction model is normally assumed as first order, $f(\alpha)=(1-\alpha)$.

$$\frac{d\alpha}{dt} = \sum_{i=0}^n F_i \left(\frac{d\alpha}{dt} \right)_i \quad (2.28)$$

The method of least squares is normally used to evaluate the kinetic parameters. Thus, the use of a scheme of three independent parallel reactions generates three sets of kinetic parameters (E_i , n_i , and k_i), which has been found to resemble the pure compounds activation energies (E) (Cardoso et al., 2011; Grønli et al., 2002; Orfão et al., 1999; Sánchez-Silva, López-González, Villaseñor, Sánchez, & Valverde, 2012; Vyazovkin et al., 2011).

However, it is important to emphasize that the use of a single heating rate is disapproved because it can generate inconsistent parameters. This fact is discussed by Anca-Couce et al. (2014) and White et al. (2011) that highlight the importance of using various heating rates in the kinetic estimations in order to satisfy an entire range of heating conditions.

In the IPRS, the overall biomass volatilized mass is accounted as the summation of volatile mass contributions of each biomass theoretical component (known as pseudo-component). These pseudo-component devolatilization reactions are commonly represented by one-step global reactions (Órfão et al., 1999). According to Liu et al. (2011) the interactions among components are different for each biomass, and their contributions in the overall biomass thermal decomposition are difficult to quantify. Consequently, biomass

pseudo-components and their contributions in the volatilized mass are considered for analysis in the IPRS. The common approach is considering three main pseudo-component reactions related to hemicellulose, cellulose and lignin.

The cellulose and hemicellulose reactions are commonly represented by a first order one-step global reaction, which is considered as a good first approach (Órfão et al., 1999; Antal & Várhegyi, 1995; Antal, Várhegyi, & Jakab, 1998; Lin et al., 2009), while lignin is normally represented by one-step global reaction with reaction order between 1 and 3 (Anca-Couce et al., 2014; Branca et al., 2005; Santos et al., 2012; Sun et al., 2011; Várhegyi et al., 1997).

Nevertheless, recently it has been clearly demonstrated that the cellulose pyrolysis reaction follows a more complex kinetic pathway and not a first order one-step global reaction (Capart et al., 2004; Mamleev et al., 2007; Sanchez-Jimenez et al., 2011; Sanchez-Jimenez et al., 2013). About this subject, Capart et al. (2004) have described the cellulose thermal decomposition through a scheme of two parallel reactions, each one described by the reaction model of nucleation. The authors validate their results by resembling ten different thermogravimetric curves at several heating rates. Mamleev et al. (2007) have proposed a multistep mechanism composed by two first-order competitive reactions, which provided a better description of cellulose thermal decomposition than the previously presented by Capart et al. (2004). Recently, some researchers (Sanchez-Jimenez et al., 2011; Sanchez-Jimenez et al., 2013) have demonstrated that cellulose thermal decomposition is better described by one-step reaction following the reaction model of random scission. This model (random scission) has described very well the auto-acceleration initial period (up to 40% of conversion), which the reaction model of first order was not able to describe. On the other hand, according to Di Blasi (2008), the hemicellulose reaction temperature range is between 200 °C and 300°C, cellulose between 250 °C and 350 °C, and lignin between 200 °C and 500 °C.

Figure 2.3 shows the logarithm of pre-exponential factor as a function of activation energy for the pseudo-components related to lignocellulosic biomass, obtained from investigations which applied IPRS (Anca-Couce et al., 2014; Barneto et al., 2010; Branca et al., 2005; Caballero et al., 1997; Grønli et al., 2002; Hu et al., 2007; Lira et al., 2010; Manara et al., 2015; Manyà et al., 2003; Naranjo et al., 2012; Órfão et al., 1999; Santos et al., 2012; Sun et al., 2011; Teng & Wei, 1998; Vamvuka et al., 2003).

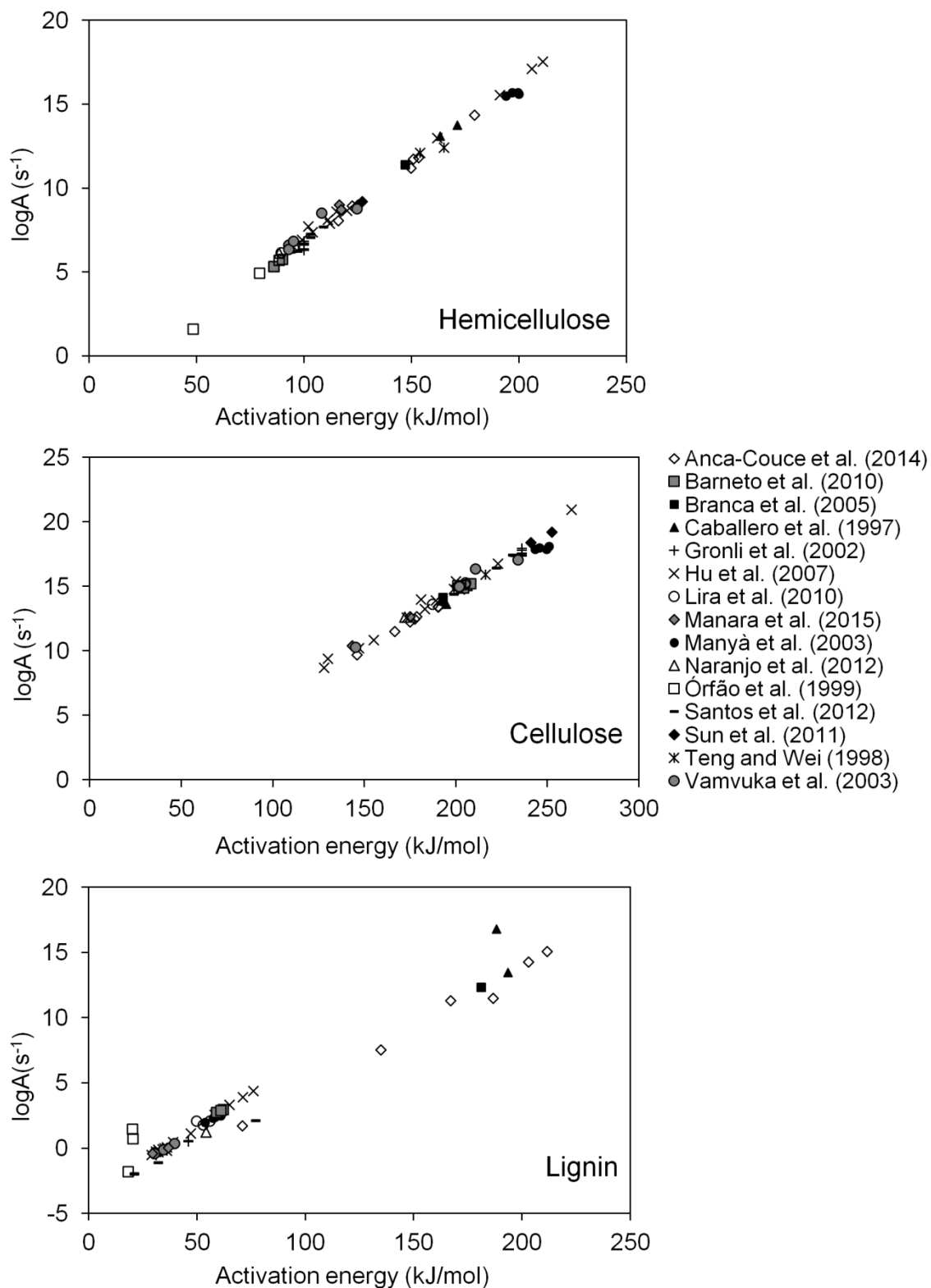


Figure 2.3. Logarithm of pre-exponential factor as a function of the activation energy of the main components of lignocellulosic biomass obtained by several researchers

In Figure 2.3 the activation energies concerning to the hemicellulose reaction were between 100 kJ/mol and 200 kJ/mol, corresponding to the pre-exponential factors from 1×10^6

to $1 \times 10^{10} \text{ s}^{-1}$. The activation energies related to the cellulose reaction were between 150 kJ/mol and 250 kJ/mol, related to the pre-exponential factors between $1 \times 10^{10} \text{ s}^{-1}$ and $1 \times 10^{20} \text{ s}^{-1}$. The range of variation of activation energies related to lignin reaction was lower than the observed for hemicellulose and cellulose, according to 30 kJ/mol – 80 kJ/mol related to the pre-exponential factors between 1 s^{-1} and $1 \times 10^5 \text{ s}^{-1}$.

Finally, in Figure 2.3 the logarithm of pre-exponential factors and the activation energies of each pseudo-component were linearly correlated. However, after determining the linear correlations, was verified that each pseudo-component correlation presented different slope, and the data were slightly scattered. This scatter effect was most significant in the kinetic parameters related to the lignin reaction, since lignin reaction have a broad decomposition temperature range which is not well defined compared with the other biomass components.

2.4.5. Distributed activation energy models

The distributed activation energy model (DAEM) was firstly presented by Anthony and Howard (1976) in order to evaluate the variation of activation energy (E) as a function of conversion in the thermal decomposition of solid fuels (biomass and coal). However, the mathematical approach was developed by Vand (1943) in the analysis of the irreversible electrical resistance changes. The DAEM concept emerged from the attempt to describe the coal thermal decomposition by a series of several first-order parallel reactions, which produced a set of several kinetic parameters. The mathematical formulation of the DAEM is presented in equation (2.29), in which the conversion (α) is expressed in terms of a distribution function of the activation energy, $f(E)$. Then, the derivative of conversion with respect of temperature ($d\alpha/dT$) can be described by equation (2.30).

$$\alpha = \int_0^{\infty} \left\{ 1 - \exp \left[- \int_{T_0}^T \frac{A}{\beta} \exp \left(\frac{-E}{RT} \right) dT \right] \right\} f(E) dE \quad (2.29)$$

$$\frac{d\alpha}{dT} = \int_0^{\infty} \left\{ \frac{A}{\beta} \exp \left[- \frac{E}{RT} - \int_{T_0}^T \frac{A}{\beta} \exp \left(\frac{-E}{RT} \right) dT \right] \right\} f(E) dE \quad (2.30)$$

In the DAEM the real distribution of activation energy is unknown. Nevertheless, according to Cai et al. (2013) is commonly used a Gaussian distribution in the analysis of the thermal decomposition of biomass and coal, presented in equation (2.31).

$$f(E) = \frac{1}{\sqrt{2\pi\sigma}} \exp\left[-\frac{(E - E_0)^2}{2\sigma^2}\right] \quad (2.31)$$

Although DAEM has been considered the most accurate to study thermal decomposition of different biomasses, the inclusion of the distributed profile generates mathematical complexities that are not observed in consecutive or parallel reactions schemes, for example (Várghegyi et al., 2009). Other disadvantages are the incapability of modeling the drying stages, and the complex or laborious mathematical manipulations that need to be applied (Cai et al., 2013; Chen, Zheng, & Zhu, 2013; Várghegyi et al., 2009). Among its advantages, DAEM avoids the underestimation of E , which is common when a global reaction scheme is used to adjust the temperature dependency (Di Blasi, 2008).

Considering all the reviewed models, numerous studies have employed multiple heating rates experiments for a three-step independent parallel reaction scheme, using different biomasses, heating rates, reaction mechanisms and temperature ranges. Other researches applied not only parallel reactions, but also DAEM, global reactions, and consecutive reactions schemes to estimate parameters such as activation energy (E) and pre-exponential factor (A). Some of these took into account biomass pseudo-components and reaction orders (n) higher than first-order. In order to exemplify the biomass pyrolysis kinetic, Table 2.4 shows a compendium of models, TGA conditions, and evaluated kinetic parameters made in the last five years. The investigations presented in Table 2.4 have been performed using nitrogen as analysis gas with the exception of the work of Sánchez-Silva et al. (2012), which used helium.

Regarding the evolution of the schemes, the global reaction model represented the first attempts to model biomass pyrolysis. It uses a linear regression method to evaluate the kinetic parameters (Vyazovkin et al., 2011). The consecutive reactions model accounts for multistep kinetics using the same principles involved in global reaction model (Várghegyi et al., 1994). However, the inherent specificity involved in the derivation of such schemes is not interesting from a practical point of view.

Table 2.4. Recent kinetics biomass studies considering TG conditions, modeling and parameters

Reference	TG conditions		Biomass	Model	Parameters	
	Sample mass	Heating rate			Temperature range	E (kJ/mol)
Becidan et al. (2007)	2.5-5 mg 5, 10 and 20 °C/min 23-600°C		Wood, coffee, and brewery grain wastes	1-step IPRS	76.0-206.0	2.5-16.4
				n-step IPRS	81.0-214.0	5.3-17.6
				3-step DAEM	175.0-236.0	12.6-20.9
Ye et al. (2010)	10 mg 10, 30 and 50 °C/min 25-800°C		Maize straw	KAS	130.1-156.0	14.2-23.7
				OFW	132.3-157.8	14.7-24.0
Cardoso et al. (2011)	6 mg 5, 10,15,20, 25,40, 50°C/min 100-900 °C		Tobacco waste Sorghum bagasse	Ozawa	77.7-132.0	-
					80.5-138.4	-
				n-step IPRS	39.7-272.0	5.2-36.8
Nascimento (2012)	2.5-10 mg 5, 10, 20, and 40°C/min 25-900 °C		Brazil nut woody shell		129.9-143.6	14.9-19.0
				Ozawa	96.6-150.2	11.7-21.7
			Sapucaia nut woody shell <i>Tucumã</i> endocarp		129.1-158.2	16.5-21.3
					131.3-138.9	15.4-20.1
				KS	135.1-142.9	17.5-20.8
	128.5-142.7	15.4-20.1				

Table 2.4. Recent kinetics biomass studies considering TGA conditions, modeling and parameters (continuation)

Reference	TGA conditions		Biomass	Model	Parameters			
	Sample mass	Heating rate			Temperature range	E (kJ/mol)	$\log A$ (s ⁻¹)	
Sánchez-Silva et al. (2012)	10 mg	5, 15, and 40 °C/min	25-900 °C	Fir wood	n-step IPRS	95.6-154.2	13.9-14.8	
						<i>Eucalyptus</i> bark	57.1-202.8	8.4-13.9
						Pine bark	91.4-166.4	12.90-14.0
						HC: 94.1-181.4	13.3-14.2	
						C: 191.3	14.54	
Pure components	L: 88.9-99.1	8.6-13.8						
Cai et al. (2013)	5 mg	10 and 20 °C/min	25-900 °C	Rice straw	3-step DAEM	HC: 187.3	13.1	
						C: 204.4	13.8	
						L: 242.6	15.9	
Anca-Couce et al. (2014)	3-20 mg	1, 2.5, 3, 5, 10,20, 80	25-500 °C	Four different beech woods	KAS	145.6-203.9	-	
						KS	127.0-313.9	-
					Three kinds of pine wood	n-step IPRS	HC: 122.5-153.4	8.1-14.4
							C: 178.6-190.2	9.7-13.5
						L: 70.8-203.0	1.7-15.1	
Ceylan and Topçu (2014)	10 mg	5, 10, and 20 °C/min	20-1000 °C	Hazelnut husk	KAS	95.0-162.0	4.8-22.8	
					OFW	102.5-161.5	5.4-22.9	

Differently from other schemes, IPRS relates to the composition of the biomass and requires the use of non-linear regression methods with initial assumptions to perform evaluations. This method is mathematically more complex but shows great improvements in the fitting quality of biomass kinetics, providing a better understanding of the process in a microscopic scale (Anca-Couce et al., 2014). The DAEM can be seen as an extension of IPRS, where E is considered to be represented by a continuous distribution of activation energies, involving the application of extremely complex methods to optimize the kinetic parameters (Cai et al., 2013)

CHAPTER 3

MATERIALS AND METHODS

In this chapter are presented the raw material, experimental set-up used to carried out the thermal decomposition analyses in inert and oxidative atmospheres, the standards used to obtain the thermal, chemical and physical characteristics of the biomass, and finally, the mathematical methodologies to obtain the kinetics parameters through four methods.

3.1. Biomass analyzed

In this work, sugarcane straw (*Saccharum officinarum* Linnaeus) was used as raw material, which was mainly composed by dry leaves. The biomass was ground (batches of 10 g in 20 s) in a hammer mill (Tigre S.A., CV2, Brazil) coupled to an induction motor of 3800 rpm, CV5 (General Electric, 25.4062.405, Brazil). Then, was separated by sieving using 28- and 35-mesh Tyler standard sieves (Granutest sieves, Brazil) and obtained the mean diameter between sieves of 510 μm . After that, a rotary cone sample divider (model laborette 27, Fritsch, Germany) was utilized to obtain a representative sample to apply in the thermogravimetric analysis.

3.1.1. Sample characterization

The sample characterization was divided into four analyses: proximate, ultimate, heating value, and chemical composition.

The proximate analysis was performed using the following standards: moisture content (ASTM E871–82), Ash content (ASTM E1755–01), volatile content (ASTM E872–82), and fixed carbon obtained by difference on a dry-basis.

The elemental analysis (CHN-O) was done using an elemental analyzer (Perkin Elmer, Series II 2400, USA), and the oxygen content was determined by difference on a dry and ash free basis.

The higher heating value (HHV) was determined using an oxygen bomb calorimeter (IKA, C200, Germany), applying the standard ASTM D240-09. The lower heating value (LHV) in kJ/kg was determined using equation (3.1), in which X_H and X_M are the percentages of hydrogen and moisture contents in the biomass, respectively (Bizzo & Sánchez, 2010).

However, due to its importance in characterization of solid fuels, there are other approaches to determine the LHV (Appendix A), which are proposed by the American Petroleum Institute (API), the Mendeleev's equation, and by the Intergovernmental Panel on Climate Change (IPCC). Therefore, in order to compare the LHV, equation (3.1), Appendix A show the results determined through the API, IPCC, and Mendeleev's approaches.

$$LHV = \left\{ \left[1 - \left(\frac{X_M}{100} \right) \right] \left[HHV - 9 \left(\frac{X_H}{100} \right) 2440 \right] \right\} - \left(\frac{X_M}{100} \right) 2440 \quad (3.1)$$

The method of Van Soest (Van Soest, Robertson & Lewis, 1991), for obtaining the neutral detergent fiber, was applied concerning to the fractions of hemicellulose and cellulose. The experimental procedure applied was the same of the association of official analytical chemist (AOAC), 17th edition (Horwitz, 2000). The lignin content in the sample was determined by the Klason's method based on acid hydrolysis (Sluiter, Hames, Ruiz, Scarlata, Sluiter, Templeton, & Crocker, 2012).

3.2. Experimental Set-up

3.2.1. Thermogravimetric analyzer

The thermal decomposition experiments were performed with a thermogravimetric analyzer from Shimadzu Corporation (TGA-50, Japan), with sample mass measuring resolution of 0.001 mg.

Thermal decomposition in nitrogen atmosphere

The samples were installed in an open sample platinum pan (6 mm internal diameter and 2.5 mm depth) with initial mass of 3.0 ± 0.2 mg. The temperature was controlled from room temperature (25 ± 3 °C) up to 900 °C at seven heating rates, 1.25 °C/min, 2.5 °C/min, 5

°C/min, 10 °C/min, 15 °C/min, 20 °C/min, and 40 °C/min. The International Confederation of Thermal Analysis and Calorimetry (ICTAC) since 2011 (Vyazovkin et al., 2011) recommend the use of at least three temperature ramps lower than 20 °C/min to perform kinetic analysis from thermogravimetry. The heating rate of 40 °C/min was selected in order to evaluate the transport phenomena effects which affect the thermogravimetric curves, and consequently the kinetic parameters. The acquisition rate of sample mass was 12 sample/min corresponding to a step of 5 s. Inert gas of high purity ($N_2=99.996\%$, 4.6 FID, White Martins, Campinas, Brazil) with flow rate of 50 mL/min was used.

Thermal decomposition in synthetic air atmosphere

Synthetic air (White Martins, $X_{\text{oxygen}}=20.00\pm 0.05\%$ e $X_{\text{nitrogen}}=80.00\pm 0.05\%$) at a flow rate of 50 mL/min was used as oxidizing atmosphere. The temperature was measured from room temperature (24.03 ± 2.44 °C) to 900 °C using heating rates (β) of 2.5°C/min, 5 °C/min and 10 °C/min, and acquisition rate of 12 samples per min. The sample was placed in an alumina pan (volume = 8 μ L), using initial mass of 3.121 ± 0.273 mg for each run.

3.2.2. Differential scanning calorimetric analyzer

The determination of the heat of reaction was carried out from heat flux (Q_{DSC}) data using differential scanning calorimetry equipment (Shimadzu, model DSC-50, Japan). The temperature was measured from room temperature (23.38 ± 0.10 °C) to 600 °C using the same heating rates, flow rate, oxidizing gas, and acquisition rate applied in the TG analysis (section 3.2.1. *Thermogravimetric analyzer*). The sample was placed in an aluminum crucible (6×1.5 mm) with pierced lid (1 mm) using initial mass of 3.14 ± 0.14 mg for each run.

3.3. Data Analysis

The thermal decomposition analysis and kinetic modeling were carried out using the software MS Office Excel 2007 (version12.0.6683.5002). The experimental data obtained from thermogravimetry (TG) and their derivatives (DTG) were normalized according to equation (3.2) and equation (3.3), respectively. This step was necessary in order to make a reliable comparison among curves at different heating rates. In equation (3.2), w represents

the normalized mass, m the mass for each time, and m_i the initial mass. The normalized DTG is represented by dw/dt in Eq. (3.3), and dm/dt is the experimental DTG in mg/s.

$$W = \frac{m}{m_i} \quad (3.2)$$

$$\frac{dW}{dt} = \frac{dm}{dt} \frac{1}{m_i} \quad (3.3)$$

For the kinetic analysis, the experimental conversion (α_e) and experimental conversion rate $(d\alpha/dt)_e$ were determined through equation (3.4) and equation (3.5), respectively. In equation (3.4) and equation (3.5), w_i , w and w_f represent the normalized mass at the beginning of the analysis (after drying, 150 °C), at a given temperature, and in the final decomposition, respectively.

$$\alpha_e = \frac{w_i - w}{w_i - w_f} \quad (3.4)$$

$$\left(\frac{d\alpha}{dt}\right)_e = -\frac{dw}{dt} \left(\frac{1}{w_i - w_f}\right) \quad (3.5)$$

The theoretical conversion rate $(d\alpha/dt)_{theoretical}$ is given by equation (3.7), in which E is the activation energy, A is the pre-exponential factor, R is the universal gas constant (8.314 J/mol K), and T is the absolute temperature. The detailed procedure is presented in Appendix B.

$$k = A \left[\exp\left(\frac{-E}{RT}\right) \right] \quad (3.6)$$

$$\left(\frac{d\alpha}{dt}\right)_{theoretical} = [f(\alpha)]k = [f(\alpha)]A \left[\exp\left(\frac{-E}{RT}\right) \right] \quad (3.7)$$

3.4. Isoconversional Methods

The kinetic analysis of the thermal decomposition reaction was done applying the isoconversional methods of Friedman (1965) in inert atmosphere, and Vyazovkin (1997) in

oxidative atmosphere. In the application of the isoconversional methods, the conversion was evaluated from 0.05 to 0.95 with a step of 0.05, resulting in 19 conversion levels, and for each one was measured a value of $(d\alpha/dt)_e$ obtained by equation (3.5) and its temperature associated at each heating rate. The procedure is presented in Appendix C.

3.4.1. Method of Friedman

The method developed by Friedman (1964) solves equation (3.7) using natural logarithm, as presented in equation (3.8). After that, it was plotted for each heating rate the value of $\ln(d\alpha/dt)$ as a function of the $1/T$, resulting in a straight line for each conversion, then the slopes are multiplied by the universal gas constant (R) to obtain the activation energies.

$$\ln\left(\frac{d\alpha}{dt}\right) = \ln A + \ln f(\alpha) - \left(\frac{E}{RT}\right) \quad (3.8)$$

3.4.2. Method of Vyazovkin

The isoconversional method of Vyazovkin (Vyazovkin, 1997) is presented in equation (3.9), in which the function $I(E_\alpha, T_\alpha) = (E_\alpha / R)[p(x)]$ for each conversion level. Thus, the E_α value which provides the minimum in the summation is the activation energy for that conversion level.

$$\sum_i^n \sum_{i \neq j}^n \frac{I(E_\alpha, T_\alpha)_i \beta_j}{I(E_\alpha, T_\alpha)_j \beta_i} = \min \quad (3.9)$$

The $p(x)$ approximate solution was carried out applying the 8th degree rational approximation presented in equation (3.10) according to Pérez-Maqueda and Criado (2000).

$$p(x) = \left(\frac{\exp(-x)}{x}\right) \left(\frac{x^7 + 70x^6 + 1886x^5 + 24920x^4 + \dots}{x^8 + 72x^7 + 2024x^6 + 28560x^5 + 216720x^4 + \dots} \right. \\ \left. \frac{\dots + 170136x^3 + 577584x^2 + 844560x + 357120}{\dots + 880320x^3 + 1794240x^2 + 1572480x + 403200} \right) \quad (3.10)$$

Assuming $\beta_1=2.5$ °C/min, $\beta_2=5$ °C/min, $\beta_3=10$ °C/min, and introducing them in equation (3.9), it was obtained equation (3.11). The Vyazovkin method was applied following equation (3.11) for each conversion level evaluated. The solution of equation (3.11) was carried out with the MS Excel optimization tool SOLVER.

$$\begin{aligned} & \frac{[I(E_\alpha, T_\alpha)_{\beta_1}]\beta_2}{[I(E_\alpha, T_\alpha)_{\beta_2}]\beta_1} + \frac{[I(E_\alpha, T_\alpha)_{\beta_1}]\beta_3}{[I(E_\alpha, T_\alpha)_{\beta_3}]\beta_1} + \frac{[I(E_\alpha, T_\alpha)_{\beta_2}]\beta_1}{[I(E_\alpha, T_\alpha)_{\beta_1}]\beta_2} + \frac{[I(E_\alpha, T_\alpha)_{\beta_2}]\beta_3}{[I(E_\alpha, T_\alpha)_{\beta_3}]\beta_2} + \dots \\ & \dots + \frac{[I(E_\alpha, T_\alpha)_{\beta_3}]\beta_1}{[I(E_\alpha, T_\alpha)_{\beta_1}]\beta_3} + \frac{[I(E_\alpha, T_\alpha)_{\beta_3}]\beta_2}{[I(E_\alpha, T_\alpha)_{\beta_2}]\beta_3} = \min \end{aligned} \quad (3.11)$$

3.4.3. Application of isoconversional methods

Figures 3.1 and 3.2 present the procedure adopted to obtain the kinetic parameters using the isoconversional methods of Ozawa-Flynn-Wall (Ozawa, 1965, Flynn & Wall, 1966), Coats-Redfern modified (Braun et al., 1991), and Friedman (Friedman, 1964). There are several considerations to be taken into account in the application of these methods (section 2.4.1. *Isoconversional methods or Model-free methods*), such as the use of at least three heating rates lower than 20 °C/min and the correct selection of the temperature/mass range in the TG curves. Nonetheless, with the intention of facilitate the understanding to beginners in the field, it was constructed a flowchart with the step-by-step to obtain accurate and reliable results.

In Figure 3.1(a) is presented a flowchart of the experimental data selection for the application of isoconversional methods. The first step correspond to the normalization of the TG/DTG data applying equations (2.1) and (2.2) transforming the units from mg and mg/s to adimensional data and s^{-1} , respectively, in order to facilitate the comparison among heating rates. The second step was the selection of the temperature/mass range in the TG curves to be analyze, and then, the calculation of the conversion (α) and conversion rate (da/dt) from the normalized data. Finally, were selected the temperatures related to each conversion, from 0,05 to 0,95, with step of 0,05 or less.

Figure 3.1(b) presents the conversion as a function of temperature for several heating rates (β) and a graphical procedure of selection of the experimental temperatures related to each conversion level. Fig. 3.1(c) shows the organization of the data for each heating rate, and

the last step corresponds to the selection of the isoconversional method to be applied. This schematic flowchart could be applied for all the isoconversional methods in literature, since they use the same experimental data.

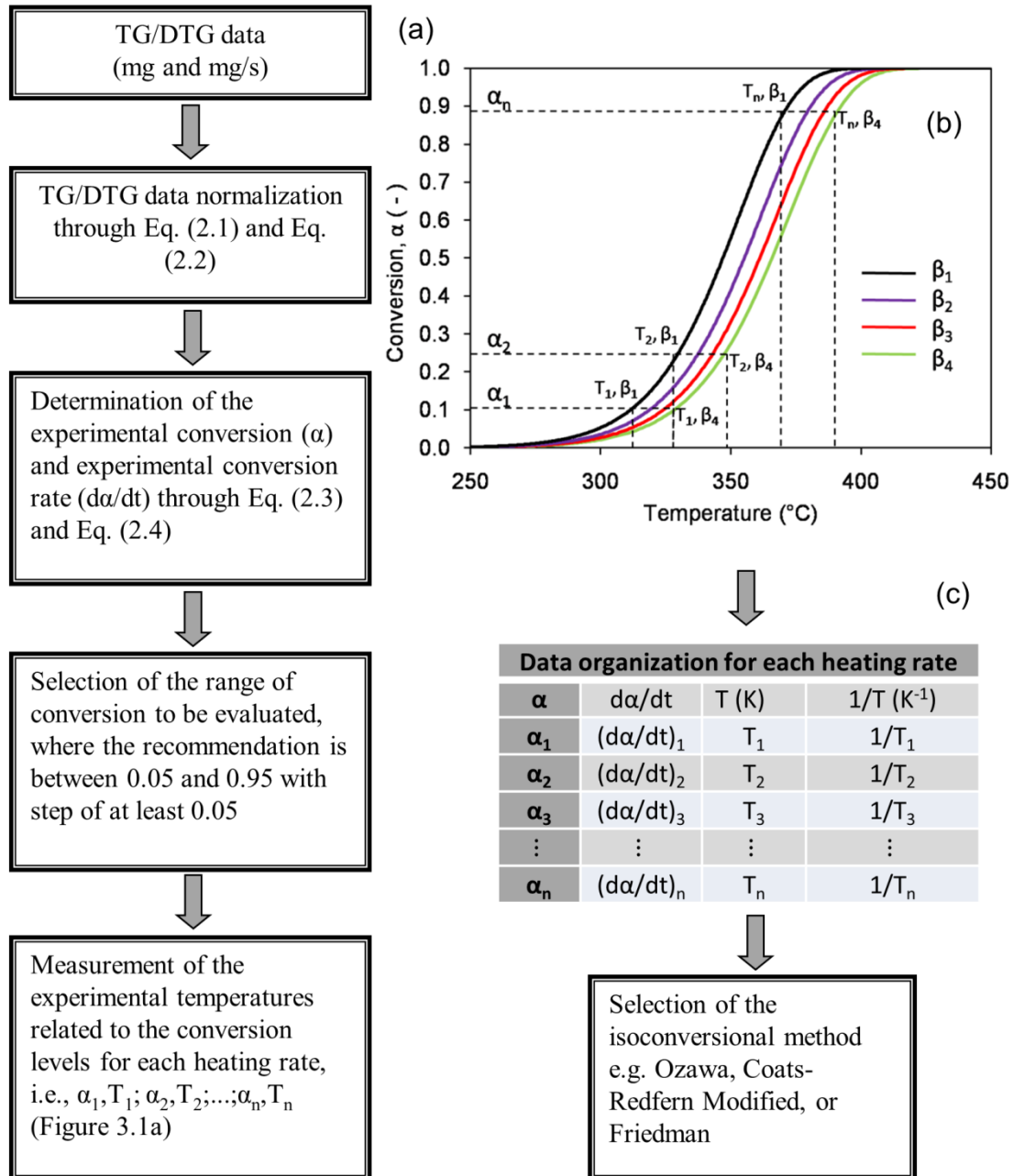


Figure 3.1. (a) Flowchart exemplifying the data selection for the application of isoconversional methods. (b) Conversion as a function of temperature for several heating rates. (c) Data organization for each heating rate

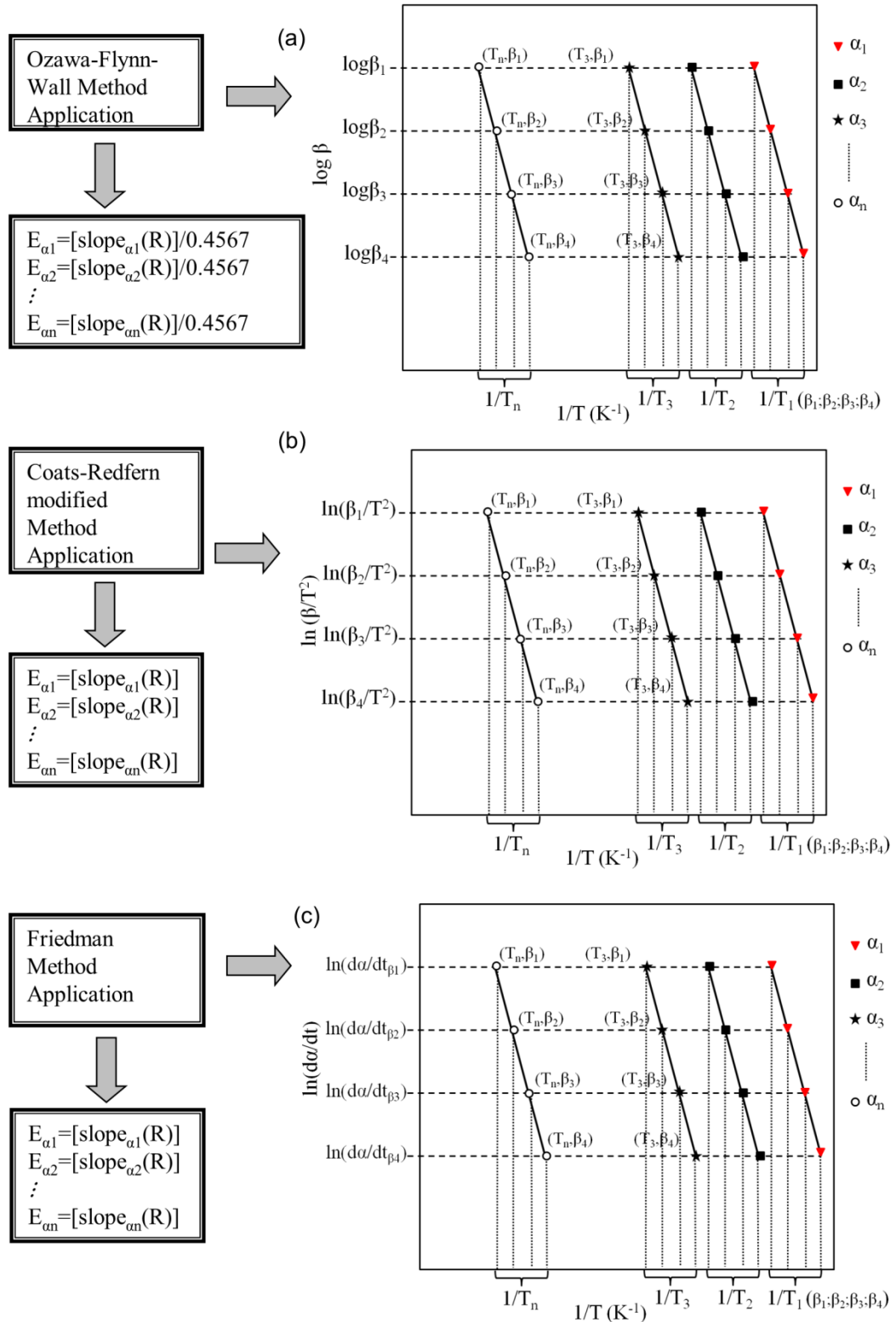


Figure 3.2. Flowchart of the determination of the activation energy through isoconversional methods. (a) Ozawa-Flynn-Wall, (b) Coats-Redfern modified, and (c) Friedman methods

Figure 3.2 presents a flowchart of the determination of activation energy through isoconversional methods. Figure 3.2(a) presents the application of the Ozawa-Flynn-Wall method (Ozawa, 1965, Flynn & Wall, 1966). In this method, for each conversion level, a straight line is formed by plotting the logarithm of each heating rate (β) as a function of the inverse of the absolute temperature, in which the slope multiplied by a constant provided the activation energy related to the conversion level selected.

In Figure 3.2(b) is presented the application of the Coats-Redfern modified method (Braun et al., 1991). The activation energy in this method was obtained by the multiplication of the slope of a straight line by the gas universal constant (R). The straight line is formed by the plot of the natural logarithm of the ratio β/T^2 as a function of the inverse of the absolute temperature for each conversion level analysed.

Figure 3.2(c) presents the methodology to apply the Friedman method (Friedman, 1964), in which the plot of the natural logarithm of the conversion rate as a function of the inverse of the absolute temperature forms a straight line. The activation energy for each conversion level was determined by the multiplication of the slope of the straight line with the gas universal constant (R).

3.4.4. Reaction model determination

The reaction model was determined following the recommendations provided by the International Confederation of Thermal Analysis and Calorimetry (ICTAC). According to Vyazovkin et al. (2011) the use of master plots is the correct way to determine the reaction model as presented in equation (3.12), in which $p(x)$ was solved as presented previously (section 3.4.4. *Method of Vyazovkin*).

$$\frac{g(\alpha)}{g(0.5)} = \frac{\frac{E_a A}{\beta R} p(x)}{\frac{E_a A}{\beta R} p(x_{0.5})} = \frac{p(x)}{p(x_{0.5})} \quad (3.12)$$

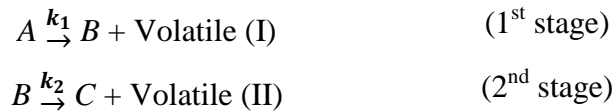
3.4.5. Pre-exponential factor determination

The determination of the pre-exponential factor was carried out as a last step, with the knowledge of the reaction model, $f(\alpha)$. Therewith, rearranging equation (3.13) and plotting the values of $\ln[(d\alpha/dt)/f(\alpha)]$ as a function of $1/T$, it was obtained a straight line, in which the intercept represents $\ln A$, and with the slope is determined the final activation energy. This activation energy should not differ more than 10% from the values provided by the Friedman's isoconversional method (Janković, 2008).

$$\ln \left[\frac{\left(\frac{d\alpha}{dt} \right)}{f(\alpha)} \right] = \ln A - \frac{E}{RT} \quad (3.13)$$

3.5. Consecutive Reactions Scheme

The consecutive reactions scheme was applied by two approaches. The first approach as recommended in literature (Guo & Lua, 2001; Chen et al., 2006; Luangkiattikhun et al., 2008; Weerachanchai et al., 2010), assuming two consecutive reactions, represented by the following scheme:



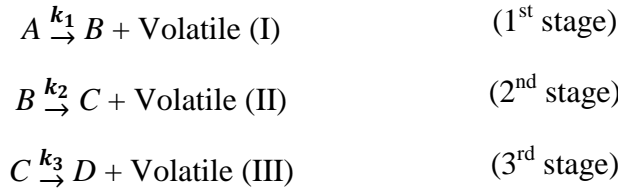
In the first approach, the reactant A was analyzed as dry biomass, which produces the solid product B through the first reaction with pre-exponential factor and activation energy, A_1 , E_1 , respectively. This product B was assumed as torrifed biomass, which is an intermediate state of the thermal decomposition process. This solid B decomposed slowly forming the final carbonaceous solid, C , at the end of the process through the second reaction, with pre-exponential factor A_2 and activation energy E_2 . Equations (3.14) to (3.16) describe mathematically the two consecutive reactions scheme.

$$\frac{d[A]}{dt} = -(A_1) \left[\exp \left(\frac{-E_1}{RT} \right) \right] [A] \quad (3.14)$$

$$\frac{d[B]}{dt} = (A_1) \left[\exp\left(\frac{-E_1}{RT}\right) \right] [A] - (A_2) \left[\exp\left(\frac{-E_2}{RT}\right) \right] [B] \quad (3.15)$$

$$\frac{d[C]}{dt} = (A_2) \left[\exp\left(\frac{-E_2}{RT}\right) \right] [B] \quad (3.16)$$

The second approach was constituted by three consecutive reactions, represented by the next scheme:



The first and the second reaction follow the same the first approach. The third reaction with pre-exponential factor A_3 and activation energy E_3 , represent the final volatile release from the carbonaceous solid (C) to obtain the final solid residue at 900°C (D), being the slowest step, and taking place at high temperatures ($>400^\circ\text{C}$). The mathematical description of the three consecutive reactions scheme is presented in equations (3.17) to (3.20).

$$\frac{d[A]}{dt} = -(A_1) \left[\exp\left(\frac{-E_1}{RT}\right) \right] [A] \quad (3.17)$$

$$\frac{d[B]}{dt} = (A_1) \left[\exp\left(\frac{-E_1}{RT}\right) \right] [A] - (A_2) \left[\exp\left(\frac{-E_2}{RT}\right) \right] [B] \quad (3.18)$$

$$\frac{d[C]}{dt} = (A_2) \left[\exp\left(\frac{-E_2}{RT}\right) \right] [B] - (A_3) \left[\exp\left(\frac{-E_3}{RT}\right) \right] [C] \quad (3.19)$$

$$\frac{d[D]}{dt} = (A_3) \left[\exp\left(\frac{-E_3}{RT}\right) \right] [C] \quad (3.20)$$

In oxidative atmosphere, the first and second steps were assumed as similar to the presented for inert atmosphere, related to the oxidative pyrolysis. However, the third reaction

(formation of the final residue D) was related to the combustion of the carbonaceous solid producing the final solid residue, mainly composed by mineral matter (ash). The concentration of each reactant considering equations (3.14) to (3.20) were $[A]$, $[B]$, $[C]$, and $[D]$ corresponding to dry biomass, torrefied biomass, carbonaceous solid, and final solid residual at 900°C , respectively.

For solution of equations (3.14) to (3.20), the initial conditions were at $T=T_0$ and $t=0$, $[A]=1$, $[B]=0$, $[C]=0$, and $[D]=0$. The initial kinetic parameters of the approaches (E_1 , E_2 , E_3 , A_1 , A_2 , and A_3) were obtained with the isoconversional methods of Friedman (nitrogen) and Vyazovkin (synthetic air), and the reaction model selected was first order reaction. The determination of the theoretical concentration and the kinetic parameters of both approaches (E_1 , E_2 , E_3 , A_1 , A_2 , and A_3) was carried out applying the fourth order Runge-Kutta method, and the modeled curve was fitted to the experimental data with the least squares method, Eq. (3.21). The quality of fit (lower than 3%) was determined with the average deviation (AD) presented in Eq. (3.22), in which $(d\alpha/dt)_{e,max}$ is the maximum experimental conversion rate, and N the data points (7499, 3597, 1798, and 898 for 1.25, 2.5, 5, and $10^{\circ}\text{C}/\text{min}$, respectively).

$$RSS = \sum_{i=0}^N \left[\left(\frac{d\alpha}{dt} \right)_{i,e} - \left(\frac{d\alpha}{dt} \right)_{i,t} \right]^2 \quad (3.21)$$

$$AD(\%) = \left[\frac{\sqrt{\frac{RSS}{N}}}{\left(\frac{d\alpha}{dt} \right)_{e,max}} \right] 100 \quad (3.22)$$

In equation (3.21), the least squares method is based on the comparison of the experimental and theoretical conversion rates, and the consecutive reactions scheme is in terms of concentration rate. Then, it is necessary to convert the concentration and concentration rate in terms of conversion (α) and conversion rate (da/dt). For that, firstly was determined the theoretical normalized mass by equation (3.23) and its derivative by equation (3.24), in which a_1 , a_2 , a_3 , and a_4 are stoichiometric constants representing the quantities of each component assumed, as presented in Figure 3.3.

$$W = a_1[A] + a_2[B] + a_3[C] + a_4[D] \quad (3.23)$$

$$\frac{dW}{dt} = a_1 \frac{d[A]}{dt} + a_2 \frac{d[B]}{dt} + a_3 \frac{d[C]}{dt} + a_4 \frac{d[D]}{dt} \quad (3.24)$$

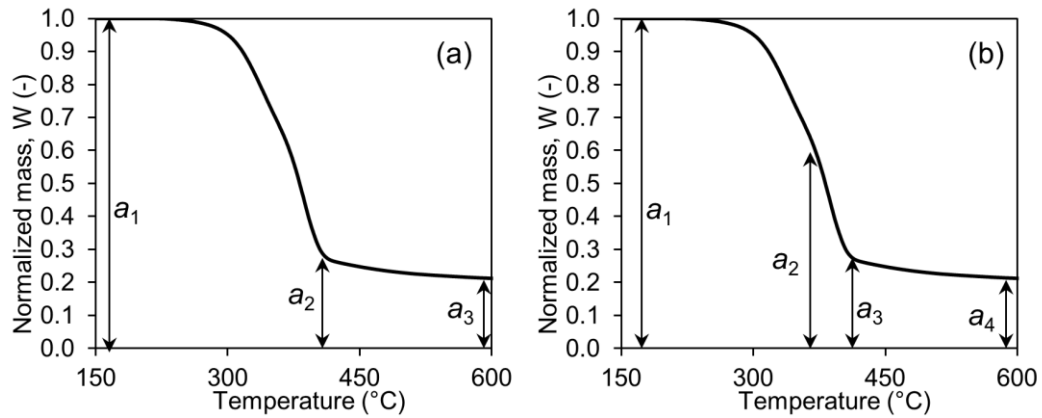


Figure 3.3. Schematic of normalized mass as a function of temperature in inert gas.

(a) Two consecutive reactions scheme. (b) Three consecutive reactions scheme

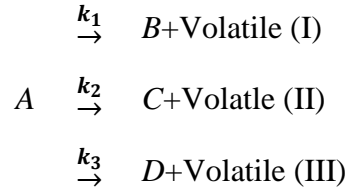
The methodology applied to determine the final kinetic parameters in a consecutive reactions scheme and the mathematical procedure applying software MS Office Excel 2007 (version 12.0.6683.5002) is presented in Appendix D.

3.6. Independent Parallel Reactions Scheme

The independent parallel reactions scheme is given by equation (3.25), in which F is the volatilized fraction related to each reaction, n is the number of reactions analyzed ($i= 1, 2, 3, \dots, n$). The conversion rate $(d\alpha/dt)_i$ for each reaction is given by Eq. (3.7), and the differential reaction model was first order, $f(\alpha)=(1-\alpha)$.

$$\frac{d\alpha}{dt} = \sum_{i=1}^n F_i \left(\frac{d\alpha}{dt} \right)_i \quad (3.25)$$

In inert atmosphere (nitrogen), the thermal decomposition of sugarcane straw was analyzed through a scheme of three independent parallel reactions, which from the reaction of A produce solid fractions represented by B , C , and D and also volatile fractions (I, II, and III), as presented in the following scheme:



The mathematical representation of the scheme of parallel reactions was composed by equations (3.26) to (3.29). Equation (3.26) presents the concentration rate of A, composed by the summation of the three Arrhenius constants k_1 , k_2 , and k_3 . The negative sign means that from A, the products B, C, and D and their volatiles are formed.

$$\frac{d[A]}{dt} = -(k_1 + k_2 + k_3)[A] \quad (3.26)$$

$$\frac{d[B]}{dt} = k_1[A] \quad (3.27)$$

$$\frac{d[C]}{dt} = k_2[A] \quad (3.28)$$

$$\frac{d[D]}{dt} = k_3[A] \quad (3.29)$$

The reactant A was analyzed as dry biomass composed by the three main biomass components, according to: hemicellulose (HC), cellulose (C), and lignin (L) as shown in equation (3.30), in which X_i represents each fraction in A (three fractions) detailed in equations (3.31) to (3.33), F_i and F_i^* are the fractions of volatilized and solid products, respectively.

$$[A]=[HC]+[C]+[L]=X_1[A]+X_2[A]+X_3[A] \quad (3.30)$$

$$X_1=F_{1(\text{volatile I})}+F_{1^*(\text{solid B})} \quad (3.31)$$

$$X_2=F_{2(\text{volatile I})}+F_{2^*(\text{solid C})} \quad (3.32)$$

$$X_3=F_{3(\text{volatile I})}+F_{3^*(\text{solid D})} \quad (3.33)$$

In order to perform the kinetic analysis in terms of conversion, equations (3.26) to (3.29) were rearranged to obtain equations (3.34) to (3.37). For that, firstly the concentration [A] was replaced by a conversion function based on the reaction model of first order, $f(\alpha)=(1-\alpha)$. Afterwards, using the composition of A presented in equation (3.30) and their fractions, equations (3.30) to (3.33), were finally obtained equations (3.34) to (3.37). The modeled

curve was fitted to the experimental data with the least squares method, Eq. (3.21). The quality of fit was determined with the average deviation (AD) presented in Eq. (3.22), as presented in the consecutive reactions scheme application (section 3.5).

$$\left(\frac{d\alpha}{dt}\right)_A = k_1[f(\alpha)]_1F_1 + k_2[f(\alpha)]_2F_2 + k_3[f(\alpha)]_3F_3 \quad (3.34)$$

$$\left(\frac{d\alpha}{dt}\right)_{HC} = k_1[f(\alpha)]_1F_1 \quad (3.35)$$

$$\left(\frac{d\alpha}{dt}\right)_c = k_2[f(\alpha)]_2F_2 \quad (3.36)$$

$$\left(\frac{d\alpha}{dt}\right)_L = k_3[f(\alpha)]_3F_3 \quad (3.37)$$

$$k_n = A_n \exp\left(\frac{E_n}{RT}\right) \quad (3.38)$$

Equation (3.38) represents the Arrhenius constant (k), in which $n=1, 2$, and 3 , depending on the reaction evaluated. The determination of the theoretical conversion was carried out applying the fourth order Runge-Kutta method, presented in its standard form in equations (3.39) to (3.43).

$$y_{n+1} = y_n + \frac{1}{6}(K_1 + K_2 + K_3 + K_4) \quad (3.39)$$

$$K_1 = h[f(x_n; y_n)] \quad (3.40)$$

$$K_2 = h\left\{f\left[x_{\left(n+\frac{h}{2}\right)}; y_{\left(n+\frac{h}{2}K_1\right)}\right]\right\} \quad (3.41)$$

$$K_3 = h\left\{f\left[x_{\left(n+\frac{h}{2}\right)}; y_{\left(n+\frac{h}{2}K_2\right)}\right]\right\} \quad (3.42)$$

$$K_4 = h\{f[x_{(n+h)}; y_{(n+hK_3)}]\} \quad (3.43)$$

The conversion rate, equation (3.44), was solved through the fourth order Runge-Kutta method applying equations (3.45) to (3.49), in which $y=\alpha$ and $x=t$, and the initial conditions were, step $h=5$ s, time $t_0=0$ s and $t=t_0+h$, temperature $T_0=150$ °C, and $\alpha_0=0$.

$$f(x, y) = \frac{d\alpha}{dt} = (1 - \alpha_i)A \exp\left[\frac{-E}{R(T_0 + \beta t_i)}\right] \quad (3.44)$$

$$K_1 = h(1 - \alpha_i) \left\{ A \exp \left[\frac{-E}{R(T_0 + \beta t_i)} \right] \right\} \quad (3.45)$$

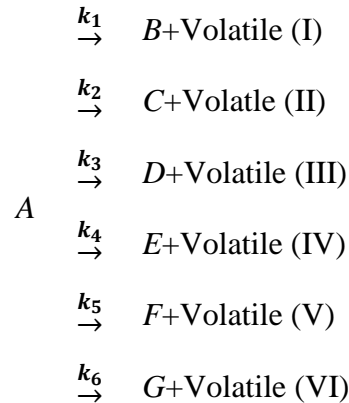
$$K_2 = h \left[1 - \left(\alpha_i + \frac{h}{2} K_1 \right) \right] \left\{ A \exp \left[\frac{-E}{R \left(T_0 + \beta \left(t_i + \frac{h}{2} \right) \right)} \right] \right\} \quad (3.46)$$

$$K_3 = h \left[1 - \left(\alpha_i + \frac{h}{2} K_2 \right) \right] \left\{ A \exp \left[\frac{-E}{R \left(T_0 + \beta \left(t_i + \frac{h}{2} \right) \right)} \right] \right\} \quad (3.47)$$

$$K_4 = h \left[1 - (\alpha_i + h K_3) \right] \left\{ A \exp \left[\frac{-E}{R(T_0 + \beta(t_i + h))} \right] \right\} \quad (3.48)$$

$$\alpha_{i+1} = \alpha_i + \left(\frac{K_1 + K_2 + K_3 + K_4}{6} \right) \quad (3.49)$$

In oxidative atmosphere (synthetic air), the thermal decomposition of sugarcane straw was analyzed through a scheme of six independent parallel reactions, in which the reaction of A produce solid fractions represented by B, C, D, E, F and G, and also volatile fractions (I, II, III, IV, V and VI) according to the following scheme:



The mathematical representation of the scheme of parallel reactions was done following the same methodology used previously in the inert atmosphere analysis, however adding three more reactions.

3.2. Heat of Reaction

The heat of reaction was determined using data from differential scanning calorimetry (DSC) and conversion (α) determined from TG/DTG. According to Rath et al. (2003), the heat flux required for heating the biomass sample (Q_S) without considering the heat of reaction is calculated using equation (3.50), in which m_0 is the dry sample mass (150 °C), m_c is the sample mass at the end of the analysis (600 °C), and the heat capacity of the sample and char was represented by $c_{p,s}$ and $c_{p,c}$, respectively.

$$Q_S = (1 - \alpha) \left(m_0 c_{p,s} \frac{dT}{dt} \right) + \alpha \left(m_c c_{p,c} \frac{dT}{dt} \right) \quad (3.50)$$

Then, assuming that transport phenomena effects were avoided, the heat flux due to exothermic or endothermic reactions (heat of reaction, Q_R) was determined by the subtraction of Q_S from the DSC data (Q_{DSC}) as presented in equation (3.51).

$$Q_R = Q_{DSC} - Q_S \quad (3.51)$$

The heat capacity (c_p) of the biomass was determined based on the investigation of Dupont et al. (2014), who studied 21 different biomasses divided into five groups (wood, short rotation forestry, perennial crops, agricultural byproducts, and energy crops) considering the temperature range between 40 and 80 °C, in which some fibers presented physical, thermal and chemical characteristics similar to sugarcane straw. The heat capacity among biomasses varied less than 20% ranging from 1300 to 2000 J kg⁻¹ K⁻¹.

Thus, from the work of Dupont et al. (2014) were obtained the heat capacity ($c_{p,s}$) of switchgrass (equation 3.52) in J/kg°C and the heat capacity of char ($c_{p,c}$), (equation 3.53).

$$Cp_s = 4.9700T + 1144.1638 \quad (3.52)$$

$$Cp_c = 1.400T + 688 \quad (3.53)$$

According to Rath et al. (2003), the heat of reaction (H_R) required or released in the process is obtained by applying equation (3.54), in which m_0 is the dried mass (150 °C). The

solution of this equation was carried out with the numerical integration tool of the software *Origin 8*. The temperature is related with time through the heating rate, in which t_1 and t_2 corresponded to the time at the temperature of 150 °C and 600 °C, respectively, using a step of 5s.

$$H_R = \frac{1}{m_0} \int_{t_1}^{t_2} Q_R dt \quad (3.54)$$

CHAPTER 4

RESULTS AND DISCUSSION

In this chapter are presented, firstly, the results of the biomass characterization, and a comparison with other investigations about sugarcane straw and bagasse. Secondly, are presented the results of the thermal decomposition. Thirdly, are presented the results of the kinetic analysis of the thermal decomposition in inert and oxidative atmospheres through three different kinetic pathways, global reaction, consecutive reactions, and independent parallel reactions. Finally, are presented the results of the determination of the heat of reaction related to the thermal decomposition in both atmospheres.

4.1. Biomass Characterization

Table 4.1 presents the proximate and ultimate analyses of sugarcane straw obtained in this work and compared with the results obtained by Mesa-Pérez et al. (2013), Leal et al. (2013), and Hoi and Martincigh (2013). Considering the composition of the sugarcane straw as dry leaves, green leaves and tops, Mesa-Pérez et al. (2013) did not present clearly the part of plant used, while Leal et al. (2013) and Hoi and Martincigh (2013) analyzed separately these three parts.

In general, the proximate and ultimate analyses, as well as the heating value are in the same magnitude order excluding the moisture content. From the proximate analysis, it was observed that the moisture was around 8% lower than Mesa-Pérez et al. (2013) and Leal et al. (2013) results. However, the latest authors present a large range of moisture from dry leaves to green leaves with an increasing of 55 wt.%, and from dry leaves to tops around 70 wt.%.

Regarding to the ash content, our result (3.85 wt.%) was similar to the average of 3.56 ± 0.81 wt.% obtained from Leal et al. (2013), whilst Mesa-Pérez et al. (2013) showed a significantly higher value (16.4wt.%). Concerning to the volatile contents, our result (86.6wt.%) was comparative to the average of 81.47 ± 2.71 wt.% obtained from Leal et al. (2013), nevertheless Mesa-Pérez et al. (2013) showed a higher difference (12.6 wt.%) probably due the high mineral contents in their samples. About fixed carbon, it was observed that the results of Mesa-Pérez et al. (2013) and Leal et al. (2013) are close (13wt.% and 14.57

wt.%, respectively), however our results presented lower data. From the ultimate analysis, it was observed that the values of C, H, N, S, and O are quite similar, with difference lower than 3 wt.%, with exception of Hoi and Martincigh (2013) for green leaves. Comparing the higher heating values the variation (max. 6.8%) could be considered negligible with exception of Leal et al. (2013) for tops of plant (13.5%).

Table 4.1. Proximate and ultimate analyses and heating values of sugarcane straw

	This work	Mesa-Pérez et al. (2013)	Leal et al. (2013)			Hoi and Martincigh (2013)		
	DL	DL	DL	GL	T	DL	GL	T
Proximate analysis wt.%								
Moisture	8.42±0.30	10.4	13.5	67.7	82.3	–	–	–
Ash ^a	3.85±0.21	16.4	2.7	3.7	4.3	–	–	–
Volatiles ^a	86.64±0.53	74.0	84.5	80.6	79.3	–	–	–
Fixed carbon ^a	9.51±0.53	13.0	11.6	15.7	16.4	–	–	–
Ultimate analysis wt.% ^{a,b}								
C	42.94±0.25	43.2	46.2	45.7	43.9	45.2	39.1	41.5
H	6.26±0.16	6.7	6.2	6.2	6.1	5.8	3.0	5.0
N	0.31±0.05	0.3	0.5	1.0	0.8	–	–	–
S	–	0.2	0.1	0.4	0.1	–	–	–
O	46.65±0.18	33.2	43.0	42.8	44.0	47.4	45.1	46.7
Heating value MJ/kg								
HHV	18.61	18.0	17.4	17.4	16.4	18.3	–	–
LHV	15.60	17.0	–	–	–	–	–	–

^awt.% on dry basis, ^bwt% on ash free basis, DL–dry leaves, GL–green leaves, T–tops

Finally, the properties obtained in this work does not differ significantly with the values obtained by other authors who studied the sugarcane straw, indicating that exists a uniformity of the material under study, providing reliability in the raw material.

Table 4.2 presents the chemical composition of sugarcane straw compared with the presented by Saad et al. (2008), Luz et al. (2010), and Costa et al. (2013). Also, in Table 4.2 were presented the results about sugarcane bagasse (Luz et al., 2010; Rocha et al., 2011; Aboyade, Görgens, Carrier, Meyer, & Knoetze, 2013) in order to correlate both biomasses.

The hemicellulose fraction in in our sample was slightly higher (6 wt.%) than the average reported in literature (26.9±0.6 wt.%). Nevertheless, comparing the average value

with the average fraction in sugarcane bagasse (26.46 wt.%) no quite difference was observed.

The cellulose fraction in our sample was 39.81 wt%, similar to the obtained by Saad et al. (2008), however, comparing it with the fraction of ~33 wt.% obtained by Luz et al. (2010) and Costa et al. (2013) our sample was 6 wt.% higher. Nonetheless, comparing the cellulose fraction in sugarcane straw with the average fraction in sugarcane bagasse (44.5 ± 0.9 wt.%), it was 5 wt.% higher than the obtained in this work and 11 wt.% higher than the reported in literature.

The lignin fraction in our sample was 21.5 wt.%, and comparing it with the lignin fractions from literature (26.1 wt.%) was 5 wt.% lower. Also, the lignin fraction obtained in this work was 2 wt.% lower than the reported in literature for sugarcane bagasse, however, this difference was considered negligible.

Table 4.2. Chemical composition of sugarcane straw and sugarcane bagasse

Sugarcane straw wt.%				
Reference	Hemicellulose	Cellulose	Lignin	Extractives
This work	33.28	39.81	21.63	5.28
Saad et al. (2008)	26.2	39.4	21.5	–
Luz et al. (2010)	27.4	33.3	26.1	10.6
Costa et al. (2013)	27.1	33.5	25.8	–
Sugarcane bagasse wt.%				
Luz et al. (2010)	28.6	43.8	23.5	2.8
Rocha et al. (2011)	27.0	45.5	21.1	4.6
Aboyade et al. (2013)	23.8	44.2	22.4	9.7

Finally, based on the previous discussion, we conclude that both biomasses, on a dry basis, presented similar characteristics. This fact is of great importance, since it opens the possibility to explore new applications for sugarcane straw, including the use of the existing thermal conversion technologies applied for sugarcane bagasse, or even explore the possibility of a mixture of both biomasses.

4.2. Thermal Decomposition Analysis in Inert Atmosphere

Figure 4.1(a) and Figure 4.1(b) present the normalized mass (W) and the normalized DTG (dW/dt) as a function of temperature, according to Eq. (3.2) and (3.3), respectively. The

thermal decomposition of the sugarcane straw was divided into three stages such as dehydration, devolatilization and carbonization.

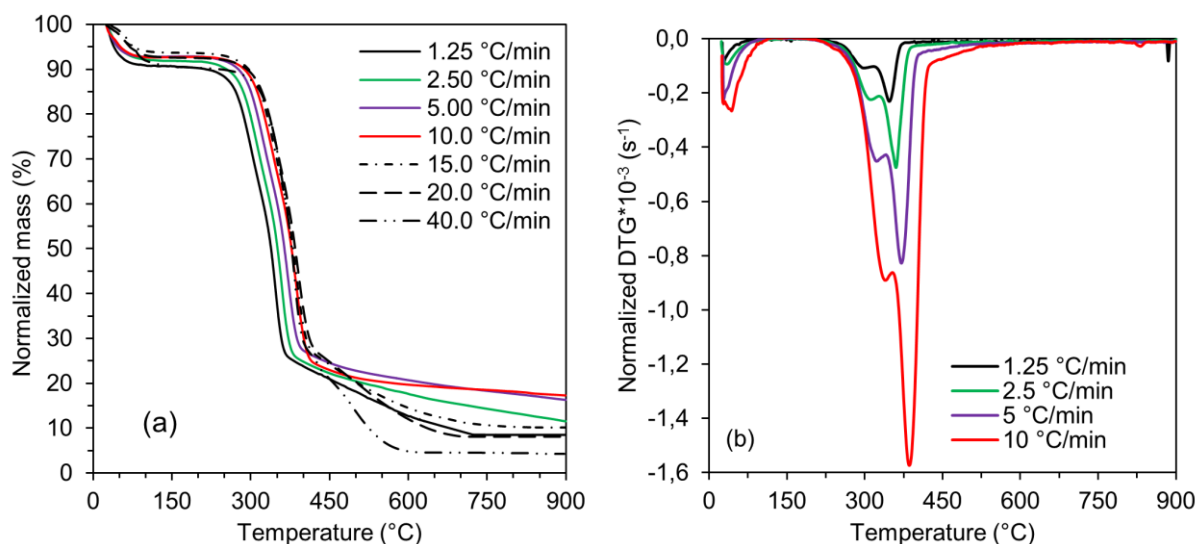


Figure 4.1. (a) Normalized mass and (b) normalized DTG as a function of temperature

4.2.1. Dehydration

The first stage in a thermal conversion process corresponds to the sample dehydration, and takes place in the temperature range between the room temperature and 150 °C. The moisture content in the sugarcane straw shown in Fig. 4.1a were 9.32%, 8.13%, 7.17%, 7.31%, 8.35%, 7.37% and 9.35% for the heating rates of 1.25, 2.5, 5, 10, 15, 20, and 40 °C/min, respectively. In the DTG curve (Fig. 4.1b) this stage presented a peak in the temperature range of 25 °C – 100 °C for all the heating rates. Above 150 °C up to 200 °C, was not registered significant mass variation (<0.5%).

4.2.2. Devolatilization

The second stage or intermediate step in a pyrolysis process is the devolatilization, which takes place in the temperature range between 200 °C and 450°C. At this stage, the biomass is completely dried, and its main components (hemicellulose, cellulose and lignin) decomposed with the temperature increasing. Different gaseous compounds are released, and a fraction of them are condensable, which are the precursors of the liquid fraction (Di Blasi, 2008). The volatilized mass of sugarcane straw, as shown in Figure 4.1a, was 69.71%, 69.63%, 68.29%, 69.73%, 69.05%, 67.87%, and 69.70% for the heating rates from 1.25

°C/min to 40 °C/min, respectively. Also, in Figure 4.1a is observed the overlapping of the curves at 15 °C/min, 20 °C/min and 40 °C/min, indicating that the use of heating rates higher than 10 °C/min involves mass and heat transfer effects which cannot be measurable. In the specific case of sugarcane straw, the last three heating rates are not recommended for kinetic analysis.

The normalized DTG curve, shown in Fig. 4.1b, was characterized by the formation of two well defined peaks at 298.7 °C and 347.3 °C, 311.6 °C and 360.3 °C, 324.7 °C and 370.8 °C, and 340.0 °C and 385.0 °C, for 1.25 °C/min, 2.5 °C/min, 5 °C/min, and 10 °C/min, respectively. However, for heating rates higher than 10 °C/min the curve pattern (two peaks) suffered modifications, at 15 °C/min and 20 °C/min the curve pattern turns into a shoulder followed by a peak, and at 40°C/min the curve is almost only one peak. This behavior indicates that the reaction time is too short to obtain a correct representation of the complexity of the thermal decomposition of sugarcane straw. Also, because in TG analysis is assumed that the inter-particle and intra-particle transport phenomena effects are avoided.

According to the literature review presented in the *Introduction section*, the hemicellulose component reacts between 200 °C and 300 °C corresponding to the first peak in the DTG curve (Fig. 4.1b). The cellulose component reacts between 250 °C and 350 °C corresponding to the main peak, and the lignin is the responsible for the final remaining solid. However, the latest component reacts in a broad temperature range, from 200 °C to 600 °C, which means that when hemicellulose and cellulose react, the lignin also is decomposing, but not governing the overall reaction.

4.2.3. Carbonization

The final stage in biomass thermal decomposition in inert atmosphere is the carbonization, occurring at temperatures above 450 °C. As observed in Fig. 4.1a, the mass released in this stage was 12.46%, 10.72%, 8.29%, 5.67%, 15.73%, 16.66% and 16.70% for the heating rates from 1.25 °C/min to 40 °C/min, respectively. The final residues, formed by the mineral content and the char fraction, were 8.61%, 11.52%, 16.30%, 17.30%, 7.65%, 8.09%, and 4.31% for the same heating rates, respectively. In Fig. 4.1b the DTG curves above 450 °C presented a small shoulder decreasing its amplitude with the temperature increasing, resembling a tail shape. This behavior is due to the lignin thermal decomposition, which is

characterized by low reaction rate and broad temperature range. However, the curves at 1.25 °C/min, 20 °C/min, and 40 °C/min presented different curve patterns with higher conversion rates and higher volatile release. The behavior at 20 °C/min and 40 °C/min confirm that were affected by transport phenomena.

In conclusion, it was observed that the higher the heating rate, the higher the final remaining mass. In other words, decreasing the heating rate, the reaction time is increased, allowing the occurrence of more reactions, breaking the polymeric linkages of biomass compounds and increasing the volatile production, and therefore, greater biomass decomposition.

4.3. Thermal Decomposition Analysis in oxidative atmosphere

Figure 4.2 presents the TG/DTG curves of thermal decomposition of sugarcane straw in synthetic air and nitrogen (section 4.2. *Thermal Decomposition Analysis in Inert Atmosphere*) in order to perform a reliable comparison between atmospheres.

Fig. 4.2a presents the thermal decomposition curves as a function of temperature, in which are observed three stages of mass loss. The first one, between room temperature and 150 °C with 10% of mass loss, was related to the moisture released. In the second stage (150-350 °C) was volatilized 55% of mass concerning to the oxidative pyrolysis. At this stage, the volatile released was mainly due to the thermal decomposition of hemicellulose and cellulose, and part of lignin. Above 350 °C, the remaining mass was mainly composed by a mixture of carbonaceous solid and mineral matter, which was oxidized producing a slow combustion reaction (smoldering), corresponding to the final stage of the thermal decomposition of sugarcane straw in synthetic air. The mass loss in the combustion stage was 30% and the final residue at 600 °C was 5% for all the heating rates, composed by the mineral matter (ash).

Also, in Fig. 4.2a was observed that the thermal decomposition in synthetic air occurred in a lower temperature range (approximately 20-30 °C) than in nitrogen (Rueda-Ordóñez and Tannous, 2015). In the normalized mass (Fig. 1a) between 0.2 and 0.3 was observed a change in the curve pattern for both atmospheres related to the end of devolatilization stage in the temperatures of 350 °C and 400 °C for synthetic air and nitrogen, respectively. In the temperature of 600 °C in synthetic air the residual mass was approximately 5%, composed by

ash, and above this temperature no more mass variations were observed. In nitrogen atmosphere the behavior was quite different, above 600 °C the carbonaceous solid was reacting and the residual mass was higher (20% mass) due to the char formed and unburned after sample devolatilization.

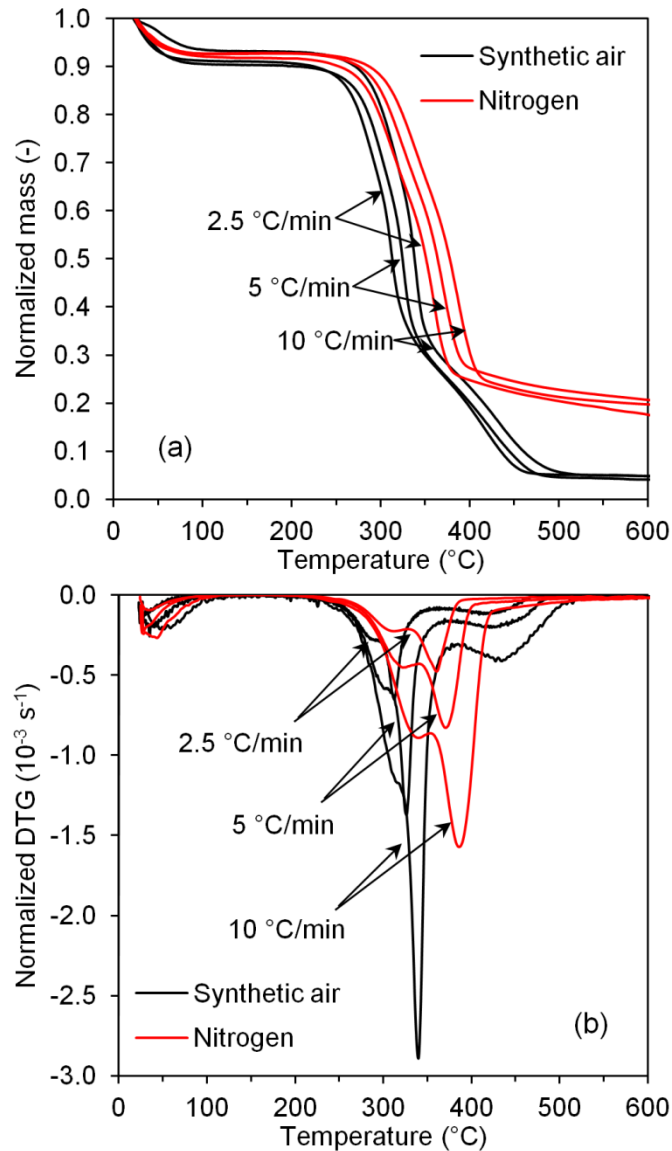


Figure 4.2. (a) TG and (b) DTG curves of thermal decomposition of sugarcane straw in synthetic air and nitrogen.

Besides that, in Figure 4.2b is showed the normalized DTG curves, in which the three stages, dehydration, oxidative pyrolysis, and combustion are clearly defined and marked by peaks. The dehydration peak was located around 50 °C for both atmospheres. The peak concerning the oxidative pyrolysis increased its amplitude and temperature with the

increasing of heating rate. This behavior is due to the differences in the reaction time for each heating rate, it means that for lower heating rates higher reaction time, and therefore, the peak temperature and amplitude are lower.

The peak temperatures and amplitudes were 312.5 °C and $-0.65 \times 10^{-3} \text{ s}^{-1}$, 325.8 °C and $-1.37 \times 10^{-3} \text{ s}^{-1}$, 339.8 °C, and $-2.89 \times 10^{-3} \text{ s}^{-1}$ for the heating rates of 2.5 °C/min, 5 °C/min, and 10 °C/min, respectively. The combustion peak presented a similar trend with temperature and amplitude of 413.2 °C and $-0.12 \times 10^{-3} \text{ s}^{-1}$, 420.4 °C and $-0.20 \times 10^{-3} \text{ s}^{-1}$, 427.2 °C and $-0.41 \times 10^{-3} \text{ s}^{-1}$, for the same heating rates, respectively.

Comparing the DTG curves between atmospheres was observed not only the difference in the temperatures previously described, but also the high reaction rate in synthetic air, which was almost twice the velocity in nitrogen. These results are in agreement with Órfão et al. (1999) observations.

4.4. Isoconversional Method Results in Inert Atmosphere

The activation energy in inert atmosphere was determined through the isoconversional method of Friedman. In order to obtain reliable kinetic parameters were used the four lower heating rates (1.25, 2.5, 5, and 10 °C/min) due to the heat and mass transfer effects in the curves at heating rates higher than 10 °C/min as previously discussed (section 4.2.2 *Devolatilization*). The kinetic analysis was carried out for the devolatilization stage, corresponding to the normalized mass between 90% and 25%, and temperature range between 200 °C and 450 °C, for all heating rates (Figure 4.1a).

Figure 4.3 presents the derivative of conversion with respect to the temperature ($d\alpha/dT$) and activation energy as a function of conversion (α). In Figure 4.3a two peaks were observed corresponding to the hemicellulose, cellulose, and lignin decomposition reactions, as described in the section 4.2.2 *Devolatilization*. The conversion range between 0.00 and 0.45 was related to the temperature range between 200 °C and 320 °C for all heating rates, concerning mainly to hemicellulose and lignin decomposition reactions.

Also, in Figure 4.3a the derivative of conversion with respect to the temperature presented a minimum at the conversion level of 0.45, representing a division between

hemicellulose and cellulose main reactions. In this conversion range (0.00 to 0.45), it was observed a small effect of heating rate on the da/dT curves, i.e., similar curve patterns were obtained for all heating rates. This effect was also verified by the comparison of the slopes between 85% and 55% in the normalized mass curve (Figure 4.1a), which were almost equal.

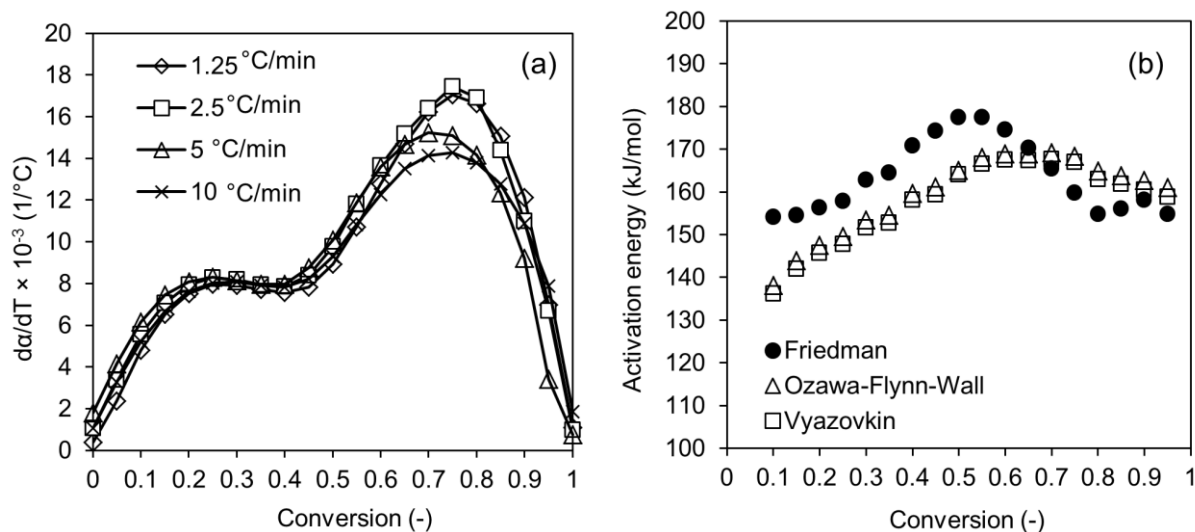


Figure 4.3. (a) Derivative of conversion with respect to temperature and (b) Activation energy as a function of conversion

For the conversion range between 0.45 and 1.00, the main decomposition reaction corresponded to cellulose and lignin. In Figure 4.3a, the curves of da/dT as a function of conversion were similar for the heating rates of 1.25 and 2.5 °C/min, but for 5 °C/min and 10 °C/min the da/dT curve decreased with the increasing of the heating rate. In this case, from the comparison of the slopes between 50% and 25% in the normalized mass curve (Figure 4.1a) were verified changes among them.

Figure 4.3b presents the activation energies obtained for the isoconversional methods of Friedman, Ozawa-Flynn-Wall, and Vyazovkin. The activation energies were between 154.1 and 177.8 kJ/mol (increasing of 15%), and average of 163.4 kJ/mol. According to Vyazovkin (1997), the variation of activation energy as a function of conversion happens by two main aspects: (1) existence of a complex kinetic pathway following more than one reaction (i.e., parallel, consecutive, or competitive reactions schemes); (2) error from experimental data by noises and lack of calibration of the equipment, which are transferred to the isoconversional methods. Also, according to Janković (2008), this variation of activation energy can be explained by the fact that the Arrhenius equation was developed for reaction kinetics of gases,

which are well described by a one-step global reaction, and in this case the evaluation is applied for solid-state reaction kinetics.

In the conversion range between 0.1 and 0.2, the average of activation energy remained in 154.66 ± 0.44 kJ/mol, corresponding to the temperature interval between 200–300 °C, related to the depolymerization of the biomass components, which is the first step in the thermal decomposition, with low energy requirements.

Above 0.2 up to 0.5 was observed an increasing in the activation energy from 153.9 to 174.0 kJ/mol due to the polymeric differences between hemicellulose and cellulose. According to Di Blasi (2008) the hemicellulose is the least thermally stable of the biomass components, and therefore, its activation energy in an inert thermal decomposition process is lower than the cellulose one. According to Liu et al. (2011), the cellulose is formed by links of β (1-4)-glucose, which are very stable links, thus, requiring more energy for their breaking and decomposition. The maximum activation energy (177.5 kJ/mol) was achieved when the cellulose decomposition was reached, corresponding to the conversion of 0.5, and therefore, no higher energy was necessary to continue the biomass decomposition. Therewith, above the conversion of 0.5 the activation energy decreased from 177.5 kJ/mol to 160.0 kJ/mol.

Above the conversion of 0.8, the biomass was almost decomposed and a carbonaceous solid was formed constituting the majority of the residue, and the activation energy became stable in 155.8 ± 1.86 kJ/mol, concerning to the lignin thermal decomposition reaction, as commented in the section 4.2.2 *Devolatilization*.

4.4.1. Reaction model and pre-exponential factor determination

Reaction model determination

The determination of the reaction model is a fundamental step in kinetic studies, since it is a theoretical function that helps to describe and improve the understanding of the reaction. In investigations of thermal decomposition of biomass which applied isoconversional methods was observed that it is commonly assumed a first or n^{th} order reaction model (Damartzis, Vamvuka, Sfakiotakis, & Zabaniotou, 2011; Slopiecka et al., 2012; Ceylan & Topçu, 2014; Baroni et al., 2015). Nevertheless, according to Vyazovkin et al. (2011), is not

recommended the assumption of a reaction model without a previous verification through master plots, since other reaction model could be more suitable to describe the reaction.

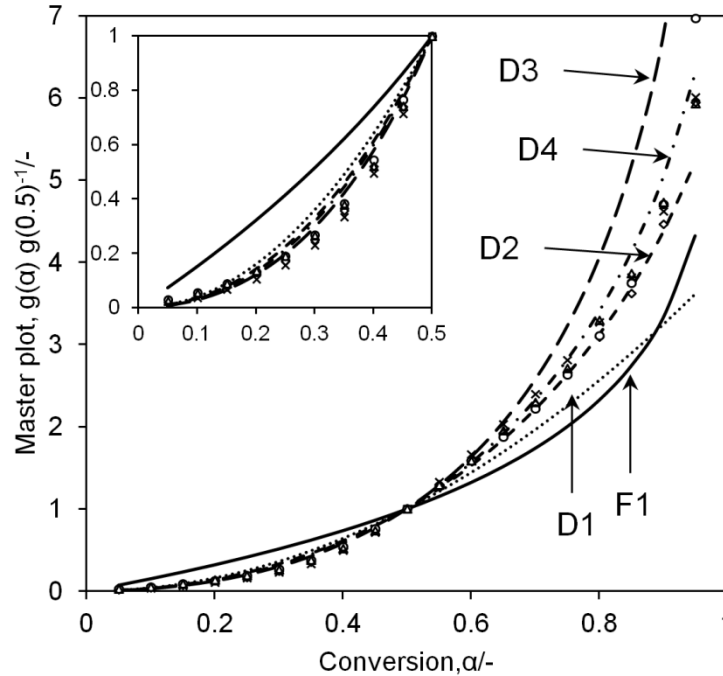


Figure 4.4. Theoretical and experimental master plots for the thermal decomposition of sugarcane straw at the heating rates of (x)1.25 °C/min, (◊)2.5 °C/min, (Δ)5 °C/min, (o)10 °C/min as a function of conversion.

In Figure 4.4 is presented the theoretical and experimental master plots as a function of conversion. The theoretical curves (lines) are for a few integral reaction models, $g(\alpha)$, (F1, D1, D2, D3 and D4 according to Table 2.3) which could represent the experimental behavior at the different heating rates evaluated, however, all the reaction models were analyzed. In Figure 4.4 is observed that the experimental master plots (symbols) at 1.25 °C/min (x), 2.5 °C/min (◊), 5 °C/min (Δ) and 10 °C/min (o) are consistent with the theoretical master plot of the reaction model D2 (Valensi-Carter equation) corresponding to two-dimensional diffusion.

According to Khawam and Flanagan (2006), the two-dimensional diffusion is derived from the assumption of a cylindrical shape solid with the reaction occurring radially from the external boundary to the center, increasing the reaction zone with time. In this present study, the two-dimensional diffusion (D2) provides an approximation to the real behavior of the biomass decomposition reaction, and taking into account that the sample of sugarcane straw

used in this work is a long fiber with cylindrical shape, the mathematical approach is correct. Nonetheless, from the kinetic point of view, is widely discussed the approximation of the thermal decomposition reaction as a one-step reaction, since it is governed by multiple complex reactions affected by the interactions between biomass components.

Pre-exponential factor determination

The pre-exponential factor was determined as a forward step, with knowledge of a suitable reaction model, $f(\alpha)$, which provided a good representation of the experimental data. The pre-exponential factor was determined by linearization of $\ln[(d\alpha/dt)/f(\alpha)]$ as a function of the $1/T$, as mentioned in the section 3.4.4. *Pre-exponential factor determination*, and presented in Figure 4.5. The linear equation obtained is given by equation (4.1), in which the slope and intercept were 18.007 and 21.322.

$$\ln[(d\alpha/dt)/f(\alpha)] = 18.007(1/T) + 21.322 \quad R^2 = 0.9658 \quad (4.1)$$

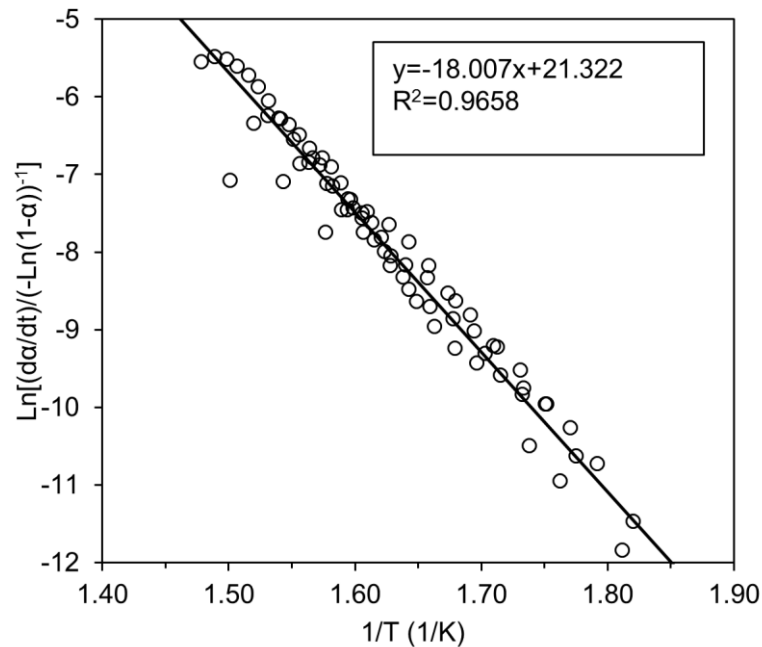


Figure 4.5. Linearization of the conversion rate equation as a function of the inverse of absolute temperature

The scattering of the experimental data in Figure 4.5 was reflected in the determination coefficient, R^2 , of 0.9658. This slight scatter effect is due to the formation of two peaks

(Figure 4.1b), associated to multiple and complex reactions in the biomass thermal decomposition, as stated by Vyazovkin et al. (2011).

The intercept represents $\ln A$, corresponding to a pre-exponential factor of $A=1.8 \cdot 10^9 \text{ s}^{-1}$. The activation energy ($E= 149.710 \text{ kJ/mol}$) was obtained through the multiplication of the slope by the universal gas constant (8.314 J/mol K). This value is slightly below (2%) of the lowest activation energy obtained by Friedman's method (154.1 kJ/mol), but it is in agreement with the range $140\text{--}200 \text{ kJ/mol}$ previously analyzed for biomass in Table 2.2.

4.4.2. Evaluation of the kinetic parameters

Figure 4.6 presents theoretical ($\alpha_{theoretical}$) and experimental (α_{exp}) conversion curves as a function of temperature obtained at different heating rates. These curves were obtained assuming the thermal decomposition reaction of sugarcane straw as a one-step global reaction (equation 4.7).

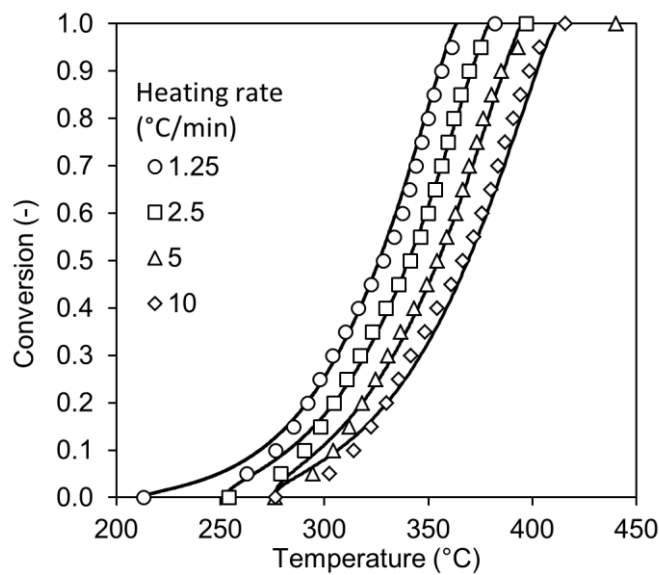


Figure 4.6. Conversion curves as a function of temperature. Modeled data as solid lines, and experimental data in symbols.

It is observed that from the conversion of 0.00 to 0.20, the theoretical data is slightly underestimated, and above 0.80 is overestimated. However, for the conversion range between 0.20 and 0.80, the theoretical curve is in good agreement with experimental data. The variation in the extremes suggests a reaction model modification.

Table 4.3 presents the kinetic parameters determined for the thermal decomposition of sugarcane straw in inert atmosphere. The kinetic parameters obtained, activation energy, pre-exponential factor, and reaction model, remained constant for all the heating rates analyzed. This fact confirms the independency of the process with the heating rate, i.e., was successfully avoided the inter-particle and intra-particle effect of the transport phenomena.

The activation energy obtained in this research was 149.710 kJ/mol, in agreement with literature for biomass (Table 2.2, section 2.4.1. *Isoconversional methods*), normally between 140 kJ/mol and 200 kJ/mol. Also, the reaction model determined for the one-step global reaction provides a better description of the experimental behavior than the reaction model normally used in literature, which is a first or n^{th} reaction order. This fact is in agreement with the results and conclusion of Baroni et al. (2015), who studied the use of first order reaction model to describe the biomass thermal decomposition, concluding that using this reaction model the results are overestimated.

Table 4.3. Kinetic parameters of sugarcane straw in inert atmosphere for a global reaction

One-step global reaction				
	$f(\alpha)$	E (kJ/mol)		$\ln A (\ln s^{-1})$
	$D2=[-\ln(1-\alpha)]^{-1}$	149.710		21.322
β (°C/min)	1.25	2.5	5	10
AD (%)	2.3%	2.2%	2.3%	3.1%

4.5. Isoconversional Method Results in Oxidative Atmosphere

The isoconversional kinetic analysis was carried out through the model-free method of Vyazovkin (Vyazovkin, 1997) applied for each stage separately, concerning to the main events of decomposition (oxidative pyrolysis and combustion).

As presented in Figure 4.2(a), the oxidative pyrolysis stage was related to the normalized mass range from 0.9 to 0.3 concerning to the temperatures between 150 °C and 350 °C, respectively, divided into 20 conversion data. The combustion stage was analyzed from 0.3 to 0.05 of normalized mass related to the temperatures of 350 °C to 600 °C, and divided into 19 conversion data. This division in stages was done in order to obtain a detailed behavior of activation energy for all the thermal decomposition process.

Figure 4.7 shows the activation energy as a function of conversion for oxidative pyrolysis and combustion. In the oxidative pyrolysis stage the activation energies varied from 148.0 kJ/mol ($\alpha=0.15$) to 352.1 kJ/mol ($\alpha=0.95$) concerning to a percentage variation of 137% and an average value of 172.0 ± 39.4 kJ/mol. In the combustion stage, the activation energy decreased from 350 kJ/mol ($\alpha=0.10$) to 159 kJ/mol ($\alpha=0.95$), with percentage variation higher than 100% and average 266.4 ± 52.7 kJ/mol.

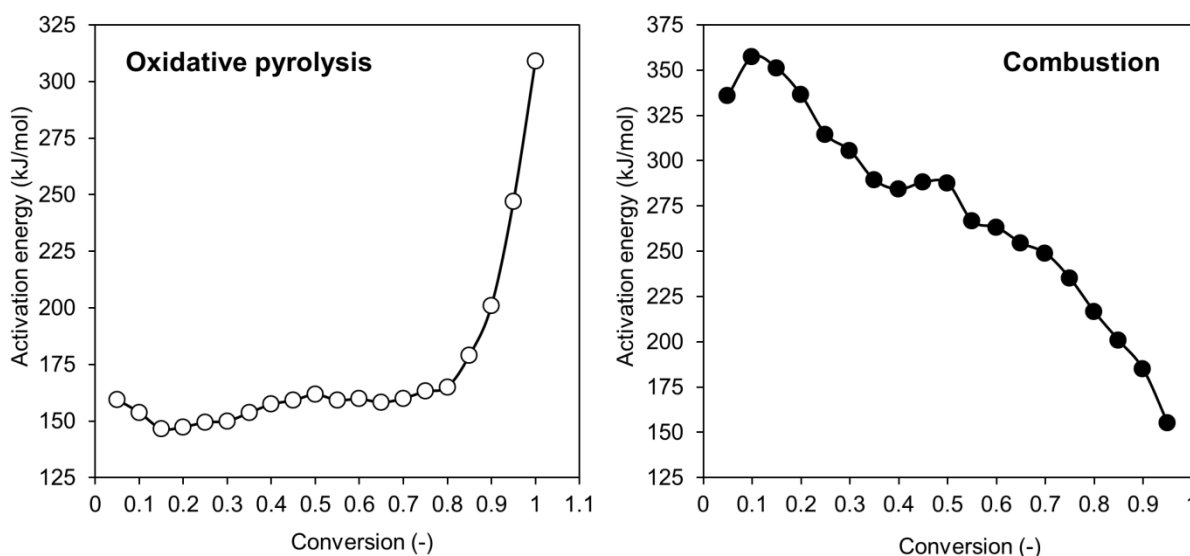


Figure 4.7. Activation energy as a function of conversion for the two stages, oxidative pyrolysis and combustion.

According to Vyazovkin et al. (2011), when the percentage variation between minimum and maximum activation energy is higher than 30%, the reaction obeys a multistep kinetic scheme, and therefore indicates that parallel reactions scheme could be applied. Also, they recommended using the average activation energy obtained as a first guess in the iterative process, in order to obtain the final activation energy for each parallel reaction analyzed.

4.6. Analysis and Considerations on Model Fitting

The kinetic modeling of biomass pyrolysis is normally carried out as an optimization analysis, using common fitting tools as the least squares method. Nevertheless, that fit is dependent on the combination of parameters used in the analysis, which in this case are the activation energy, pre-exponential factor, and the peak temperature.

As aforementioned, Section 2.4.4. *Independent parallel reactions scheme*, these parameters showed an interdependency that cannot be ignored. Thus, in order to evaluate the parametric interdependency, were simulated reaction rate curves of a first order one-step global reaction by using equation (3.7) with $f(\alpha)=(1-\alpha)$. As the heating rate (β) affects the results, were simulated curves from 1 to 20 °C/min, with a step of 1 °C/min, and also 30, 40, and 50 °C/min. For each value of $\log A$ analyzed were evaluated five different activation energies, 100, 125, 150, 175, and 200 kJ/mol, and were measured the values of peak conversion rate, $(d\alpha/dt)_p$, and its related temperature (T_p). The value of $\log A$ was increased from 4 to 10, with a step of 1.

$$\left(\frac{d\alpha}{dt}\right) = A(1 - \alpha) \left[\exp\left(\frac{-E}{RT}\right) \right] \quad (3.7)$$

In Figure 4.8 are presented curves of conversion rate as a function of temperature obtained from simulated data. Figure 4.8a shows the conversion rate as a function of temperature, in which twelve curves were simulated, each one representing different combination of parameters. The curves were obtained from simulations using four different $\log A$, 5, 7, 9, and 11 $\log s^{-1}$, and three activation energies 100, 150, and 200 kJ/mol at a heating rate (β) of 10 °C/min in order to evaluate the effect of $\log A$. For each $\log A$ are presented three conversion rate curves, from left to right, each one represents a reaction with activation energy of 100, 150, and 200 kJ/mol. The increasing in $\log A$, results in a shift of the reaction to the left, decreasing the peak temperature and reaction temperature range, and increasing the peak amplitude.

Figure 4.8b presents the conversion rate as a function of temperature, in which twelve curves were simulated, each one representing different combination of parameters. The curves were obtained from simulations using four heating rates (β), 4, 6, 8, and 10 °C/min and three activation energies 100, 150, and 200 kJ/mol with $\log A=10 \log s^{-1}$. As above presented, each heating rate evaluated correspond to three conversion rate curves, from left to right, each one represents a reaction with activation energies of 100, 150, and 200 kJ/mol. The increasing in the heating rate, results in an increasing in the peak amplitude, and therefore a shift in the peak temperature to the right.

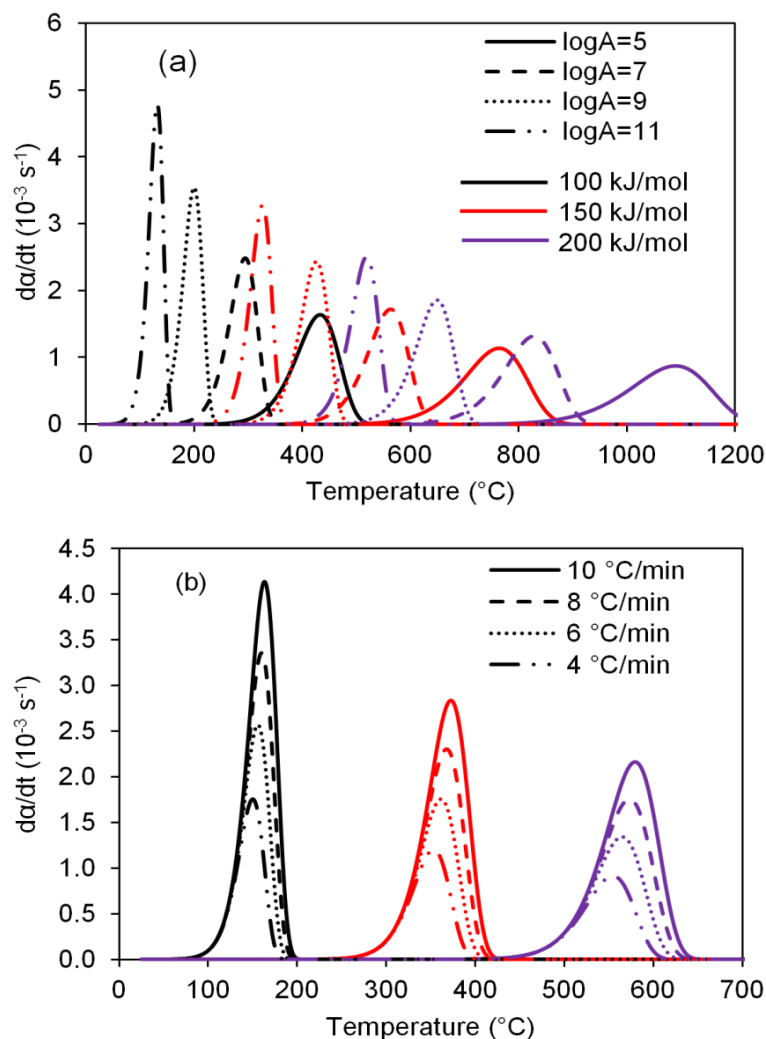


Figure 4.8. Results of the conversion rate simulation. (a) Effect of the pre-exponential factor at $10^{\circ}C/min$, and (b) Effect of the heating rate (β) using $\log A = 10 \log s^{-1}$.

The overall results obtained with the simulation showed that the activation energy (E) is linearly dependent on the peak temperature (T_p), following the function presented in equation (4.2). The linear constants, a and b in this correlation increase linearly with $\log A$, as showed in equation (4.3) and equation (4.4). Also, it was observed that the peak conversion rate $(da/dt)_p$ decreased with the increasing of peak temperature (T_p), following a logarithmic function according to equation (4.5). The constants c and d in equation (4.5) increased linearly with $\log A$ as shown in equation (4.6) and equation (4.7).

The parameters x and y represent the slope and linear coefficients of equations (4.3), (4.4), (4.6), and (4.7).

$$E=a(T_p)+b \quad (4.2)$$

$$a=x_0(\log A)+y_0 \quad (4.3)$$

$$b=x_1(\log A)+y_1 \quad (4.4)$$

$$(d\alpha/dt)_p=c\ln(T_p) + d \quad (4.5)$$

$$c= x_2\log A+y_2 \quad (4.6)$$

$$d= x_3\log A+y_3 \quad (4.7)$$

Figure 4.9 summarizes the results obtained with the correlations in two diagrams, which corresponds to data at a heating rate (β) of 5 °C/min. Figure 4.9a presents the peak conversion rate $(d\alpha/dt)_p$ as a function of the peak temperature (T_p) for different values of $\log A$. Figure 4.9b shows the activation energy as a function of the peak temperature.

For the determination of the kinetic parameter through the diagrams above presented is necessary to know the T_p and the $(d\alpha/dt)_p$, which must be the experimentally obtained at a heating rate (β) of 5 °C/min. Then, with these data in Fig. 4.9a is obtained the $\log A$ related to them, and afterward, with the T_p and the $\log A$ is determined the activation energy.

These kinetic parameters, even obtained at a heating rate (β) of 5 °C/min, must adjust to the data obtained experimentally at different heating rates. However, the inverse process, i.e., measuring the experimental T_p and $(d\alpha/dt)_p$ at a different heating rate, will provide different results as showed in Figure 4.8b.

Thus, to avoid the construction of these diagrams at different heating rates to attend all the experimental requirements, it was deeply analyzed the effect produced by the heating rate in order to state correlations which attend all the requirements.

Table 4.4 presents the parameters x_0 , x_1 , x_2 , x_3 , y_0 , y_1 , y_2 , and y_3 obtained through simulation of each heating rate from 1 °C/min to 50 °C/min. In Figure 4.10 it was discussed the behavior of each parameter of the correlations with the increasing of heating rate in order to present a complete analysis.

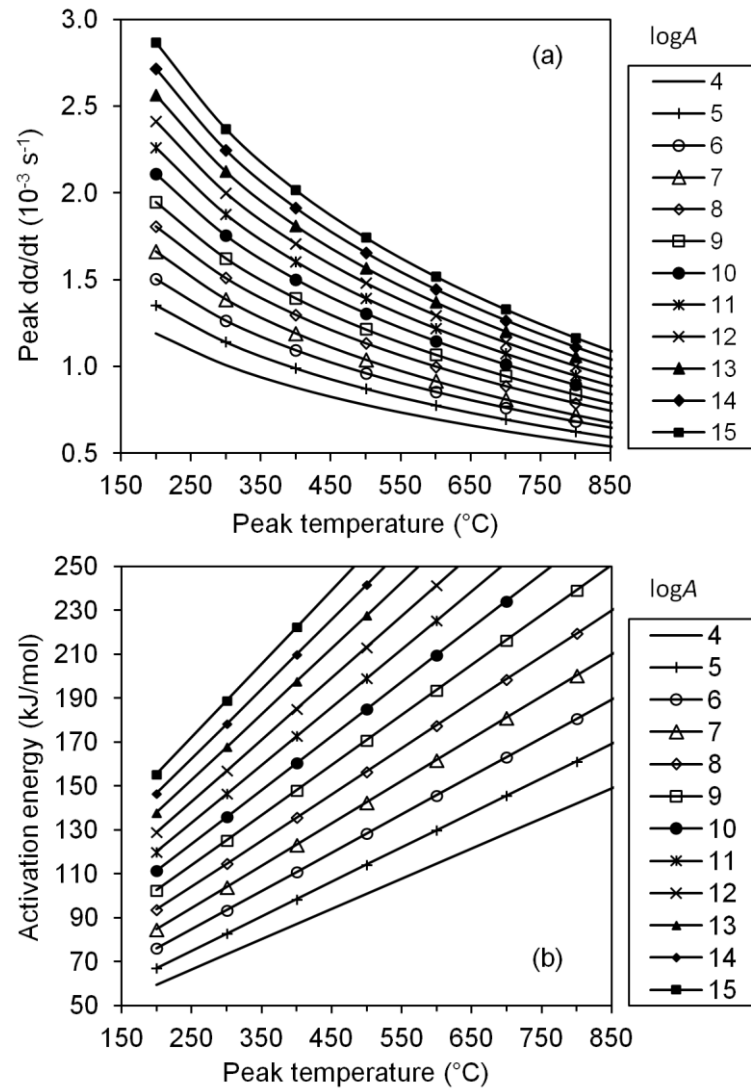


Figure 4.9. Diagrams obtained using the proposed correlations for a heating rate (β) of $5^\circ\text{C}/\text{min}$. (a) Peak conversion rate as a function of peak temperature and (b) activation energy as a function of peak temperature.

It was observed in Table 4.4 that x_0 and x_1 presented negligible variations, and therefore, their average values were $0.017747 \pm 4 \times 10^{-5}$ and $5.271271 \pm 7 \times 10^{-2}$, respectively. In Figure 4.10(a) and (b) the parameters y_0 and y_1 were fitted to logarithmic functions according to equations (4.8) and (4.9), respectively.

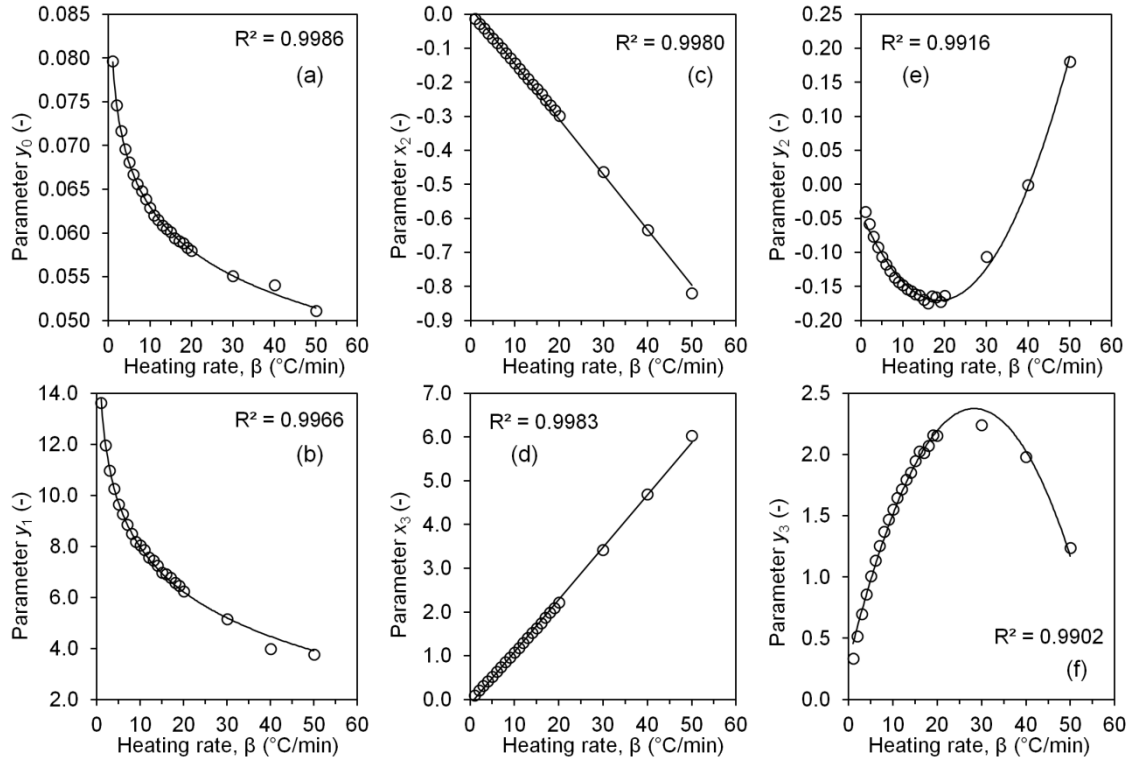


Figure 4.10. Analysis of the behavior of each parameter with the increasing of heating rate, from 1 °C/min to 50 °C/min. Empirical parameters (a) y_0 , (b) y_1 , (c) x_2 , (d) x_3 , (e) y_2 , and (f) y_3 .

In Figure 4.10(c) and (d) are presented the parameters x_2 and x_3 , which were linearly dependents on heating rate following equations (4.10) and (4.11), respectively. In Figure 4.10(e) and (f) are showed the parameters y_2 and y_3 , which followed a quadratic function according to equations (4.12) and (4.13), respectively.

$$y_0 = -0.007189 \ln \beta + 0.079554 \quad (4.8)$$

$$y_1 = -2.521793 \ln \beta + 13.773328 \quad (4.9)$$

$$x_2 = -0.016251 \beta + 0.016647 \quad (4.10)$$

$$x_3 = 0.119792 \beta - 0.112870 \quad (4.11)$$

$$y_2 = 0.000366 \beta^2 - 0.013657 \beta - 0.043026 \quad (4.12)$$

$$y_3 = -0.002565 \beta^2 + 0.145388 \beta + 0.315596 \quad (4.13)$$

The results presented in Table 4.4, when replaced in equations (4.2) and (4.5), and rearranging them, constitute an accurate mathematical form to obtain the activation energy and pre-exponential factor of first order one-step global reactions.

Table 4.4. Empirical parameters for the correlations proposed at several heating rates

β ($^{\circ}\text{C}/\text{min}$)	x_0	y_0	x_1	y_1	x_2	y_2	x_3	y_3
1	0.0178622	0.0796687	5.2206308	13.6356102	-0.0126541	-0.0405803	0.0961224	0.3342259
2	0.0178295	0.0746108	5.2296412	11.9562757	-0.0273469	-0.0580003	0.2047306	0.5148583
3	0.0178096	0.0716479	5.2349267	10.9712004	-0.0415116	-0.0765490	0.3103101	0.6973137
4	0.0177927	0.0695644	5.2426241	10.2604768	-0.0558243	-0.0921367	0.4168785	0.8584221
5	0.0177541	0.0681175	5.2564995	9.6425677	-0.0701578	-0.1062455	0.5236978	1.0078676
6	0.0177637	0.0666806	5.2491872	9.2674486	-0.0847999	-0.1172253	0.6325165	1.1358561
7	0.0177470	0.0656290	5.2568783	8.8474097	-0.0995212	-0.1270672	0.7418333	1.2557065
8	0.0177201	0.0647731	5.2632573	8.4948714	-0.1141352	-0.1365869	0.8507809	1.3702717
9	0.0177216	0.0638948	5.2639988	8.1895578	-0.1291838	-0.1434160	0.9621569	1.4701051
10	0.0177599	0.0628710	5.2488765	8.0468956	-0.1443969	-0.1480546	1.0747335	1.5536758
11	0.0177688	0.0620384	5.2490566	7.8587854	-0.1592889	-0.1540906	1.1853191	1.6454303
12	0.0177667	0.0615279	5.2520635	7.5637035	-0.1748860	-0.1567571	1.3003558	1.7153106
13	0.0177646	0.0608451	5.2480533	7.4497806	-0.1897419	-0.1615266	1.4110417	1.7961571
14	0.0177433	0.0604425	5.2453768	7.2605771	-0.2054882	-0.1624946	1.5274383	1.8522063
15	0.0177007	0.0601225	5.2697437	6.9698073	-0.2197915	-0.1696480	1.6346026	1.9476066
16	0.0177564	0.0594144	5.2440016	6.9082891	-0.2347915	-0.1747111	1.7464011	2.0280691
17	0.0177042	0.0590908	5.2661308	6.7771466	-0.2518386	-0.1644283	1.8705878	2.0132329
18	0.0176870	0.0588241	5.2698264	6.5775612	-0.2671584	-0.1661215	1.9844877	2.0714965
19	0.0177162	0.0583308	5.2558865	6.4519361	-0.2818030	-0.1725601	2.0940441	2.1603424
20	0.0176834	0.0580045	5.2891745	6.2387741	-0.2986507	-0.1636716	2.2168346	2.1545488
30	0.0176801	0.0550696	5.2929845	5.1495232	-0.4627221	-0.1061113	3.4256986	2.2420163
40	0.0175147	0.0540216	5.3499952	3.9908691	-0.6346033	-0.0007418	4.6896883	1.9826756
50	0.0177507	0.0510894	5.2927744	3.7707851	-0.8195419	0.1806022	6.0352192	1.2396206

Equations (4.14) and (4.15) summarize all the correlations obtained and represent the method developed, in which only three experimental parameters are strictly necessary, the heating rate (β) in $^{\circ}\text{C}/\text{min}$, the peak temperature (T_p) in $^{\circ}\text{C}$ and the peak conversion rate $(d\alpha/dt)_p$ in 10^{-3} s^{-1} . The results obtained are logarithm of pre-exponential factor (A) in logs^{-1} and the activation energy in kJ/mol .

$$\log A = \frac{\left(\frac{d\alpha}{dt}\right)_p - y_3 - y_2 \ln T_p}{x_2 \ln T_p + x_3} \quad (4.18)$$

$$E = (x_0 \log A + y_0)T_p + x_1 \log A + y_1 \quad (4.19)$$

In order to verify the accuracy and reliability of the mathematical correlations above proposed were simulated three curves of conversion rate (da/dt) at $10^{\circ}\text{C}/\text{min}$ (Figure 4.11) with activation energies of 100 kJ/mol , 150 kJ/mol , and 200 kJ/mol , and pre-exponential factor (A) of $10 \times 10^{10} \text{ s}^{-1}$ corresponding to $\log A = 10 \text{ logs}^{-1}$.

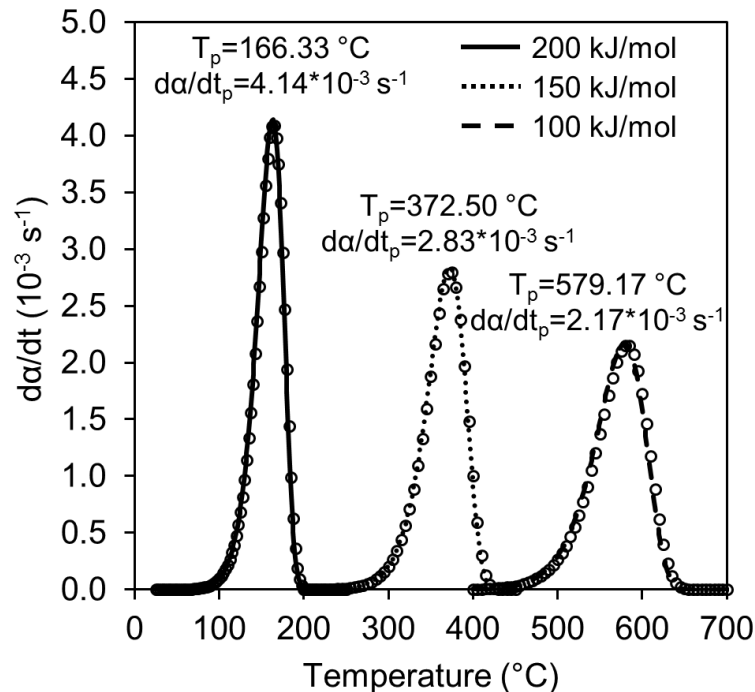


Figure 4.11. Model validation, heating rate of $10^{\circ}\text{C}/\text{min}$ and $\log A = 10 \text{ logs}^{-1}$. Simulated curve as solid line and curve obtained with correlation in symbols (o).

Figure 4.11 presents the simulated conversion rate curves as a solid line and the curve obtained with data from model in symbols (o). The fourth order Runge-Kutta method was used to obtain the conversion, using step of 5s and temperature controlled as a linear increment dependent on the heating rate from initial temperature 25 °C to 1100 °C.

The three curves presented as solid lines were assumed as experimental data, in which the peak temperatures (166.33 °C, 372.50 °C and 579.17 °C) and the peak conversion rates ($4.14 \times 10^{-3} \text{ s}^{-1}$, $2.83 \times 10^{-3} \text{ s}^{-1}$, and $2.17 \times 10^{-3} \text{ s}^{-1}$) were the experimental parameters applied in equation (4.14). The empirical constants in equation (4.14) were $x_2 = -0.1443969$, $x_3 = 1.0747335$, $y_2 = -0.1480546$, and $y_3 = 1.5536758$, obtained from Table 4.4 for $\beta = 10 \text{ °C/min}$. Then, considering the peak temperatures, peak conversion rates, and empirical constants in equation (4.14) each $\log A$ was determined, according to $9.9 \log \text{ s}^{-1}$, $9.9 \log \text{ s}^{-1}$, and $10 \log \text{ s}^{-1}$.

The empirical constants in equation (4.15) were $x_0 = 0.0177599$, $x_1 = 5.2488765$, $y_0 = 0.0628710$, and $y_1 = 8.04689$ obtained from Table 4.4, and with the values of $\log A$ from equation (4.14) were determined the following activation energies, 99.4 kJ/mol, 149.0 kJ/mol, and 200.7 kJ/mol. Comparing the determined values through the empirical correlations, equations (4.14) and (4.15), with those selected to simulate the curves (100, 150, and 200 kJ/mol), the percentage error between kinetic parameters was less than 1% for the three cases. It was also observed that the curves obtained with the kinetic parameters determined with the correlations fits very well with the simulated ones (Figure 4.11), with average deviation (AD) of 0.82%, 0.65%, and 1.87%, from left to right.

4.6.1. Application of the correlations in complex reaction schemes

In the thermal decomposition of lignocellulosic biomass, the cellulose reaction is dominant, and it is the component responsible for the highest amount of volatile released, and also, its chemical structure does not represent considerable changes among biomasses (Antal and Várhegyi, 1995). Thus, for the application of the independent parallel reactions scheme (IPRS), is accepted the use of cellulose activation energy in the range between 180 kJ/mol and 250 kJ/mol, and pre-exponential factor between 1×10^{10} and $1 \times 10^{20} \text{ s}^{-1}$ as shown in Figure 2.3 (section 2.4.4. *Independent parallel reactions scheme*). However, as the range is wide and the pseudo-component fraction is an important parameter in this selection, it will be presented two approaches to easily obtain the kinetic parameters.

The first one is selecting the activation energy for each pseudo-component, which could be the average value in the range cited in the section 2.4.4. *Parallel reactions scheme* (Figure 2.3), i.e., 125, 215, and 75 kJ/mol for hemicellulose, cellulose, and lignin, respectively. Then, depending on the biomass behavior and heating rate, is selected a desired peak temperature for each pseudo-component, e.g., 290–330 °C, 340–390 °C, 410–500 °C for hemicellulose, cellulose and lignin, respectively. Then, from Table 4.6 are obtained the constants x_0 , x_1 , y_0 , and y_1 , related to the heating rate used, and with equation (4.15) is determined the pre-exponential factor.

Therefore, the fit of the pseudo-component reactions will be only dependent on the fraction, which is 0.2 to 0.3 for hemicellulose, 0.4-0.5 for cellulose, and for lignin from 0.15 to 0.25. Finally, using equation (3.7) and equation (3.34) the complete reaction scheme is obtained.

The second approach to select the activation energy is the recommended by Vyazovkin et al. (2011), using isoconversional methods to obtain a first value of activation energy. After this process is repeated the steps previously presented to obtain the other kinetic parameters. The requirement to use default activation energies is due to the IPRS resemble a reaction composed by three or more one-step global reactions of first order, and the correlations were developed for obtaining the kinetic parameter of only one reaction of first order.

4.7. Results of the Consecutive Reactions Scheme in Inert and Oxidative Atmospheres

The biomass thermal decomposition is often modeled by isoconversional methods due to their easy application and rapid understanding. However, in the isoconversional methods is assumed a one-step global reaction scheme, which introduces errors and restrictions in the modeling. As presented in the section 4.4. *Isoconversional Method Results in Inert Atmosphere*, the model only represented data between 150 °C and 450°C, underestimating part of the experimental behavior. Also, in the section 4.5. *Isoconversional Method Results in Oxidative Atmosphere*, the activation energies as a function of conversion varied more than 100%, meaning that the process cannot be modeled by a one-step global reaction scheme.

Then, it is necessary a more complex scheme of reactions to represent the biomass thermal decomposition. As presented in the section 2.4.3. *Consecutive reactions scheme*, a

scheme constituted by two consecutive reactions is the commonly applied for biomass thermal decomposition. Nevertheless, in this investigation, when used the scheme of two consecutive reactions, the modeled data above 450 °C were underestimated, as showed in Figure 4.12.

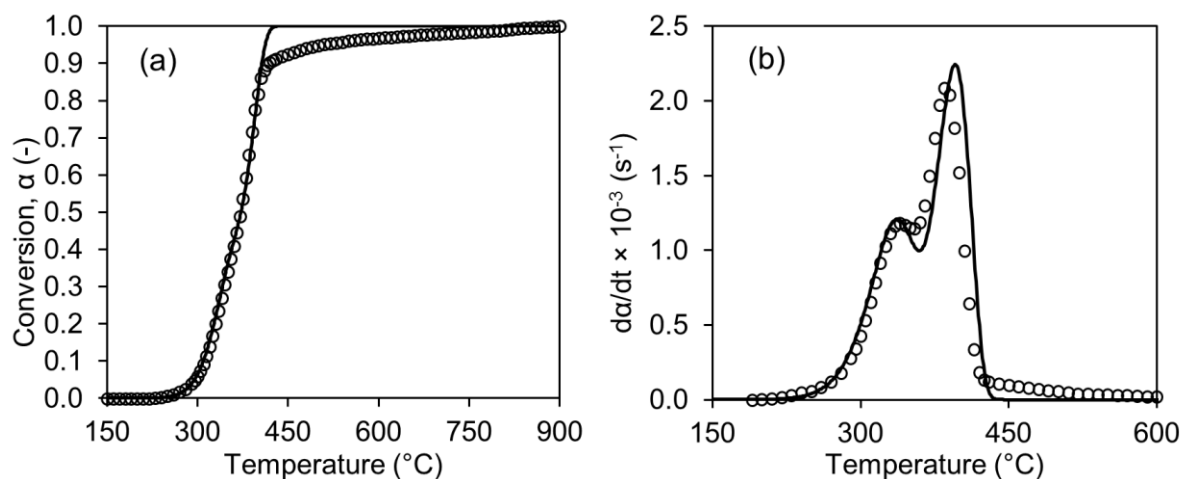


Figure 4.12. (a) Conversion and (b) conversion rate as a function of temperature at 10 °C/min in inert atmosphere applying two consecutive reactions. Experimental data in symbol (O), model in solid line.

Therefore, in order to overcome the underestimation problem and improve the kinetic model, one extra reaction was complement composing three consecutive reactions. Also, in the kinetic modeling of the biomass thermal decomposition through the consecutive reactions scheme were assumed all reactions with first order reaction model.

In both atmospheres analyzed, the activation energies of the three decomposition reactions remained equal for the different heating rates. In inert atmosphere, the activation energies were $E_1=133.774$ kJ/mol, $E_2=198.258$ kJ/mol, and $E_3=56.612$ kJ/mol for the four heating rates between 1.25 and 10 °C/min. In oxidative atmosphere, the activation energies $E_1=200$ kJ/mol, $E_2=350$ kJ/mol, and $E_3=100$ kJ/mol were obtained for the same heating rates. The activation energies in synthetic air were higher than nitrogen atmosphere for the same three consecutive reactions. This behavior could be explained by the fact that the conversion rate in oxidative atmosphere was nearly twice the amplitude in inert atmosphere.

In Table 4.5 and Table 4.6 are presented the pre-exponential factors, A , determined for each reaction considered in this scheme, as well as the constant values a_i applied in equations

(3.23) and (3.24) in inert and oxidant atmospheres, respectively. The average deviation (*AD*) remained lower than 3% for all heating rates in both atmospheres, which means that the parameters obtained provided a good agreement between experimental and theoretical data.

Table 4.5. Parameters of the consecutive reactions scheme in nitrogen atmosphere

Parameters	Heating Rate			
	1.25 °C/min	2.5 °C/min	5 °C/min	10 °C/min
E_1 (kJ/mol)			133.774	
E_2 (kJ/mol)			198.258	
E_3 (kJ/mol)			56.612	
A_1 (1/s)	1.979×10^9	2.305×10^9	2.336×10^9	2.336×10^9
A_2 (1/s)	5.671×10^{13}	5.728×10^{13}	5.375×10^{13}	4.450×10^{13}
A_3 (1/s)	0.689	0.547	2.315	7.163
a_1	1.000	1.000	1.000	1.000
a_2	0.727	0.727	0.720	0.703
a_3	0.256	0.250	0.277	0.261
a_4	0.095	0.125	0.175	0.186
<i>AD</i> (%)	2.476	2.590	2.715	1.994

Table 4.6. Parameters of the consecutive reactions scheme in synthetic air

Parameters	Heating rate (°C/min)		
	2.5	5	10
E_1 (kJ/mol)		200	
E_2 (kJ/mol)		350	
E_3 (kJ/mol)		100	
A_1 (1/s)	2.651×10^{16}	1.400×10^{16}	1.230×10^{16}
A_2 (1/s)	6.583×10^{28}	2.626×10^{28}	1.200×10^{28}
A_3 (1/s)	5.470×10^4	7.070×10^4	1.005×10^5
a_1	1.000	1.000	1.000
a_2	0.750	0.719	0.745
a_3	0.371	0.337	0.334
a_4	0.055	0.044	0.049
<i>AD</i> (%)	2.707	2.825	2.535

Figures 4.13 and 4.14 present the curves of conversion, conversion rate, and concentration as a function of temperature in inert atmosphere for the heating rates of 1.25 and 2.5 °C/min, and 5 and 10 °C/min, respectively.

Figures 4.13 (a) and (d) present the conversion as a function of temperature for heating rates of 1.25 and 2.5 °C/min. The theoretical conversion for both heating rates showed an excellent agreement with experimental conversion between 0.00 and 0.80 (150 to 380 °C). The model at 1.25 °C/min (Figure 4.13a) underestimated the data between 380 °C and 410

°C, but above this temperature the data was accurate and reliable. However, the model at 2.5 °C/min (Figure 4.13d) decreased its accuracy above 380 °C, reflected in fluctuations around the experimental conversion.

Figures 4.14 (a) and (d) present the conversion as a function of temperature for heating rates of 5.0 and 10 °C/min. In Figure 4.14a, the model at 5 °C/min was in agreement with the experimental data from 150 °C up to 600 °C (conversion of 0.95), and at higher temperatures the model underestimate the experimental behavior. The best representation was obtained at 10 °C/min (Figure 4.14d), in which the model described the thermal decomposition of sugarcane in inert atmosphere in the complete range of temperatures analyzed (150 °C – 900 °C). The differences in the quality of fitting and in the representation of the experimental data among heating rates is due to the use of the same activation energy for each one of the three reaction analyzed.

Figure 4.13 (b) and (e), and Figure 4.14 (b) and (e) present the conversion rate as a function of temperature at 1.25, 2.5, 5, and 10 °C/min, respectively in inert atmosphere. In these figures it is easy to recognize the main thermal decomposition stage, which was between 150 °C and 400 °C, and that the models for all heating rates represented this stage with accuracy.

Figure 4.13 (c) and (f), and Figure 4.14 (c) and (f) present the concentration of the analyzed reactions as a function of temperature at 1.25, 2.5, 5, and 10 °C/min, respectively. The thermal decomposition of *A* or dry biomass, for all heating rates, initiated at 150 °C and finished at 350 °C, in which the concentration [*A*] decreased while was forming the product *B* or torrefied biomass. The concentration [*B*] varied between 200 °C and 400 °C, which rapidly reach its maximum of 0.85 at ~300 °C, and above this temperature was decomposed forming the carbonaceous solid or product *C*. The biomass thermal decomposition turns very slow above 400°C, and therefore, the formation of product *D* (final solid residue at 900°C) from *C*. The concentration [*C*] increased from 300 °C to reach its maximum of 0.97 at 375 °C. Above this temperature, the product *D* increased slowly finishing its formation at 800 °C, as observed in the curve of concentration [*D*].

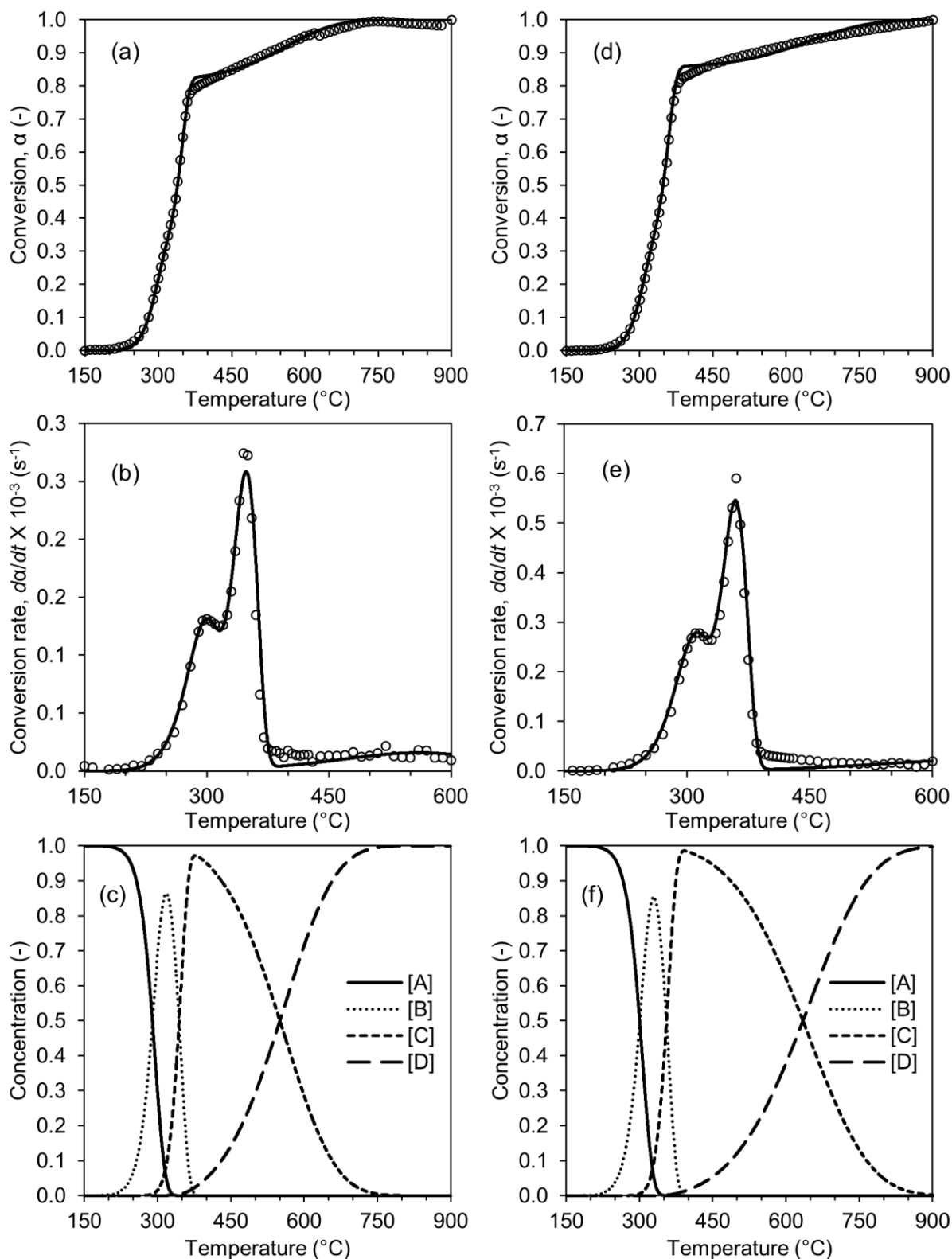


Figure 4.13. (a) and (d) Conversion; (b) and (e) Conversion rate, and (c) and (f) Concentration as a function of temperature in inert atmosphere. (a), (b), and (c) data at 1.25 °C/min. (d), (e), and (f) data at 2.5 °C/min.

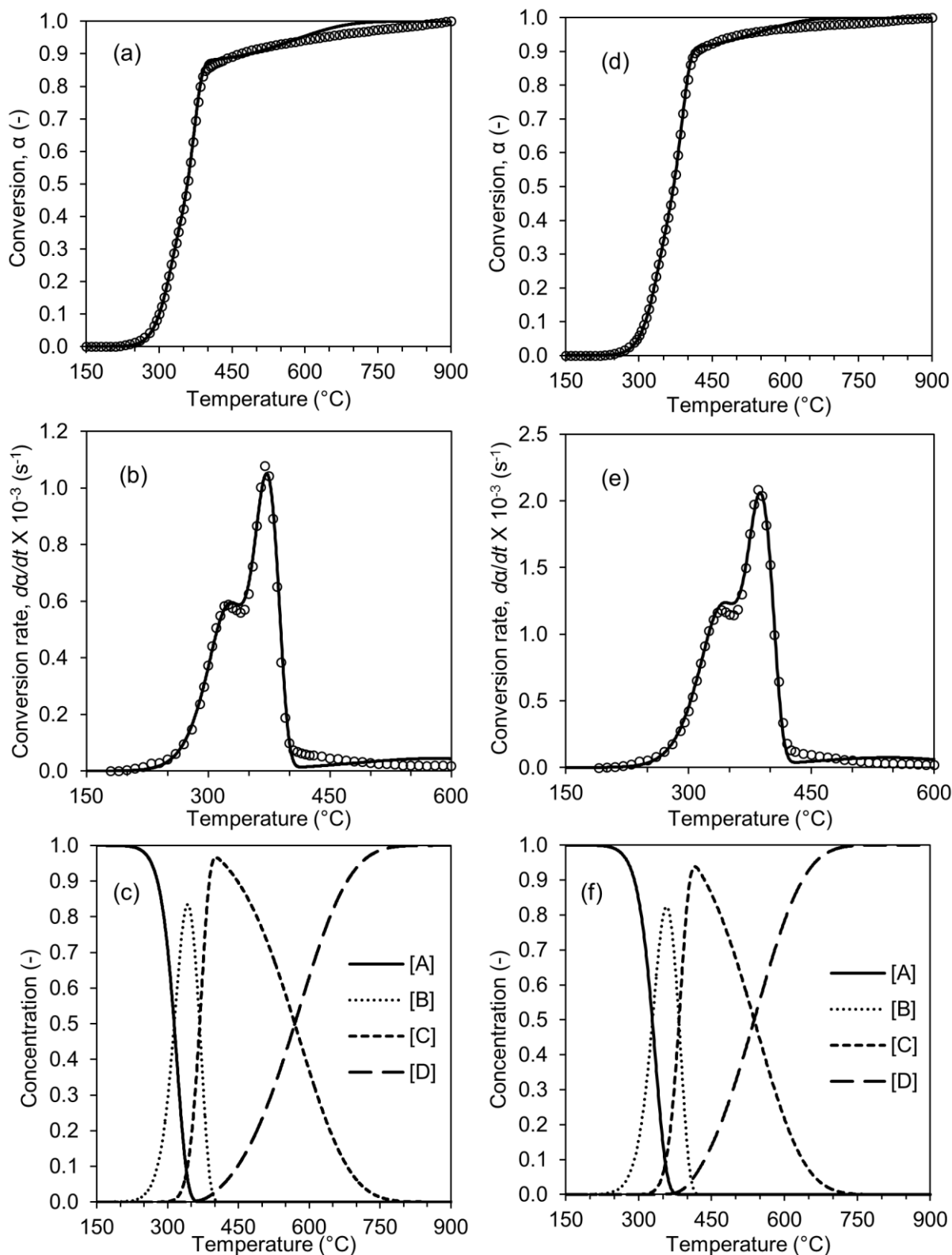


Figure 4.14. (a) and (d) Conversion; (b) and (e) Conversion rate, and (c) and (f) Concentration as a function of temperature in inert atmosphere. (a), (b), and (c) data at 5 °C/min. (d), (e), and (f) data at 10 °C/min.

Figures 4.15 and 4.16 presents the curves of conversion, conversion rate, and concentration as a function of temperature in oxidative atmosphere for the heating rates of 2.5 and 5 °C/min, and 10 °C/min, respectively.

Figure 4.15 (a) and (d), and Figure 4.16 (a) present the conversion as a function of temperature at 2.5, 5, and 10 °C/min, respectively. The modeled data for all heating rates underestimate the experimental behavior between 325 °C and 400 °C (between 0.6 and 0.7 of conversion). Above of the latest temperature the agreement between experimental and model data was accurate and reliable. The best representation of the experimental data was obtained at 10 °C/min (Figure 4.16a), describing the reactions in the complete range of temperatures analyzed (150 °C – 900 °C).

Figure 4.15 (b) and (e), and Figure 4.16 (b) present the conversion rate as a function of temperature at 2.5, 5, and 10 °C/min, respectively. In these figures are showed with more detail the underestimated data between 325 °C and 400 °C. However, it is also observed that the models applied for all the heating rates represented the smoldering reaction with high accuracy, since the average deviation was lower than 3% (Table 4.6) as recommended in literature (Orfão et al., 1999; Anca-Couce et al., 2014).

Figure 4.15 (c) and (f), and Figure 4.16 (c) present the concentration of the analyzed reactions in oxidative reactions as a function of temperature at 2.5, 5, and 10 °C/min, respectively. The thermal decomposition of *A* or dry biomass, for all heating rates, started at 150 °C and finished at 300 °C, in which the concentration [*A*] decreased while was forming the product *B* or torried biomass. The concentration [*B*] varied between 200 °C and 350 °C, which rapidly reach its maximum of 0.90 at 275 °C, and above this temperature was decomposing forming the carbonaceous solid or product *C*. The biomass thermal decomposition turns slow above 325 °C, and therefore, also the formation of product *D* (mineral matter - ash at 900°C) from *C*. The concentration [*C*] increased from 300 °C to reach its maximum of 0.97 at 325 °C, and above of this temperature the product *D* increased slowly finishing its formation at 500 °C, as observed in the curve of concentration [*D*].

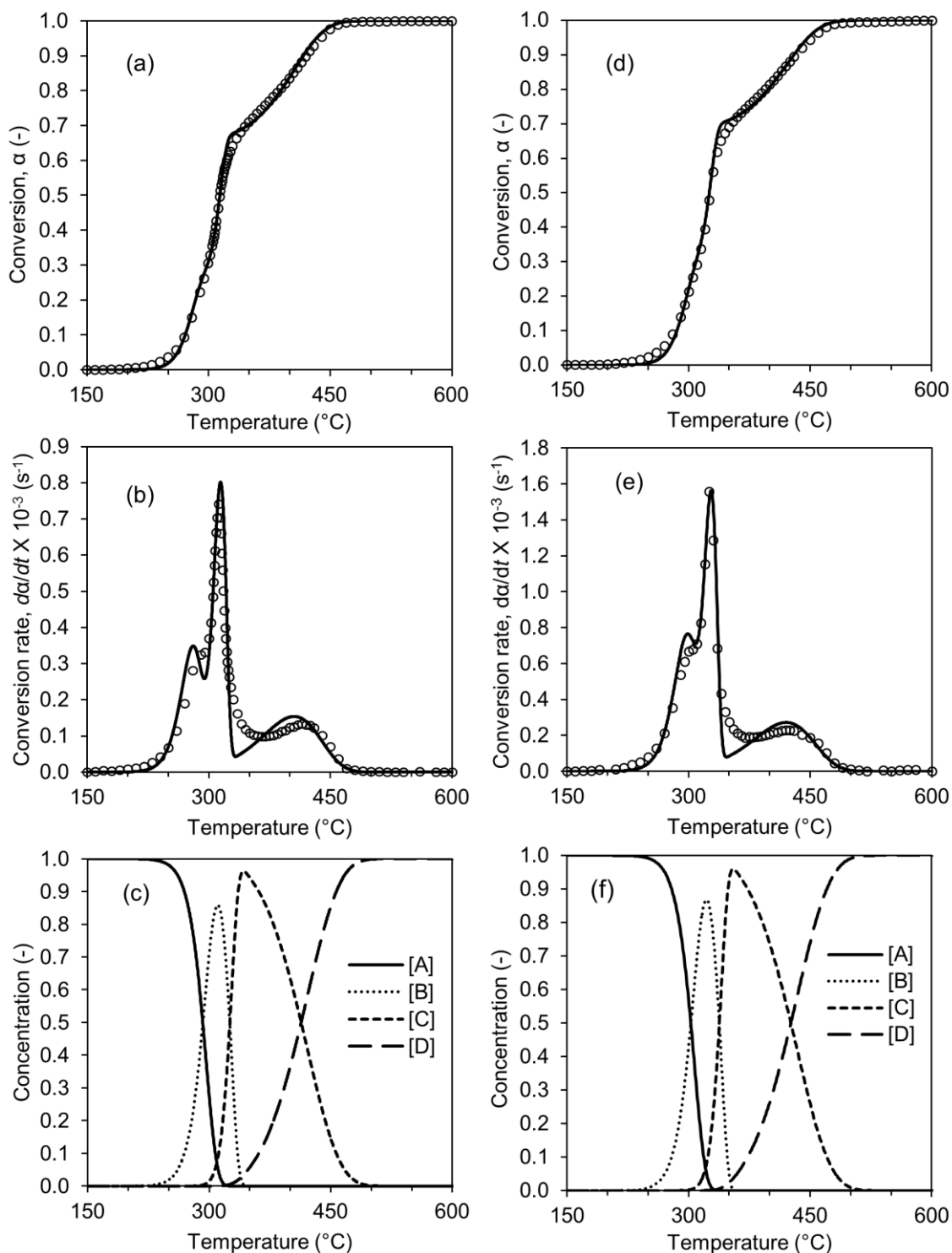


Figure 4.15. (a) and (d) Conversion; (b) and (e) Conversion rate, and (c) and (f) Concentration as a function of temperature in oxidative atmosphere. (a), (b), and (c) data at 2.5 °C/min. (d), (e), and (f) data at 5 °C/min.

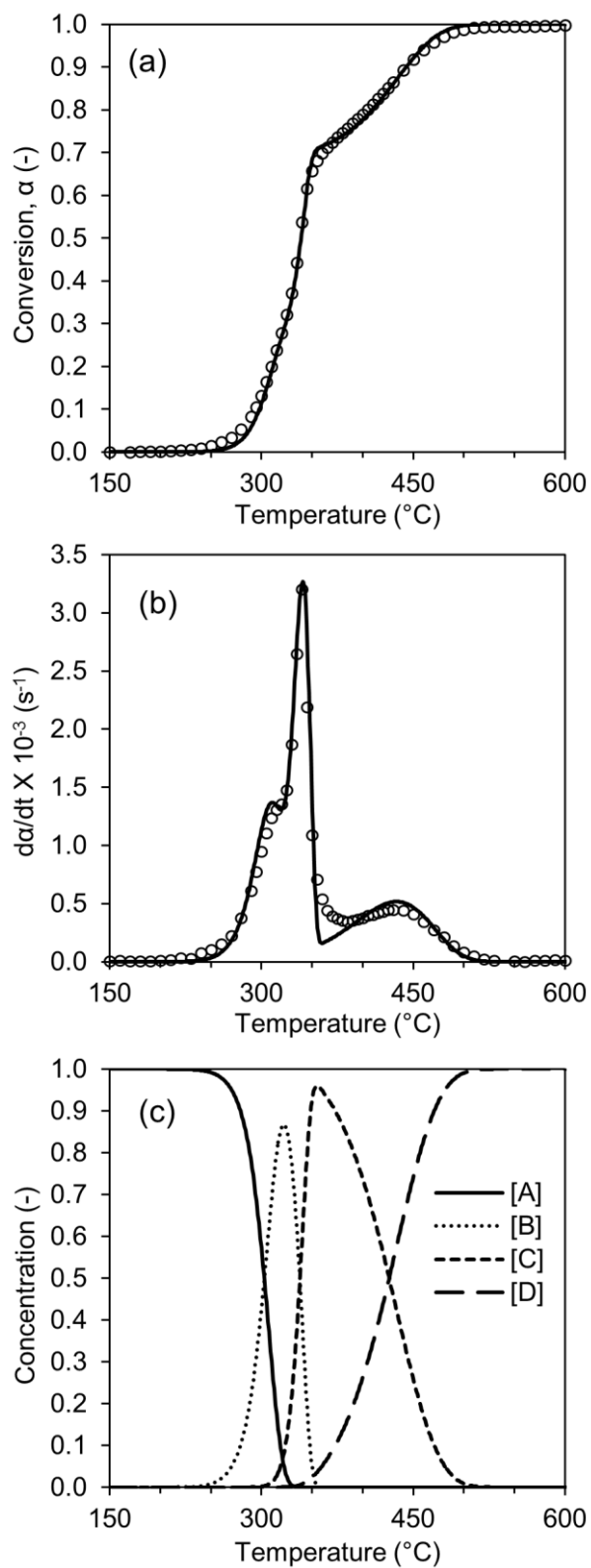


Figure 4.16. (a) Conversion; (b) Conversion rate, and (c) Concentration as a function of temperature at 10 $^{\circ}\text{C}/\text{min}$ in oxidative atmosphere

In conclusion, the results obtained analyzing the thermal decomposition of sugarcane straw through the consecutive reactions scheme showed to be accurate ($AD < 3\%$) and reliable for both atmospheres evaluated. In nitrogen (inert atmosphere), the modelled data were in agreement with the experimental conversion for all heating rates (1.25, 2.5, 5, and 10 °C/min), mainly in the devolatilization stage, considered the most important in biomass thermal decomposition. In synthetic air (oxidative atmosphere), also the modelled data described well the experimental conversion for all the heating rates evaluated.

4.8. Results of the Independent Parallel Reactions Scheme in Inert Atmosphere

The kinetic parameters determination was done using the two approaches previously detailed. In the first approach, were used as initial guess activation energies of 125, 215, and 75 kJ/mol for hemicellulose, cellulose, and lignin, respectively, which are the average values in the range obtained from literature (Anca-Couce et al., 2014; Barneto et al., 2010; Branca et al., 2005; Caballero et al., 1997; Grønli et al., 2002; Hu et al., 2007; Lira et al., 2010; Manara et al., 2015; Manyà et al., 2003; Naranjo et al., 2012; Órfão et al., 1999; Santos et al., 2012; Sun et al., 2011; Teng and Wei, 1998; Vamvuka et al., 2003). Table 4.7 presents the peak temperatures and constants used in equations (4.14) and (4.15) for the different heating rates to obtain the kinetic parameters related to the thermal decomposition of sugarcane straw by independent parallel reactions scheme. The constants y_0 and y_1 for the heating rates of 1.25 °C/min and 2.5 °C/min were determined according to the equations (4.8) and (4.9), respectively, since these heating rates are not included in Table 4.4.

In the second approach, was used the activation energy of 195 kJ/mol for cellulose pseudo-component, which is also in the literature range, and obtained by applying the isoconversional method of Ozawa (1965), detailed in Rueda-Ordóñez et al., (2013). For hemicellulose and lignin, the activation energies used were the same used previously 125 and 75 kJ/mol, respectively. In the application of this approach the parameters used in the correlations were the same presented in Table 4.7.

Figure 4.17 presents the conversion rate curves as a function of temperature for the heating rates of 1.25, 2.5, 5, and 10 °C/min. The first dotted curve concerns to the hemicellulose pseudo-component, which reaction temperature range is between 200 °C and 400 °C. The second dotted curve was related to the cellulose pseudo-component, located

between 300 °C and 410 °C, and the third was related to the lignin pseudo-component with reaction temperature range between 300 °C and 600 °C.

Table 4.7. Empirical parameters for the correlations proposed to obtain the kinetic parameters of sugarcane straw by independent parallel reactions scheme

Peak temperature (°C)				
β (°C/min)	1.25	2.5	5	10
Hemicellulose	295.0	305.4	319.1	333.3
Cellulose	346.3	357.7	370.1	385.9
Lignin	487.6	551.8	436.1	410.1
Constants for Eq. (14)				
β (°C/min)	1.25 ^{a,b}	2.5 ^{a,b}	5	10
x_0	0.017747	0.017747	0.0177541	0.0177599
y_0	0.077898	0.072929	0.0681175	0.0628710
x_I	5.271271	5.271271	5.2564995	5.2488765
y_I	13.27200	11.50667	9.6425677	8.0468956

^a y_0 determined by Eq.(4.8), ^b y_I determined by Eq. (4.9)

For the determination of the average deviation the maximum experimental conversion rates were $0.2817 \times 10^{-3} \text{ s}^{-1}$, $0.5913 \times 10^{-3} \text{ s}^{-1}$, $1.081 \times 10^{-3} \text{ s}^{-1}$ and $2.085 \times 10^{-3} \text{ s}^{-1}$ for the heating rates of 1.25, 2.5, 5, and 10 °C/min, respectively. The modeled curves obtained with both approaches fitted very well with the experimental data, presenting an average deviation (*AD*) less than 3%, which indicates a very good agreement, since the acceptable values must achieve $AD \leq 5\%$. Table 4.8 presents the kinetic parameters obtained through the different approaches. The cellulose activation energy varied between 195 kJ/mol and 212 kJ/mol, due to the two approaches applied. The hemicellulose and lignin activation energies were 142 kJ/mol and 40 kJ/mol, respectively, for both approaches.

Also, the so-called compensation effect, widely discussed by Di Blasi (2008) and White et al. (2011), is easily avoided with the correlations here presented, just knowing the activation energy at a certain heating rate for each pseudo-component reaction. Then, applying equation (4.15) is determined the $\log A$ related to the peak temperature at different heating rates, depending on the fraction for the best fitting.

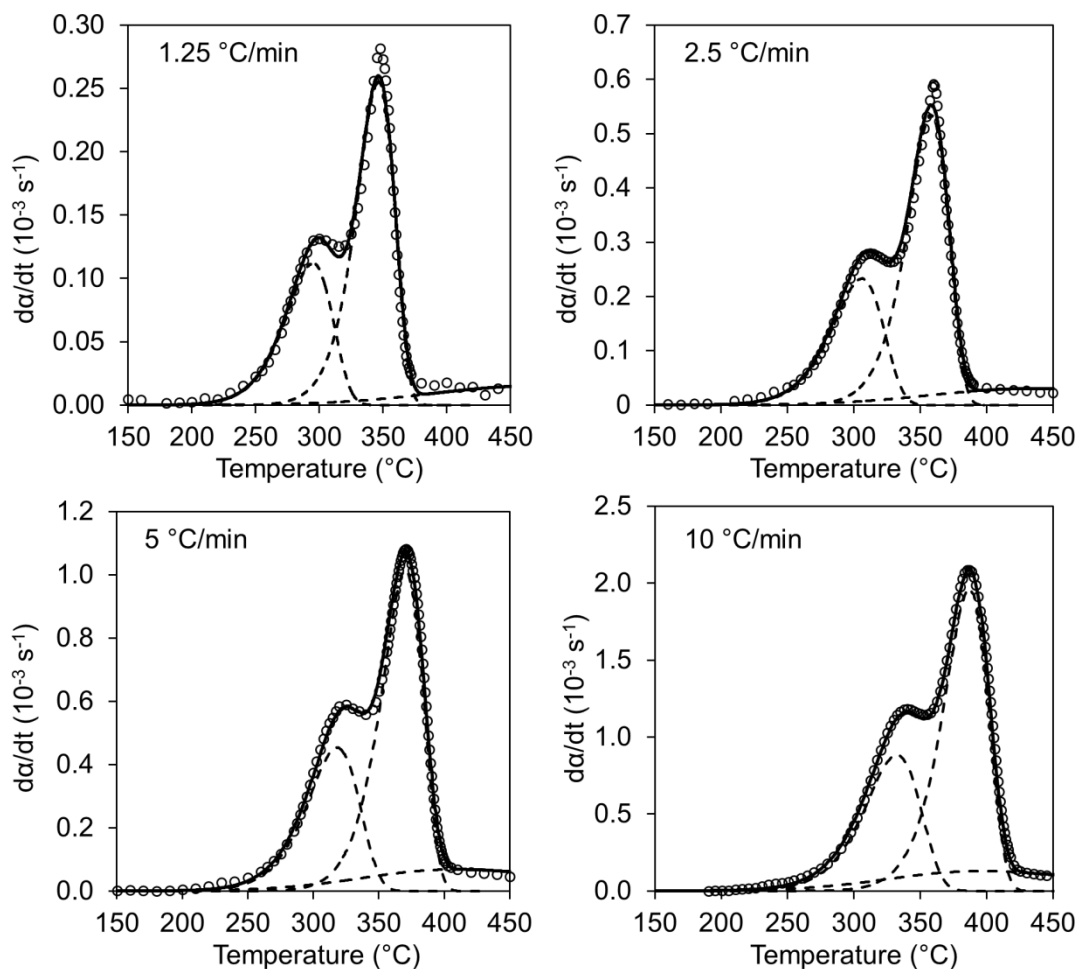


Figure 4.17. Conversion rate curves as a function of temperature for different heating rates. Experimental data in symbol (o), IPRS model as a solid line and pseudo-components as dotted lines.

Table 4.8. Kinetic parameters of sugarcane straw

First approach			
Parameter	Hemicellulose	Cellulose	Lignin
E (kJ/mol)	142.00±0.00	212.00±0.00	40.00±0.00
logA (logs ⁻¹)	10.13±0.03	14.92±0.10	-0.47±0.66
<i>F</i> *	0.28±0.01	0.51±0.01	0.21±0.02
<i>AD</i> (%)	1.8		
Second approach			
Parameter	Hemicellulose	Cellulose	Lignin
E (kJ/mol)	142.00±0.00	195.00±0.00	40.00±0.00
logA (logs ⁻¹)	10.13±0.09	13.50±0.10	-0.47±0.47
<i>F</i> *	0.27±0.01	0.54±0.01	0.20±0.02
<i>AD</i> (%)	2.1		

*Volatilized fraction concerning to each pseudo-component

Here was not addressed the following subjects, reaction order and reaction model, since the biomass pyrolysis reaction can be well modeled through a scheme of three independent reactions of first order reaction model. Therefore, the ranges of activation energy and fraction will change if is used other reaction schemes, as the reaction order is increased the conversion rate amplitude is decreased. Nonetheless, the correlation obtained between activation energy, $\log A$, and peak temperature (equation 4.15) is not affected by this effect, it means that can be globally used for different reaction orders.

Finally, it is recommended to work in the activation energy range of 100-150 kJ/mol, 180-250 kJ/mol, and 40-100 kJ/mol for hemicellulose, cellulose, and lignin, respectively. For the hemicellulose, the fraction suggested is between 0.20 and 0.35, for cellulose between 0.35 and 0.55, and lignin between 0.15-0.35. These fractions depend on the biomass nature, and therefore, the kinetic parameters are also influenced, being this the main reason to remain undefined an activation energy globally accepted, generating large variation in the literature results as showed in Figure 2.3 (Section 2.4.4. *Independent parallel reactions scheme*).

4.9. Results of the Independent Parallel Reactions Scheme in Oxidative Atmosphere

The smoldering reaction of sugarcane straw could not be modeled by isoconversional kinetics for one-step global reaction, suggesting that a complex kinetic pathway would improve the description of the thermal decomposition in synthetic air. Thus, based on the independent parallel reactions scheme, three reactions for the oxidative pyrolysis and other three reactions for the combustion of the carbonaceous residue, were suggested.

The kinetic pathway is detailed in Figure 4.18 following the model proposed by Amutio et al. (2012) for the thermal decomposition reaction in oxidative atmosphere. The oxidative pyrolysis reaction was divided into three reactions of devolatilization corresponding to the main components of lignocellulosic biomass (hemicellulose-HC, cellulose-C, and lignin-L). From the three reactions of the oxidative pyrolysis stage, it was assumed that the carbonaceous solid residue was composed by amounts provided by each biomass component. Therefore, for the combustion reaction was assumed three reactions of the carbonaceous solid contributions in oxidative pyrolysis stage.

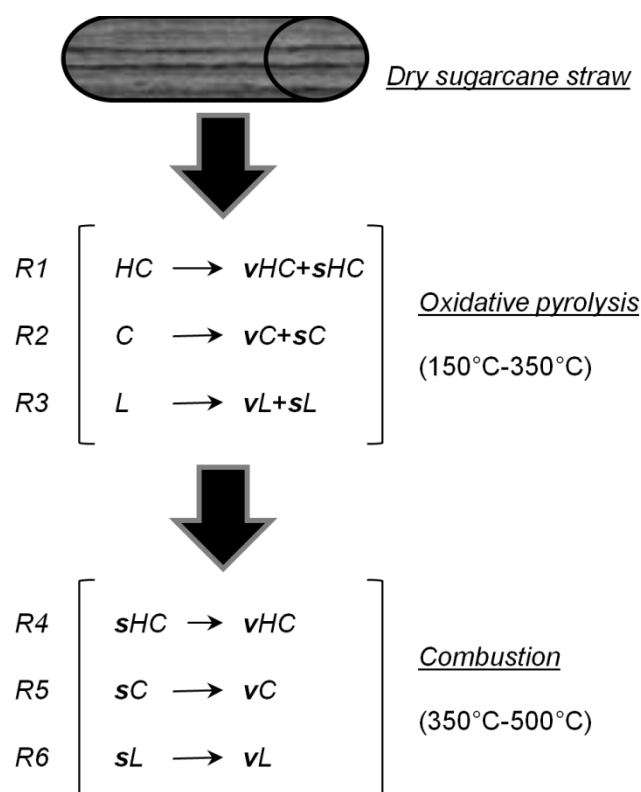


Figure 4.18. Independent parallel reaction scheme for biomass smoldering reaction.

The determination of the kinetic parameters by independent parallel reactions must have a first guess that was obtained from the results with the isoconversional method of Vyazovkin. Thus, for the oxidative pyrolysis stage, the activation energies applied as first guess were 148 kJ/mol ($\alpha=0.15$), 352 kJ/mol ($\alpha=0.95$), and 172 kJ/mol (average) for HC, C, and L reactions, respectively. In the combustion stage was assumed only the activation energy of 159 kJ/mol ($\alpha=0.95$) due to the high variation observed with conversion and the low conversion rate. The determination of $\log A$ was carried out with equation (4.15), using peak temperatures between 250–350 °C, 300–350 °C, 300–400 °C, 350–400 °C, 400–450 °C, and 450–500 °C for the six reactions, respectively for all heating rates.

Table 4.9 presents the kinetic parameters obtained for the six reactions. The reaction 1 (R1), reaction 2 (R2), and reaction 3 (R3) were related to the oxidative pyrolysis of the hemicellulose, cellulose, and lignin fractions, respectively. The activation energies presented in Table 2 for R1, R2, and R3 were 176, 313, and 150 kJ/mol, respectively. The values of R1 and R3 were in the same magnitude order reported by Amutio et al. (2012) for these reactions, according to 133 and 62 kJ/mol for pinewood sawdust.

Nonetheless, the activation energy of R2 (cellulose) was higher than the commonly published in literature, such as 206 kJ/mol by Amutio et al. (2012), 150.37 kJ/mol for Esparto grass, 239.63 kJ/mol for straw, and 255.98 kJ/mol for Posidonea Oceanica by Conesa and Domene (2011). This high activation energy of cellulose does not affect the overall results, since the fitting was very good, meaning that for a mathematical modeling of the process, these data will provide reliable and accurate results. However, from the kinetic point of view, there is no evidence of such value of activation energy for the real cellulose smoldering reaction.

Table 4.9. Kinetic parameters of smoldering reaction of sugarcane straw

Reactions	E (kJ/mol)	logA (log s ⁻¹)	F*
R1	176.00	14.00±0.00	0.20
R2	313.00	25.33±0.35	0.40
R3	150.00	10.30±0.00	0.10
R4	80.00	3.70±0.00	0.08
R5	150.00	8.36±0.10	0.08
R6	100.00	4.77±0.21	0.15

*Pseudo-component volatilized fraction

Comparing the results obtained for the thermal decomposition of sugarcane straw in nitrogen atmosphere (section 4.8 *Results of the Independent Parallel Reactions Scheme in inert atmosphere*), the activation energy in the oxidative pyrolysis stage were significantly higher. The activation energies in nitrogen atmosphere were 142 kJ/mol, 212 kJ/mol, and 40 kJ/mol for the pseudo-components hemicellulose (R1), cellulose (R2), and lignin (R3), respectively. The activation energy of the R2 and R3 in the atmosphere of synthetic air was around 100 kJ/mol higher than in nitrogen atmosphere. This effect is due to the differences in reaction rates between atmospheres as observed in Fig. 1, since in synthetic air, the peak reaction rate is almost twice the value in nitrogen, and therefore, requiring more energy.

Table 4.9 presents the kinetic parameters obtained for the reaction 4 (R4), reaction 5 (R5), and reaction 6 (R6) corresponding to the combustion of the hemicellulose, cellulose, and lignin fractions, respectively. The activation energies presented in Table 4.9 for R4, R5, and R6 were 80 kJ/mol, 150 kJ/mol, and 100 kJ/mol, respectively. These activation energies were lower than those obtained in the oxidative pyrolysis, because the conversion rate in this stage (combustion) was considerably lower than the previous stage (oxidative pyrolysis).

Also, in Table 4.9 the kinetic parameters remained equal for all the heating rates evaluated, which means that the transport phenomena effects by contact between particles and intra-particles thermal conduction were successfully avoided.

The volatilized fractions in Table 4.9 represent the summation of the amounts of each biomass component, in which R1 and R4, R2 and R5, and R3 and R6, were the amounts of hemicellulose, cellulose, and lignin, respectively. For hemicellulose, the volatilized fractions of R1 and R4 were 0.20 and 0.08, respectively, corresponding to 28% of this component in the sugarcane straw composition. For cellulose, the volatilized fraction of R2 was 0.40 and 0.08 for R5, which correspond to a 48%. For lignin was 25% concerning to the volatilized fraction of R3 and R6 of 0.10 and 0.15, respectively. This theoretical sugarcane straw composition corresponded to the variation of the experimental data presented previously (Section 4.1. *Biomass Characterization*) according to 18.4–28.9% hemicellulose, 33.3–36.1% cellulose, and 25.8–40.7% lignin.

Figure 4.19 presents the conversion rate curves as a function of temperature, for the different heating rates analyzed. The temperature intervals concerning reaction 1, reaction 2, and reaction 3 were 200–350 °C, 250–330 °C, and 250–400 °C, respectively, for all the heating rates. These temperature ranges are in agreement with literature (Santos et al., 2012; Amutio et al., 2013; Anca-Couce et al., 2014) to describe the pyrolysis stage with three independent parallel reactions. The temperature ranges for the combustion stage, described by the reaction 4, reaction 5, and reaction 6 were 300–500 °C, 300–500 °C, and 350–550 °C, respectively, for all the heating rates.

Finally, Figure 4.19 shows the comparison between experimental and modeled curves of conversion rate as a function of temperature. It can be observed that the agreement between curves is very good, reflecting the average deviation percentage of 2.762%, 2.212%, and 1.499% for 2.5 °C/min, 5 °C/min, and 10 °C/min, respectively. These results show that the kinetic parameters could be used in mathematical models to predict different processes involving smoldering reaction of sugarcane straw.

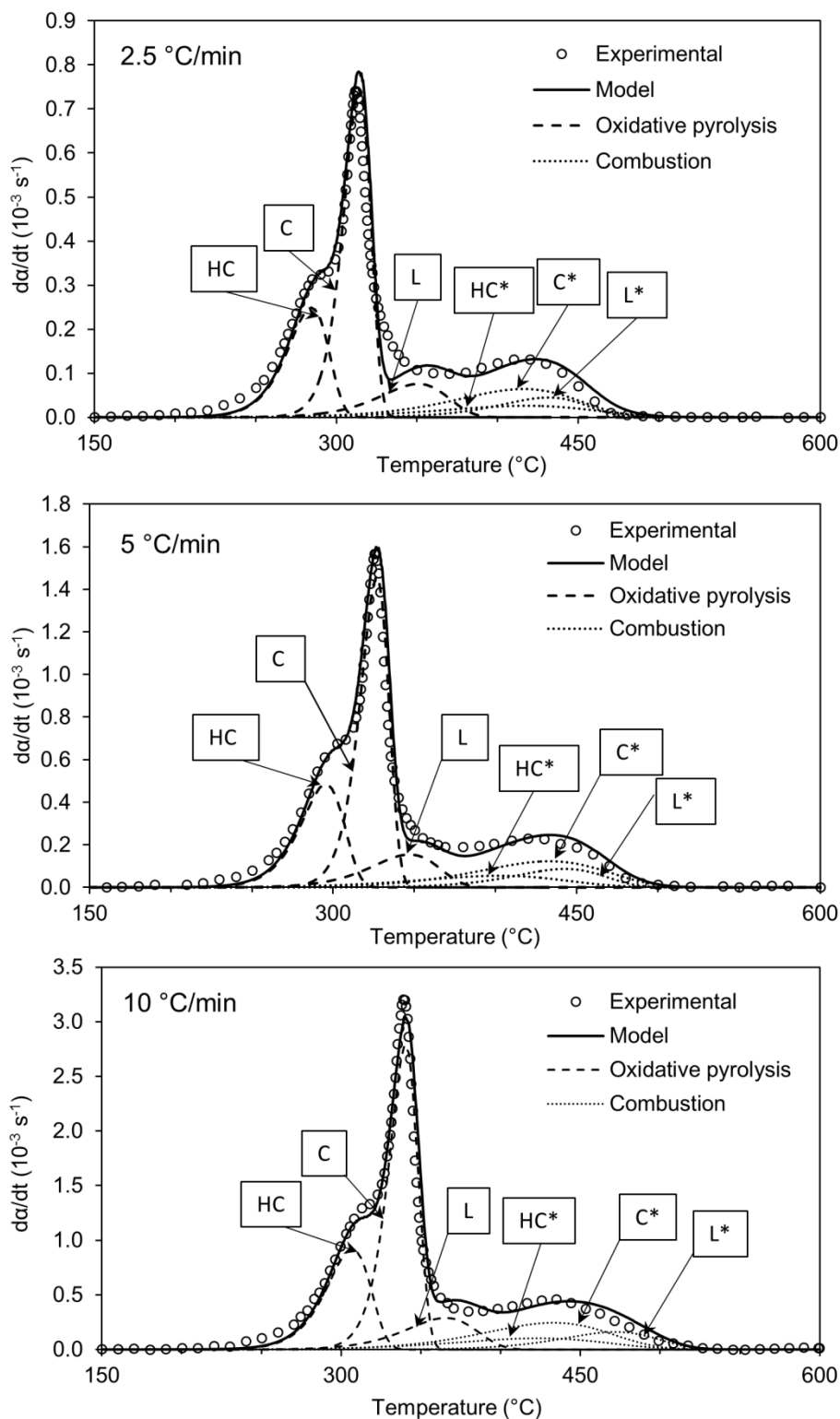


Figure 4.19. Conversion rate as a function of temperature obtained with the independent parallel reaction scheme. The capital letters HC, C, and L are related to hemicellulose, cellulose, and lignin, respectively. The symbol (*) represent combustion reaction

4.10. Summary of the Kinetic Analysis of Thermal Decomposition of Sugarcane Straw

In this investigation were studied three kinetic pathways for modeling the thermal decomposition of sugarcane straw in inert and oxidative atmospheres, which were global reaction, consecutive reactions, and parallel reactions. In order to conclude this investigation were summarized all the results concerning to the kinetic modeling. Tables 4.10 and 4.11 presents the summary of the kinetic analysis results in nitrogen and in synthetic air, respectively.

Table 4.10. Summary of the results of the kinetic analysis in nitrogen

Kinetic scheme	Mathematical representation	Parameters
Global Reaction $A(s) \xrightarrow{K} B(g) + C(s)$	$\frac{d\alpha}{dt} = k[f(\alpha)]$	$E=149.71$ kJ/mol $A=1.82 \times 10^9$ 1/s $f(\alpha)=[-\ln(1-\alpha)]^{-1}$
3 Consecutive Reactions $A(s) \xrightarrow{K_1} B(s) + V_I(g)$ $B(s) \xrightarrow{K_2} C(s) + V_{II}(g)$ $C(s) \xrightarrow{K_3} D(s) + V_{III}(g)$	$\frac{d[A]}{dt} = -k_1[A]$ $\frac{d[B]}{dt} = k_1[A] - k_2[B]$ $\frac{d[C]}{dt} = k_2[B] - k_3[C]$ $\frac{d[D]}{dt} = k_3[C]$ $W = a_1[A] + a_2[B] + a_3[C] + a_4[D]$ $\frac{d[W]}{dt} = a_1 \frac{d[A]}{dt} + a_2 \frac{d[B]}{dt} + a_3 \frac{d[C]}{dt} + a_4 \frac{d[D]}{dt}$	$E_1=133.77$ kJ/mol $E_2=198.26$ kJ/mol $E_3=56.61$ kJ/mol $A_1=2.24 \times 10^9$ 1/s $A_2=5.31 \times 10^{13}$ 1/s $A_3=3.39 \times 10^0$ 1/s $a_1=1.0$ $a_2=0.72$ $a_3=0.26$ $a_4=0.15$
3 Parallel reactions $A(s) \xrightarrow{k_1} B(s) + V_I(g)$ $A(s) \xrightarrow{k_2} C(s) + V_{II}(g)$ $A(s) \xrightarrow{k_3} D(s) + V_{III}(g)$	$\left(\frac{d\alpha}{dt}\right)_A = F_1 \left(\frac{d\alpha}{dt}\right)_B + F_2 \left(\frac{d\alpha}{dt}\right)_C + F_3 \left(\frac{d\alpha}{dt}\right)_D$ $\left(\frac{d\alpha}{dt}\right)_B = k_1[f(\alpha)]_1$ $\left(\frac{d\alpha}{dt}\right)_C = k_2[f(\alpha)]_2$ $\left(\frac{d\alpha}{dt}\right)_D = k_3[f(\alpha)]_3$ $\alpha_A = F_1 \alpha_B + F_2 \alpha_C + F_3 \alpha_D$	$E_1=142.0$ kJ/mol $E_2=212.0$ kJ/mol $E_3=40.0$ kJ/mol $A_1=1.35 \times 10^{10}$ 1/s $A_2=8.32 \times 10^{14}$ 1/s $A_3=3.39 \times 10^{-1}$ 1/s $F_1=0.28$ $F_2=0.51$ $F_3=0.21$

Table 4.11. Summary of the results of the kinetic analysis in synthetic air

Kinetic scheme	Mathematical representation	Parameters
Global Reaction $A(s) \xrightarrow{K} B(g) + C(s)$	$\frac{d\alpha}{dt} = k[f(\alpha)]$	-
3 Consecutive Reactions $A(s) \xrightarrow{K_1} B(s) + V_I(g)$ $B(s) \xrightarrow{K_2} C(s) + V_{II}(g)$ $C(s) \xrightarrow{K_3} D(s) + V_{III}(g)$	$\frac{d[A]}{dt} = -k_1[A]$	$E_1=200.0$ kJ/mol
	$\frac{d[B]}{dt} = k_1[A] - k_2[B]$	$E_2=350.0$ kJ/mol
	$\frac{d[C]}{dt} = k_2[B] - k_3[C]$	$E_3=100.0$ kJ/mol
	$\frac{d[D]}{dt} = k_3[C]$	$A_1=1.76 \times 10^{16}$ 1/s
	$W = a_1[A] + a_2[B] + a_3[C] + a_4[D]$	$A_2=3.47 \times 10^{28}$ 1/s
	$\frac{d[W]}{dt} = a_1 \frac{d[A]}{dt} + a_2 \frac{d[B]}{dt} + a_3 \frac{d[C]}{dt} + a_4 \frac{d[D]}{dt}$	$A_3=7.53 \times 10^4$ 1/s
		$a_1=1.0$
		$a_2=0.74$
		$a_3=0.35$
		$a_4=0.05$
6 Parallel reactions $A(s) \xrightarrow{k_1} B(s) + V_I(g)$ $A(s) \vdots \vdots \vdots$ $A(s) \xrightarrow{k_6} G(s) + V_{VI}(g)$	$\left(\frac{d\alpha}{dt}\right)_A = F_1 \left(\frac{d\alpha}{dt}\right)_B + F_2 \left(\frac{d\alpha}{dt}\right)_C + F_3 \left(\frac{d\alpha}{dt}\right)_D$ $+ F_4 \left(\frac{d\alpha}{dt}\right)_E$ $+ F_5 \left(\frac{d\alpha}{dt}\right)_F + F_6 \left(\frac{d\alpha}{dt}\right)_G$	$E_1=176.0$ kJ/mol
		$E_2=313.0$ kJ/mol
		$E_3=150.0$ kJ/mol
		$E_4=80.0$ kJ/mol
		$E_5=150.0$ kJ/mol
		$E_6=100.0$ kJ/mol
	$\left(\frac{d\alpha}{dt}\right)_B = k_1[f(\alpha)]_1$	$A_1=1.0 \times 10^{14}$ 1/s
	$\left(\frac{d\alpha}{dt}\right)_C = k_2[f(\alpha)]_2$	$A_2=2.14 \times 10^{25}$ 1/s
	$\left(\frac{d\alpha}{dt}\right)_D = k_3[f(\alpha)]_3$	$A_3=2.0 \times 10^{10}$ 1/s
	$\left(\frac{d\alpha}{dt}\right)_E = k_4[f(\alpha)]_4$	$A_4=5.01 \times 10^3$ 1/s
$\left(\frac{d\alpha}{dt}\right)_F = k_5[f(\alpha)]_5$	$A_5=2.29 \times 10^8$ 1/s	
$\left(\frac{d\alpha}{dt}\right)_G = k_6[f(\alpha)]_6$	$A_6=5.88 \times 10^4$ 1/s	
$\alpha_A = F_1\alpha_B + F_2\alpha_C + F_3\alpha_D + F_4\alpha_E + F_5\alpha_F + F_6\alpha_G$	$F_1=0.20$	
	$F_2=0.40$	
	$F_3=0.10$	
	$F_4=0.08$	
	$F_5=0.08$	
	$F_6=0.15$	

4.11. Heat of Reaction in Nitrogen and Synthetic Air Atmospheres

The heat of reaction of the thermal decomposition of sugarcane straw in nitrogen and synthetic air atmospheres was determined experimentally from DSC measurements presented in Figure 4.20.

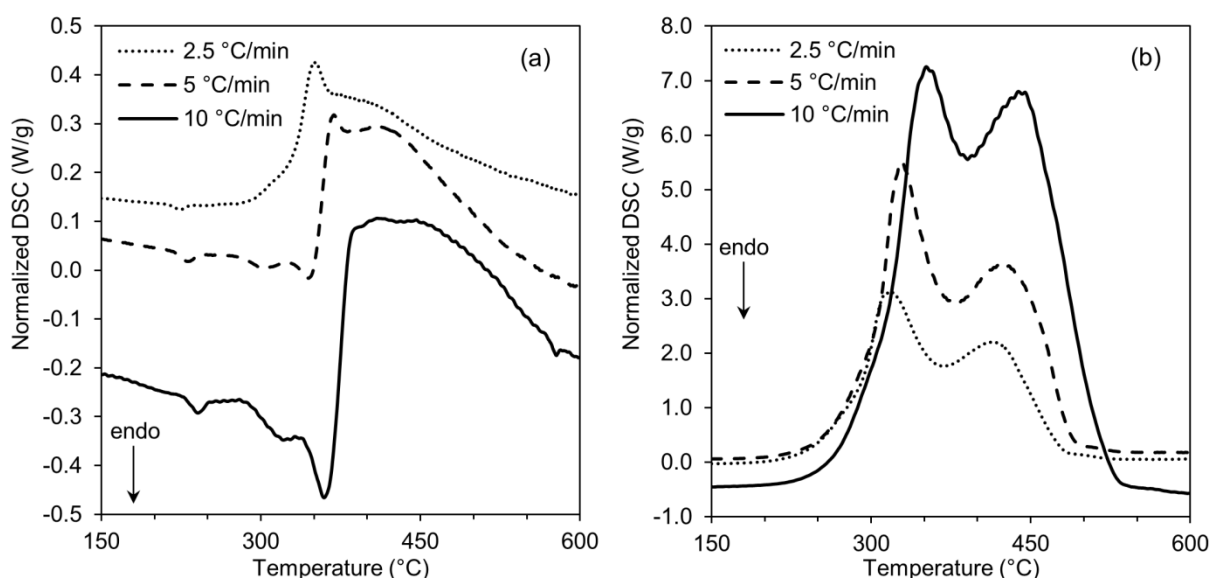


Figure 4.20. Experimental heat measurements obtained with DSC of the thermal decomposition of sugarcane straw in atmosphere of (a) Nitrogen, and (b) Synthetic air.

In Figure 4.20a is presented the curves of DSC for nitrogen atmosphere at 2.5 °C/min, 5 °C/min, and 10 °C/min. The DSC curve was characterized by three endothermic peaks between 200 °C and 400 °C, corresponding to the sugars, hemicellulose, and cellulose decomposition reactions. The peaks related to the sugars appear at 225.4, 231.4, and 240.5 °C for the three heating rates, respectively. The endothermic peaks related to hemicellulose and cellulose reactions were not well detailed at 2.5 and 5 °C/min, while at 10 °C/min are well marked at 321.1 and 359.3 °C. An exothermic peak appears for the heating rates of 2.5 and 5 °C/min at 350.1 and 368.4 °C concerning to the decomposition reaction of lignin, however, this peak at 10 °C/min was imperceptible.

Figure 4.20b presents the curves of DSC for synthetic air atmosphere at the different heating rate applied. The DSC curve was characterized by two exothermic peaks between 200 and 500 °C concerning to the oxidative pyrolysis and combustion stages, respectively. The peak temperatures of oxidative pyrolysis were 316.5, 327.3, and 351.8 °C at 2.5, 5, and 10

°C/min, respectively. The peak temperatures of combustion were 413.4, 422.5, and 438.2 °C, for the same heating rates, respectively. These results confirm the existence of two different stages of thermal decomposition.

In Fig. 4.20b it was also observed that the first peak was higher than the peak of the combustion stage. The heat released by the sample oxidation contributes to the rapid increasing in the sample temperature providing a fast conversion rate. Therefore, the decomposition temperature was lower than in nitrogen, explaining the large differences between atmospheres observed in Fig. 1 for the sugarcane straw thermal.

Finally, the heat of reaction as a function of temperature determined for the thermal decomposition of sugarcane straw is presented in Figure 4.21. In the analysis of the atmosphere of nitrogen, the reaction was endothermic for the main volatile release stage (i.e., between 150 and 350 °C), as presented in Figure 4.21a. Then, in this figure, the heat of reaction was defined as the heat required for the pyrolysis reaction, which was 945 kJ/kg at 350 °C, and remained constant up to 500 °C. Figure 4.21b presents the heat released as a function of temperature for the thermal decomposition of sugarcane straw in synthetic air atmosphere.

The heat released by the combustion of the sugarcane straw reached 8 MJ/kg. This value was almost half of the higher heating value (18.6 MJ/kg). This behavior can be explained due to the following aspects:

- (1) Pure oxygen (White Martins, $O_2=99.99\%$, Air<20ppm) was used in the bomb calorimeter, while in the DSC analyzer was synthetic air (White Martins, $X_{oxygen}=20.00\pm 0.05\%$ e $X_{nitrogen}=80.00\pm 0.05\%$);
- (2) DSC heat flux measurement was non-isothermal at very low heating rates <20 °C/min, while in the bomb calorimeter the combustion reaction is extremely fast;
- (3) The synthetic air used in the DSC analyzer is at atmospheric pressure, while the bomb calorimeter uses pressure of 30 kgf/cm².

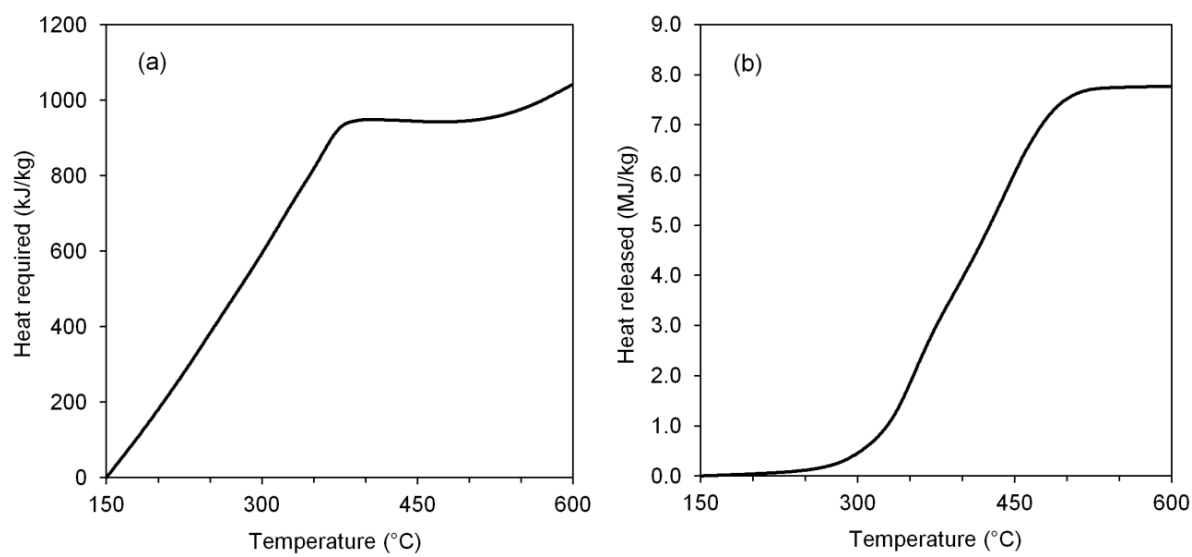


Fig. 4.21. Heat of reaction as a function of temperature for the thermal decomposition of sugarcane straw in atmosphere of (a) Nitrogen, and (b) Synthetic air.

CONCLUSIONS

The thermal decomposition of sugarcane straw presented three stages in the two atmospheres analyzed (i) in nitrogen, were drying, devolatilization, and carbonization; (ii) in synthetic air, were drying, oxidative pyrolysis (devolatilization), and combustion of the remaining carbonaceous solid.

The thermal decomposition of sugarcane straw in nitrogen could be mathematically well represented through the assumption of one-step global reaction, with the reaction model corresponding to a two-dimensional diffusion, $f(\alpha)=[-\ln(1-\alpha)]^{-1}$, pre-exponential factor of $1.82 \times 10^9 \text{ s}^{-1}$, and activation energy of 149.7 kJ/mol. However, the assumption of this kinetic scheme involved some restrictions:

- (a) The experimental data was represented only in the normalized mass range between 0.3 and 0.9 corresponding to the devolatilization step, i.e., hemicellulose and cellulose thermal decomposition, occurring between 150 and 450 °C.
- (b) This scheme did not describe the experimental behavior above the main devolatilization step, normally corresponding to the lignin decomposition (15% of the volatilized mass).

The analysis of the thermal decomposition in synthetic air through one-step global reaction resulted in large variation of activation energy, and therefore, allows concluding that is not possible to describe mathematically this process by this kinetic pathway.

The application of the kinetic scheme of three consecutive reactions for modeling the thermal decomposition in nitrogen and synthetic air showed to be a representative kinetic pathway, since it was obtained a very good agreement between experimental and modeled data for both atmospheres. Nevertheless, if is applied a kinetic scheme of two consecutive reactions, as widely recommended in literature, the modeling presented the same restrictions when analyzed as one-step global reaction, and therefore, is not a recommendable kinetic pathway.

The fitting method for one-step global reactions with first-order reaction model could be used accurately through the application of the empirical correlations developed in this work. Also, these correlations showed to be useful in the accurate and reliable determination of the kinetic parameters in complex kinetic schemes.

The thermal decomposition of sugarcane straw in nitrogen and synthetic air was mathematically well represented through the kinetic scheme of three and six parallel first-order reactions, respectively. The application of this kinetic pathway provided results without any of the restrictions presented with the one-step reaction scheme.

Also, for all the kinetic pathways applied for modeling the thermal decomposition of sugarcane straw in both atmospheres (nitrogen and synthetic air), the activation energies remained equal for different heating rates, therefore, the inter-particle and intra-particle transport phenomena were successfully avoided.

Finally, from the analysis of the heat of reaction, the thermal decomposition reaction in inert atmosphere (pyrolysis) was endothermic up to 350 °C with maximum heat requirement of 1 MJ/kg, remaining constant up to 600 °C. In oxidative atmosphere (combustion), the reaction was completely exothermic releasing 8 MJ/kg, almost half (0.43) of the higher heating value (18.6 MJ/kg). Then, the heat released by burning of part of the sugarcane straw would provide the energy requirements in a pyrolysis process, which is the principle of the oxidative pyrolysis.

REFERENCES

- Abbasi, T., & Abbasi, S. A. (2010). Biomass energy and the environmental impacts associated with its production and utilization. *Renewable and Sustainable Energy Reviews*, *14*(3), 919–937. doi:10.1016/j.rser.2009.11.006
- Aboulkas, A., & El Harfi, K. (2008). Study of the Kinetics and Mechanisms of Thermal Decomposition of Moroccan Tarfaya Oil Shale and Its Kerogen. *Oil Shale*, *25*(4), 426–443. doi:10.3176/oil.2008.4.04
- Aboyade, A.O., Görgens, J.F., Carrier, M., Meyer, E.L., & Knoetze, J.H. (2013). Thermogravimetric study of the pyrolysis characteristics and kinetics of coal blends with corn and sugarcane residues. *Fuel Processing Technology*, *106*, 310-320.
- Amutio, M., Lopez, G., Aguado, R., Bilbao, J., & Olazar, M. (2012). Biomass oxidative flash pyrolysis: Autothermal operation, yields and product properties. *Energy & Fuels*, *26*, 1353-1362.
- Amutio, M., Lopez, G., Aguado, R., Artetxe, M., Bilbao, J., & Olazar, M. (2012). Kinetic study of lignocellulosic biomass oxidative pyrolysis. *Fuel*, *95*, 305-311.
- Amutio, M., Lopez, G., Jon, A., Moreira, R., Duarte, G., Nunes, J., Bilbao, J. (2013). Pyrolysis kinetics of forestry residues from the Portuguese Pyrolysis kinetics of forestry residues from the Portuguese Central Inland Region. *Chemical Engineering Research and Design*, *91*, 2682–2690.
- Anca-Couce, A., Zobel, N., Berger, A., & Behrendt, F. (2012). Smouldering of pine wood: Kinetics and reaction heats. *Combustion and Flame*, *159*, 1708-1719.
- Anca-Couce, A., Berger, A., & Zobel, N. (2014). How to determine consistent biomass pyrolysis kinetics in a parallel reaction scheme. *Fuel*, *123*, 230–240. doi:10.1016/j.fuel.2014.01.014
- Antal, M.J., & Várhegyi, G. (1995). Cellulose pyrolysis kinetics: the current state of knowledge. *Industrial and Engineering Chemistry Research*, *34*, 703-717.
- Antal, M.J., Várhegyi, G., & Jakab, E. (1998). Cellulose pyrolysis kinetics: revisited. *Industrial and Engineering Chemistry Research*, *37*, 1267-1275.

Anthony, D.B., & Howard, J.B. (1976). Coal devolatilization and hidrogasification. *AIChE Journal*, 22, 625-656.

Baroni, E.G., Tannous, K., Rueda-Ordóñez, Y.J., & Tinoco-Navarro, L.K. (2015). The applicability of isoconversional models in estimating the kinetic parameters of biomass pyrolysis. *Journal of Thermal Analysis and Calorimetry*. doi: 10.1007/s10973-015-4707-9.

Barneto, A.G., Carmona, J.A., Alfonso, J.E.M., & Serrano, R.S. (2010). Simulation of the thermogravimetry analysis of three non-wood pulps. *Bioresource Technolgy*, 101, 3220-3229.

Basu, P. (2010). Biomass Gasification and Pyrolysis Practical Design and Theory. *Elsevier*, (pp.1–364). Kidlington, Oxford: Academic Press .

Becidan, M., Várhegyi, G., Hustad, J. E., & Skreiberg, Ø. (2007). Thermal decomposition of biomass wastes. A kinetic study. *Industrial & Engineering Chemistry Research*, 46(8), 2428–2437. doi:10.1021/ie061468z

Bizzo, W.A., Sánchez, C.G. (2010). Estequiometria das reações de combustão e gaseificação, in: Sánchez, C.G. (Ed.), *Tecnologia da Gaseificação de Biomassa*. Atómo, Campinas.

Branca, C., Albano, A., & Di Blasi, C. (2005). Critical evaluation of global mechanisms of wood devolatilization. *Thermochimica Acta*, 429, 133-141.

Branca, C., & Di Blasi, C., 2015. A lumped kinetic model for banana peel combustion. *Thermochim. Acta*. 614, 68-75.

Bradbury, A. G. W., Sakai, Y., & Shafizadeh, F. (1979). A kinetic model for pyrolysis of cellulose. *Journal of Applied Polymer Science*, 23(11), 3271–3280. doi:10.1002/app.1979.070231112

Branca, C., & Di Blasi, C. (2013). Char structure and combustion kinetics of a phenolic-impregnated honeycomb material. *Industrial & Engineering Chemistry Research*, 52(41), 14574-14582. doi:10.1021/ie402470z

Braun, R. L., Burnham, A. K., Reynolds, J. G., & Clarkson, J. E. (1991). Pyrolysis kinetics for lacustrine and marine source rocks by programmed micropyrolysis. *Energy and Fuels*, 5(1), 192–204. doi:10.1021/ef00025a033

Broido, A. (1976). Kinetics of solid-phase cellulose pyrolysis. In F. Shafizadeh, K. V. Sarkanen, & D. A. Tillman (Eds.), *Thermal uses and properties of carbohydrates and lignins* (pp. 19–36). New York: Academic Press.

Brown, W.E., Dollimore, D., & Galwey, A.K. (1980). Theory of solid state reaction kinetics. In Bamford, C.H., & Tipper, C.F.H (Eds.), *Chemical Kinetics, Volume 22 Reactions in the solid state* (pp. 41-113). Amsterdam: Elsevier.

Caballero, J.A., Conesa, J.A., Font, R., & Marcilla, A. (1997). Pyrolysis kinetics of almond shells and olive stones considering their organic fractions. *Journal of Analytical and Applied Pyrolysis*, *42*, 159-175.

Cai, J., Wu, W., Liu, R., & Huber, G. W. (2013). A distributed activation energy model for the pyrolysis of lignocellulosic biomass. *Green Chemistry*, *15*(5), 1331–1340. doi:10.1039/c3gc36958g

Cancellieri, D., Leroy-Cancellieri, V., Leoni, E., Simeoni, A., Kuzin, A.Y., Filkov, A.I., Rein, G. (2012). Kinetic investigation on the smouldering combustion of boreal peat. *Fuel*, *93*, 479-485.

Capart, R., Khezami, L., & Burnham, A.K. (2004). Assessment of various kinetic models for the pyrolysis of a microgranular cellulose. *Thermochimica Acta*, *417*, 79-89.

Cardoso, C. R., Miranda, M. R., Santos, K. G., & Ataíde, C. H. (2011). Determination of kinetic parameters and analytical pyrolysis of tobacco waste and sorghum bagasse. *Journal of Analytical and Applied Pyrolysis*, *92*(2), 392–400. doi:10.1016/j.jaap.2011.07.013

Ceylan, S., & Topçu, Y. (2014). Pyrolysis kinetics of hazelnut husk using thermogravimetric analysis. *Bioresource Technology*, *156*, 182–188. doi:10.1016/j.biortech.2014.01.040

Chen, H., Liu, N., & Fan, W. (2006). Two-step consecutive reaction model and kinetic parameters relevant to the decomposition of Chinese forest fuels. *Journal of Applied Polymer Science*, *102*(1), 571–576. doi:10.1002/app.24310

Chen, D., Zheng, Y., & Zhu, X. (2013). In-depth investigation on the pyrolysis kinetics of raw biomass. Part I: Kinetic analysis for the drying and devolatilization stages. *Bioresource Technology*, *131*, 40-46. doi:10.1016/j.biortech.2012.12.136

Coats, A. W., & Redfern, J. P. (1965). Kinetic parameters from thermogravimetric data. II. *Journal of Polymer Science Part B: Polymer Letters*, *3*(11), 917–920. doi:10.1002/pol.1965.110031106

Conesa, J. A., & Domene, A., 2011. Biomasses pyrolysis and combustion kinetics through n-th order parallel reactions. *Thermochimica Acta*, *523*, 176– 181.

- Conesa, J. A., & Rey, L., 2015. Thermogravimetric and kinetic analysis of the decomposition of solid recovered fuel from municipal solid waste. *Journal of Thermal Analysis and Calorimetry*, 120, 1233-1240.
- Costa, S.M., Mazzola, P.G., Silva, J.C.A.R., Pahl, R., Pessoa Jr, A., & Costa, S.A. (2013). Use of sugarcane straw as a source of cellulose for textile fibre production. *Industrial Crops and Production*, 42, 189-194.
- Czernik, S., & Bridgwater, A.V. (2004). Overview of applications of biomass fast pyrolysis oil. *Energy and Fuels*, 18, 590-598.
- Damartzis, T., Vamvuka, D., Sfakiotakis, S., & Zabaniotou, A. (2011). Thermal degradation studies and kinetic modeling of cardoon (*Cynara cardunculus*) pyrolysis using thermogravimetric analysis. *Bioresource Technology*, 102, 6230-6238.
- Demirbas, M. F., & Balat, M. (2007). Biomass pyrolysis for liquid fuels and chemicals: A review. *Journal of Scientific and Industrial Research*, 66(10), 797–804.
- Di Blasi, C. (2008). Modeling chemical and physical processes of wood and biomass pyrolysis. *Progress in Energy and Combustion Science*, 34(1), 47–90. doi:10.1016/j.pecs.2006.12.001
- Di Blasi, C., & Russo, G. (1993). Modeling of transport phenomena and kinetics of biomass pyrolysis, in: Bridgwater A.V. (Ed.), *Advances in thermochemical biomass conversion*. Dordrecht: Springer Netherlands; 1993, pp. 906-921.
- Doyle, C.D. (1961). Kinetic Analysis of Thermogravimetric Data, *Journal of Applied Polymer Science*, 5(15), 285–292. doi:10.1002/app.1961.070051506
- Dupont, C., Chiriac, R., Gauthier, G., Toche, F., 2014. Heat capacity measurements of various biomass types and pyrolysis residues. *Fuel*. 115, 644-651.
- Ebrahimi-Kahrizsangi, R., & Abbasi, M.H. (2008). Evaluation of reliability of Coats-Redfern method for kinetic analysis of non-isothermal TGA. *Transactions of Nonferrous Metals Society of China*, 18(1), 217–221. doi:10.1016/S1003-6326(08)60039-4
- Fiori, L., Valbusa, M., Lorenzi, D., & Fambri, L. (2012). Modeling of the devolatilization kinetics during pyrolysis of grape residues. *Bioresource Technology*, 103(1), 389–397. doi:10.1016/j.biortech.2011.09.113

Flynn, J. H., & Wall, L. A. (1966). General Treatment of the Thermogravimetry of Polymers. *Journal of Research of the National Bureau of Standards*, 70(6), 487–523. doi:10.6028/jres.070A.044

Friedman, H. L. (1964). Kinetics of thermal degradation of char-forming plastics from thermogravimetry. Application to a phenolic plastic. *Journal of Polymer Science Part C: Polymer Symposia*, 6(1), 183–195. doi:10.1002/polc.5070060121

Garg, A., Kazunari, K., & Pulles, T. (2006). Introduction, in: Eggleston, S., Buendia, L., Miwa, K., Ngara, T., & Tanabe, K. (Eds.), *2006 IPCC Guidelines for national gas inventories Volume 2 Energy*. Institute for Global Environmental Strategies, Hayama, p. 1-29.

Grønli, M. G., Várhegyi, G., & Di Blasi, C. (2002) Thermogravimetric analysis and devolatilization kinetics of wood. *Industrial & Engineering Chemistry Research*, 41(17),4201-4208. doi:10.1021/ie0201157

Güneş, M., & Güneş, S. (2002). A direct search method for determination of DAEM kinetic parameters from nonisothermal TGA data (note). *Applied Mathematics and Computation*, 130(2-3), 619–628. doi:10.1016/S0096-3003(01)00124-2

Guo, J., & Lua, A.C. (2001). Kinetic study on pyrolytic process of oil-palm solid waste using two-step consecutive reaction model. *Biomass and Bioenergy*, 20, 223-233.

He, F., Yi, W., & Bai, X. (2006). Investigation on caloric requirement of biomass pyrolysis using TG–DSC analyzer. *Energy Conversion and Management*, 47, 2461-2469.

He, F., Yi, W., & Zha, J. (2009). Measurement of the heat of smoldering combustion in straws and stalks by means of simultaneous thermal analysis. *Biomass & Bioenergy*, 33, 130-136.

Hoi, L.W.S., & Martincigh, B.S. (2013). Sugar cane plant fibres: separation and characterization. *Industrial Crops and Production*, 47, 1-12.

Horowitz, H. H., & Metzger, G. (1963). A new analysis of thermogravimetric traces. *Analytical Chemistry*, 35(10), 1464–1468. doi: 10.1021/ac60203a013

Horwitz, W. (Ed.). (2000). Official Methods of Analysis of AOAC International. 17th edition. *AOAC International*, (pp.1-2200). Gaithersburg, Maryland.

Hu, S., Jess, A., & Xu, M. (2007). Kinetic study of Chinese biomass slow pyrolysis: comparison of different kinetic models. *Fuel*, 86, 2778-2788.

Huang, X., & Rein, G. (2014). Smouldering combustion of peat in wildfires: Inverse modeling of the drying and the thermal and oxidative decomposition kinetics. *Combustion and Flame*, *161*, 1633-1644.

Huang, X., Rein, G., & Chen, H. (2015). Computational smoldering combustion: Predicting the roles of moisture and inert contents in peat wildfires. *Proceedings of the Combustion Institute*, *35*, 2673-2681.

Huang, X., & Rein, G. (2016). Thermochemical conversion of biomass in smouldering combustion across scales: The roles of heterogeneous kinetics, oxygen and transport phenomena. *Bioresource Technology*, *207*, 409-421.

Janković, B. (2008). Kinetic analysis of the nonisothermal decomposition of potassium metabisulfite using the model-fitting and isoconversional (model-free) methods. *Chemical Engineering Journal*, *139*, 128-135.

Jenkins, B.M., Baxter, L.L., Miles Jr., T.R., & Miles, T.R. (1998). Combustion properties of biomass. *Fuel Processing Technology*, *54*, 17-46.

Khawam, A., & Flanagan, D.R. (2006). Solid-state kinetic models: basics and mathematical fundamentals. *Journal of Physical Chemistry B*, *110*, 17315-17328.

Kajaste, R. (2014). Chemical from biomass-managing greenhouse gas emissions in biorefinery production chains-a review. *Journal of Cleaner Production*, *75*, 1-10. doi:10.1016/j.jclepro.2014.03.070

Kissinger, H. E. (1957). Reaction kinetics in differential thermal analysis. *Analytical Chemistry*, *29*(11), 1702-1706. doi:10.1021/ac60131a045

Lanzetta, M., & Di Blasi, C. (1998). Pyrolysis kinetics of wheat and corn straw. *Journal of Analytical and Applied Pyrolysis*, *44*(2), 181-192. doi:10.1016/S0165-2370(97)00079-X

Lautenberger, C., Fernandez-Pello, C. (2009). A model for the oxidative pyrolysis of wood. *Combustion and Flame*, *156*, 1503-1513.

Lisboa, A. C. L., & Watkinson, A. P. (1999). Operating conditions for oil shale thermogravimetry. *Powder Technology*, *101*(2), 151-156. doi:10.1016/S0032-5910(98)00166-1

Leal, M.R., Galdos, M.V., Scarpore, F.V., Seabra, J.E.A., Walter, A., & Oliveira, C.O.F. (2013). Sugarcane straw availability, quality, recovery and energy use: A literature review. *Biomass and Bioenergy*, *53*, 11-19.

- Leroy-Cancellieri, V., Cancellieri, D., Leoni, E., Simeoni, A., & Filkov, A. I., 2014. Energetic potential and kinetic behavior of peats. *Journal of Thermal Analysis and Calorimetry*, 117, 1497-1508.
- Lin, Y., Cho, J., Tompsett, G.A., Westmoreland, P.R., & Huber, G.W., 2009. Kinetics and mechanism of cellulose pyrolysis. *Journal of Physical Chemistry*, 113, 20097-20107.
- Lira, T.S., Santos, K.G., Murata, V.V., Giancesella, M., & Barrozo, M.A.S. (2010). The use of nonlinearity measures in the estimation of kinetic parameters of sugarcane bagasse pyrolysis. *Chemical Engineering and Technology*, 33, 1699-1705.
- Liu, Q., Zhong, Z., Wang, S., & Luo, Z. (2011). Interactions of biomass components during pyrolysis: A TG-FTIR study. *Journal of Analytical and Applied Pyrolysis*, 90(2), 213–218. doi:10.1016/j.jaap. 2010.12.009
- Lua, A. C., & Su, J. (2006). Isothermal and non-isothermal pyrolysis kinetics of Kapton® polyimide. *Polymer Degradation and Stability*, 91(1), 144–153. doi:10.1016/j.polymdegradstab.2005.04.021
- Luangkiattikhun, P., Tangsathitkulchai, C., Tangsathitkulchai, M. (2008). Non-isothermal thermogravimetric analysis of oil-palm solid wastes. *Bioresource Technology*, 99, 986-997.
- Lu, C., Song, W., Lin, W. (2009). Kinetics of biomass catalytic pyrolysis. *Biotechnology Advances*, 27(5), 583–587. doi:10.1016/j.biotechadv.2009.04.014
- Luz, S.M., Gonçalves, A.R., Del'Arco Jr, A.P., Leão, A.L., Ferrão, P.M.C., & Rocha, G.J.M. (2010). Thermal properties of polypropylene composites reinforced with different vegetable fibres. *Advanced Material Research*, 123-125, 1199-1202.
- Mamleev, V., Bourbigot, S., & Yvon, J. (2007). Kinetic analysis of the thermal decomposition of cellulose: the change of the rate limitation. *Journal of Analytical and Applied Pyrolysis*, 80, 141-150.
- Manara, P., Vamvuka, D., Sfakiotakis, S., Vanderghem, C., Richel, A., & Zabaniotou, A. (2015). Mediterranean agri-food processing wastes pyrolysis after pre-treatment and recovery of precursor materials: A TGA-based kinetic modeling study. *Food Research International*, 73, 44-51.
- Manyà, J.J., Velo, E., & Puigjaner, L. (2003). Kinetics of biomass pyrolysis: a reformulated three-parallel-reactions model. *Industrial & Engineering Chemistry Research*, 42, 434-441.

McKendry, P. (2002). Energy production from biomass (part 1): overview of biomass. *Bioresource Technology*, 83(1), 37–46. doi:10.1016/S0960-8524(01)00118-3

Mendeleev, D.I. (1949). Compositions (collection of works), in: Reports from the Science Academy of Union of Soviet Socialist Republics, Moscow, vol. 15, pp. 115–118.

Menon, V., & Rao, M. (2012). Trends in bioconversion of lignocellulose: Biofuels, platform chemicals & biorefinery concept. *Progress in Energy and Combustion Science*, 38(4), 522–550. doi:10.1016/j.pecs.2012.02.002

Mesa-Pérez, J., Rocha, J., Barbosa-Cortez, L., Penedo-Medina, M., Luengo, C., & Cascarosa, E. (2013). Fast oxidative pyrolysis of sugar cane straw in a fluidized bed reactor. *Applied Thermal Engineering*, 56, 167–175.

Mettler, M. S., Vlachos, D. G., & Dauenhauer, P. J. (2012). Top ten fundamental challenges of biomass pyrolysis for biofuels. *Energy and Environmental Science*, 5(7), 7797–7809. doi:10.1039/C2EE216 79E

Mishra, G., & Bhaskar, T. (2014). Non isothermal model free kinetics for pyrolysis of rice straw. *Bioresource Technology*, 169, 614–621.

Mohan, D., Pittman, C.U., & Steele, P.H. (2006). Pyrolysis of wood/biomass for bio-oil: a critical review. *Energy and Fuels*, 20, 848–889.

Moraes, M., Georges, F., Almeida, S., Damasceno, F., Maciel, G., Zini, C., Jacques, R., & Caramão, E. (2012). Analysis of products from pyrolysis of Brazilian sugar cane straw. *Fuel Processing Technology*, 101, 35–43.

Naranjo, R.A., Conesa, J.A., Pedretti, E.F., & Romero, O.R. (2012). Kinetic analysis: Simultaneous modelling of pyrolysis and combustion processes of dichrostachyscinerea. *Biomass and Bioenergy*, 36, 170–175.

Nascimento, V. F. (2012). *Caracterização de biomassas amazônicas-ouriço de castanha do brasil, ouriço de sapucaia e caroço do fruto do tucumã-visando sua utilização em processos de termoconversão*. (Master dissertation). Retrieved from Acervus Unicamp dissertations and Theses database. (T/UNICAMP N17C)

Orfão, J. J. M., Antunes, F. J. A., & Figueiredo, J. L. (1999). Pyrolysis kinetics of lignocellulosic materials - three independent reactions model. *Fuel*, 78(3), 349–358. doi: 10.1016/S0016-2361(98)00156-2

Ounas, A., Aboulkas, A., El harfi, K., Bacaoui, A., & Yaacoubi, A. (2011). Pyrolysis of olive residue and sugarcane bagasse: Non-isothermal thermogravimetric analysis. *Bioresource Technology*, *102*, 11234-11238.

Ozawa, T. (1965). A new method of analyzing thermogravimetric data. *Bulletin of the chemical Society of Japan*, *38*(11), 1881–1886. doi:10.1246/bcsj.38.1881.

Parthasarathy, P., & Narayanan, S. K. (2014). Determination of kinetic parameters of biomass samples using thermogravimetric analysis. *Environmental Progress & Sustainable Energy*, *33*(1), 256–266. doi:10.1002/ep.11763

Pasangulapati, V., Ramachandriya, K.D., Kumar, A., Wilkins, M.R., Jones, C.L., & Huhnke, R.L. (2012). Effects of cellulose, hemicellulose and lignin on thermochemical conversion characteristics of the selected biomass. *Bioresource Technology*, *114*, 663-669.

Pella, E., & Colombo, B. (1973). Study of carbon, hydrogen and nitrogen determination by combustion-gas chromatography. *Mikrochimica Acta*, *61*(5), 697-719. doi: 10.1007/BF01218130.

Pérez-Maqueda, L.A., & Criado, J.M. (2000). The accuracy of Senum and Yang's approximations to the Arrhenius integral. *Journal of Thermal Analysis and Calorimetry*, *60*, 909-15.

Pippo, W. A., Luengo, C. A., Alberteris, L. A. M., Garzone, P., & Cornacchia, G. (2011). Energy recovery from sugarcane-trash in the light of 2nd generation biofuels. Part 1: Current situation and environmental aspects. *Waste and Biomass Valorization*, *2*(1), 1-16. doi:10.1007/s12649-010-9048-0

Poletto, M., Dettenborn, J., Pistor, V., Zeni, M., & Zattera, A.J. (2010). Materials produced from plant biomass. Part I: Evaluation of thermal stability and pyrolysis of wood. *Material Research*, *13*, 375-379.

Ramajo-Escalera, B., Espina, A., García, J. R., Sosa-Arnao, J. H., & Nebra, S. A. (2006). Model-free kinetics applied to sugarcane bagasse combustion. *Thermochimica Acta*, *448*, 111-116.

Ranzi, E., Cuoci, A., Faravelli, T., Frassoldati, A., Migliavacca, G., Pierucci, S., & Sommariva, S. (2008). Chemical Kinetics of Biomass Pyrolysis. *Energy & Fuels*, *22*(6), 4292–4300. doi:10.1021/ef800551t

Rath, J., Wolfinger, M. G., Steiner, G., Krammer, G., Barontini, F., & Cozzani, V. (2003). Heat of wood pyrolysis. *Fuel*, *82*, 81-91.

Rocha, G.J.M., Martin, C., Soares, I.B., Maior, A.M.S., Baudel, H.M., & Abreu, C.A.M. (2011). Dilute mixed-acid pretreatment of sugarcane bagasse for ethanol production. *Biomass and Bioenergy*, 35, 663-670.

Rueda-Ordóñez, Y. J., Olivares-Gómez, E., & Tannous, K (2013). Thermogravimetric study and kinetic analysis of sugarcane straw. In *Proceedings of the 22nd International Congress of Mechanical Engineering (COBEM, 2013)*. Ribeirão Preto, SP, Brazil. ABCM.

Rueda-Ordóñez, Y.J., Baroni, E.G., Tinoco-Navarro, L.K., & Tannous, K. (2015). Modeling the kinetics of lignocellulosic biomass pyrolysis, in: Tannous, K. (Ed.), *Innovative Solutions in Fluid-Particle Systems and Renewable Energy Management*. IGI Global, Hershey, pp. 92-130. DOI:10.4018/978-1-4666-8711-0.ch004

Rueda-Ordóñez, Y.J., & Tannous, K. (2015). Isoconversional kinetic study of the thermal decomposition of sugarcane straw for thermal conversion processes. *Bioresource Technology*, 196, 136-144.

Rueda-Ordóñez, Y. J., Tannous, K., & Olivares-Gómez, E., 2015. An empirical model to obtain the kinetic parameters of lignocellulosic biomass pyrolysis in an independent parallel reactions scheme. *Fuel Processing Technology*, 140, 222-230.

Saad, M.B.W., Oliveira, L.R.M., Cândido, R.G., Quintana, G., Rocha, G.J.M., & Gonçalves, A.R. (2008). Preliminary studies on fungal treatment of sugarcane straw for organosolv pulping. *Enzyme and Microbial Technology*, 43, 220-225.

Sanchez, M. E., Otero, M., Gómez, X., & Morán, A. (2009). Thermogravimetric kinetic analysis of the combustion of biowastes. *Renewable Energy*, 34(6), 1622–1627. doi:10.1016/j.renene.2008.11.011.

Sanchez-Jimenez, P.E., Perez-Maqueda, L.A., Perejon, A., Pascual-Cosp, J., Benitez-Guerrero, M., & Criado, J.M. (2011). An improved model for the kinetic description of the thermal degradation of cellulose. *Cellulose*, 18, 1487-1498.

Sanchez-Jimenez, P.E., Perez-Maqueda, L.A., Perejon, A., & Criado, J.M. (2013). Generalized master plots as a straightforward approach for determining the kinetic model: The case of cellulose pyrolysis. *Thermochimica Acta*, 552, 54-59.

Sanchez-Silva, L., López-González, D., Villaseñor, J., Sánchez, P., & Valverde, J. L., (2012). Thermogravimetric-mass spectrometry analysis of lignocellulosic and marine biomass pyrolysis. *Bioresource technology*, 109, 163-172. doi:10.1016/j.biortech.2012.01.001

Santos, K.G., Lobato, F.S., Lira, T.S., Murata, V.V., & Barrozo, M.A.S. (2012). Sensitivity analysis applied to independent parallel reaction model for pyrolysis of bagasse. *Chemical Engineering Research and Design*, 90, 1989-1996.

Sbirrazzuoli, N., Vincent, L., Mija, A., & Guigo, N. (2009). Integral, differential and advanced isoconversional methods - Complex mechanisms and isothermal predicted conversion–time curves. *Chemometrics and Intelligent Laboratory Systems*, 96(2), 219–226. doi:10.1016/j.chemolab.2009. 02.002

Senneca, O., Chirone, R., & Salatino, P. (2004). Oxidative pyrolysis of solid fuels. *Journal of Analytical and Applied Pyrolysis*, 71, 959-970.

Shen, J., Igathinathane, C., Yu, M., & Pothula, A. K., 2015. Biomass pyrolysis and combustion integral and differential reaction heats with temperatures using thermogravimetric analysis/differential scanning calorimetry. *Bioresource Technology*, 185, 89-98.

Shires, T.M., Loughran, C.J, Jones, S., Hopkins, E. (2009). Compendium of Greenhouse Gas Emissions Estimation Methodologies for the Oil and Natural Gas Industry. *American Petroleum Institute*, (pp.1-807). Washington.

Slopiecka, K., Bartocci, P., & Fantozzi, F. (2012). Thermogravimetric analysis and kinetic study of poplar wood pyrolysis. *Applied Energy*, 97, 491-497.

Sluiter, A., Ruiz, R., Scarlata, C., Sluiter, J., & Templeton, D. (2008). Determination of extractives in biomass. Technical report NREL/TP-510-42619. National Renewable Energy Laboratory. http://www.nrel.gov/biomass/analytical_procedures.html

Sluiter, A., Hames, B., Ruiz, R., Scarlata, C., Sluiter, J., Templeton, D., & Crocker, D. (2012). Determination of structural carbohydrates and lignin in biomass. Technical report NREL/TP-510-42618. National Renewable Energy Laboratory. http://www.nrel.gov/biomass/analytical_procedures.html

Starink, M. (1996). A new method for the derivation of activation energies from experiments performed at constant heating rate. *Thermochimica Acta*, 288, 97–104. doi:10.1016/S0040-6031(96)03053-5

Sun, L., Chen, J.Y., Negulescu, I.I., Moore, M.A., & Collier, B.J. (2011). Kinetics modeling of dynamic pyrolysis of bagasse fibres. *Bioresource Technology*, 102; 1951-1958.

Tang, W., Liu, Y., Zhang, H., & Wang, C. (2003). New approximate formula for Arrhenius temperature integral. *Thermochimica Acta*, 408(1-2), 39–43. doi:10.1016/S0040-6031(03)00310-1

Teng, H., & Wei, Y. (1998). Thermogravimetric studies on the kinetics of rice hull pyrolysis and the influence of water treatment. *Industrial & Engineering Chemistry Research*, 37, 3806-3811.

Tonbul, Y. (2008). Pyrolysis of pistachio shell as a biomass. *Journal of Thermal Analysis and Calorimetry*, 91(2), 641–647. doi:10.1007/s10973-007-8428-6

Upadhyay, S.K. (2006). Chemical kinetics and reactions dynamics. *Springer*, (pp.1-251). Dordrecht: Springer.

Vamvuka, D., Kakaras, E., Kastanaki, E., Grammelis, P. (2003). Pyrolysis characteristics and kinetics of biomass residual mixtures with lignite. *Fuel*, 82, 1949-1960.

Van Krevelen, D., Van Heerden, C., & Huntjens, F. (1951). Physicochemical aspects of the pyrolysis of coal and related organic compounds. *Fuel*, 30, 253–259.

Van Soest, P.J., Robertson, J.B., & Lewis, B.A. (1991). Methods for dietary fiber, neutral detergent fiber, and nonstarch polysaccharides in relation to animal nutrition. *Journal of Dairy Science*, 74, 3583-3597. doi:10.3168/jds.S0022-0302(91)78551-2

Van de Velden, M., Baeyens, J., Brems, A., Janssens, B., & Dewil, R. (2010). Fundamentals, kinetics and endothermicity of the biomass pyrolysis reaction. *Renewable Energy*, 35(1), 232–242. doi:10.1016/j.renene.2009.04.019

Várhegyi, G., Antal Jr., M. J., Szekely, T., & Szabó, P. (1989). Kinetics of the thermal decomposition of cellulose, hemicellulose, and sugar cane bagasse. *Energy & Fuels*, 3(3), 329–335. doi:10.1021/ef00015a012

Várhegyi, G., Jakab, E., & Antal Jr., M. J. (1994). Is the Broido-Shafizadeh model for cellulose pyrolysis true?. *Energy & Fuels*, 8(6), 1345-1352. doi: 10.1021/ef00048a025

Várhegyi, G., Antal Jr., M. J., Jakab, E., & Szabó, P. (1997). Kinetic modeling of biomass pyrolysis. *Journal of Analytical and Applied Pyrolysis*, 42(1), 73–87. doi:10.1016/S0165-2370(96)00971-0

Várhegyi, G., Czégény, Z., Jakab, E., McAdam, K., & Liu, C. (2009). Tobacco pyrolysis. Kinetic evaluation of thermogravimetric–mass spectrometric experiments. *Journal Analytical and Applied Pyrolysis*, 86(2), 310–322. doi:10.1016/j.jaap.2009.08.008

Vassilev, S. V., Baxter, D., Andersen, L. K., & Vassileva, C. G. (2010). An overview of the chemical composition of biomass. *Fuel*, 89(5), 913–933. doi:10.1016/j.fuel.2009.10.022

Vassilev, S. V., Baxter, D., Andersen, L. K., Vassileva, C. G., & Morgan, T. J. (2012). An overview of the organic and inorganic phase composition of biomass. *Fuel*, 94, 1–33. doi:10.1016/j.fuel.2011.09.030

Vlaev, L. T., Markovska, I. G., & Lyubchev, L. A. (2003). Non-isothermal kinetics of pyrolysis of rice husk. *Thermochimica Acta*, 406(1–2), 1–7. doi:10.1016/S0040-6031(03)00222-3

Vyazovkin, S., 1997. Advanced isoconversional method. *Journal of Thermal Analysis and Calorimetry*, 49, 1493-1499.

Vyazovkin, S., Burnham, A. K., Criado, J. M., Pérez-Maqueda, L. A., Popescu, C., & Sbirrazzuoli, N. (2011). ICTAC Kinetics Committee recommendations for performing kinetic computations on thermal analysis data. *Thermochimica Acta*, 520(1–2), 1–19. doi:10.1016/j.tca.2011.03.034

WanJun, T., Cunxin, W., & Donghua, C. (2005). Kinetic studies on the pyrolysis of chitin and chitosan. *Polymer Degradation and Stability*, 87(3), 389–394. doi:10.1016/j.polymdegradstab.2004.08.006

Waters, D., Van Zwieten, L., Singh, B., Downie, A., Cowie, A.L., & Lehmann, J. (2011). Biochar in soil for climate change mitigation and adaptation, in: Singh, B., Cowie, A.L., Chan, K.Y. (Eds.). *Soil health and climate change*. New York: Springer Berlin Heidelberg; 2011, pp. 345-368.

Weerachanchai, P., Tangsathitkulchai, C., & Tangsathitkulchai, M. (2010). Comparison of pyrolysis kinetic models for thermogravimetric analysis of biomass. *Suranaree Journal of Science and Technology*, 17, 387-400.

White, J. E., Catallo, W. J., & Legendre, B. L. (2011). Biomass pyrolysis kinetics: A comparative critical review with relevant agricultural residue case studies. *Journal of Analytical and Applied Pyrolysis*, 91(1), 1–33. doi:10.1016/j.jaap.2011.01.004

Winsley, P. (2007). Biochar and bioenergy production from climate change mitigation. *New Zealand Science Review*, 64, 5-10.

Yao, F., Wu, Q., Lei, Y., Guo, W., & Xu, Y. (2008). Thermal decomposition kinetics of natural fibers: Activation energy with dynamic thermogravimetric analysis. *Polymer Degradation and Stability*, 93(1), 90–98. doi:10.1016/j.polymdegradstab.2007.10.012

Ye, N., Li, D., Chen, L., Zhang, X., & Xu, D., (2010). Comparative studies of the pyrolytic and kinetic characteristics of maize straw and the seaweed *ulva pertusa*. *Journal PLOS ONE*, 5(9), 1-6. doi:10.1371/journal.pone.0012641

Yuan, H. R., & Liu, R. H. (2007). Study on pyrolysis kinetics of walnut shell. *Journal of Thermal Analysis and Calorimetry*, 89(3), 983–986. doi:10.1007/s10973-006-7688-x

FUTURE RESEARCH DIRECTIONS

- Investigate the kinetics of mixtures of sugarcane bagasse and straw in micro and macro TG analyzer under inert and oxidizing atmospheres, comparing among kinetic parameters obtained in micro and macro scales in order to study the transport phenomena effects involved in the reaction;
- The study of the thermal decomposition of sugarcane straw in a macro thermogravimetric analyzer applying mass sample higher than 1g, under inert and oxidizing atmospheres in order to obtain a kinetic representation of the reactor. Afterward, perform a comparison among kinetic parameters obtained in micro and macro scales in order to study the transport phenomena effects involved in the reaction;
- Investigate the torrefaction process of the sugarcane straw testing several conditions such as reaction temperature, time of reaction, sample mass, particle diameter, flow gas, and non-isothermal conditions;
- Perform a phenomenological modeling of the thermal decomposition of sugarcane straw using pellets with uniform geometrical conditions. In this case, several conditions must be analyzed such as, geometry, radial and axial temperature, reaction temperature and reaction time.

PUBLICATIONS RELATED TO THE THESIS

BOOK CHAPTER

Rueda-ordóñez, Y. J., Baroni, E. G., Tinoco-Navarro, L. K., & Tannous, K. Modeling the kinetics of lignocellulosic biomass pyrolysis. In: Tannous, K. (Org.). **Innovative Solutions in Fluid-Particle Systems and Renewable Energy Management**. 1ed.Hershey: IGI Global, 2015, p. 92-130.

PAPERS IN SCIENTIFIC JOURNALS

Rueda-Ordóñez, Y. J., & Tannous, K. Isoconversional kinetic study of the thermal decomposition of sugarcane straw for thermal conversion processes. **Bioresource Technology**, v. 196, p. 136-144, 2015.

Rueda-Ordóñez, Y. J., Tannous, K., & Olivares-Gómez, E. An empirical model to obtain the kinetic parameters of lignocellulosic biomass pyrolysis in an independent parallel reactions scheme. **Fuel Processing Technology**, v. 140, p. 222-230, 2015.

Rueda-Ordóñez, Y. J., & Tannous, K. Thermal decomposition of sugarcane straw, kinetics and heat of reaction in synthetic air. **Bioresource Technology**, v. 211, p. 231-239, 2016.

PAPERS IN INTERNACIONAL CONFERENCES

Rueda-Ordóñez, Y. J., Tannous, K., & Olivares-Gómez, E. Thermogravimetric study and kinetic analysis of sugarcane straw. In: Proceedings of the **22nd International Congress of Mechanical Engineering**, p. 6006-6014, Ribeirão Preto/SP.

Rueda-Ordóñez, Y. J., & Tannous, K. (2014). Estudo cinético da pirólise de biomassas mediante o método das reações paralelas independentes. In: Anais do **IX Congresso Brasileiro de Análise Térmica e Calorimetria**, p. 1-6, Serra Negra/SP.

APPENDIX A

Lower heating value calculations

The lower heating value (LHV) is an important parameter used in the characterization of fuels. However, in the analysis of solid fuels there are different approaches to obtain this parameter. Therefore, here are presented three different correlations commonly applied to obtain the LHV.

The first correlation, equation (A1.1), to obtain the LHV is recommended by the Intergovernmental Panel on Climate Change (IPCC), in which X_H , X_M , and X_O are the percentage of hydrogen, moisture, and oxygen in the biomass, respectively (Garg, Kazunari, & Pulles, 2006).

$$LHV \text{ [MJ/kg]} = HHV - 0.212X_H - 0.245X_M - 0.008X_O \quad (\text{A1.1})$$

The second correlation was proposed by Mendeleev (1949) and presented in the equation (A1.2), in which X_C , X_H , X_O , X_S , and X_M are the percentage of carbon, hydrogen, oxygen, sulphur (obtained by elemental analysis), and moisture content of the biomass, respectively. The sulphur content was not taken into account, since no measurement was carried out in this work.

$$LHV \text{ [MJ/kg]} = 4.187[81X_C + 300X_H - 26(X_O - X_S) - 6(X_M + 9X_H)] \quad (\text{A1.2})$$

The third correlation is the simplest one, used by the American Petroleum Institute (API) to obtain the LHV of solid fuels, which assume that the LHV is lower than 5% of the HHV, as presented in equation (A1.3) according to Shires, Loughran, Jones & Hopkins (2009).

$$LHV = HHV - 0.05HHV \quad (\text{A1.3})$$

The results obtained by equations (A1.1), (A1.2), and (A1.3) were 16.68, 15.72, and 17.68 MJ/kg, respectively.

APPENDIX B

Preparation of TG/DTG data for thermal and kinetic analyses

1. Determination of normalized mass (TG) and normalized DTG from thermogravimetric data

The first step in thermal analysis through thermogravimetry is the data normalization carried out with Eqs. (3.2) and (3.3) for TG and DTG, respectively.

$$W = \frac{m}{m_i} \quad (3.2)$$

$$\frac{dW}{dt} = \frac{dm}{dt} \frac{1}{m_i} \quad (3.3)$$

However, before making the normalization, were corrected the data by subtracting the baseline, which correspond to the experiment runs in the similar conditions (heating rates and temperature ranges) with the empty pan. Table A1 presents the application of these equations in excel for the normalization of the experimental TG/DTG data.

Table A1. Experimental TG/DTG data normalization procedure

1	A	B	C	D	E
2	T (°C)	TG (mg)	DTG (mg/s)	W (-)	dW/dt (1/s)
3	25	3.010	-0.00060	=B3/\$B\$3	=C3/\$B\$3
4	26	3.008	-0.00065	=B4/\$B\$3	=C4/\$B\$3
5	27	3.006	-0.00070	=B5/\$B\$3	=C5/\$B\$3
⋮	⋮	⋮	⋮	⋮	⋮
877	900	0.100	-0.00080	=B877/\$B\$3	=C877/\$B\$3

2. Determination of conversion and conversion rate from normalized mass (TG) and normalized DTG

The normalized TG/DTG was used to analyse the overall thermal behavior. However, from these data is also selected the range of normalized mass for the kinetic analysis, which is carried out based on the experimental conversion and conversion rate, given by Eqs. (3.4) and (3.5), respectively.

$$\alpha_e = \frac{w_i - w}{w_i - w_f} \quad (3.4)$$

$$\left(\frac{d\alpha}{dt}\right)_e = -\frac{dw}{dt} \left(\frac{1}{w_i - w_f}\right) \quad (3.5)$$

In Table A2 is presented the procedure in MS Office Excel 2007 version 12.0.6683.5002 applying the Eqs. (3.4) and (3.5) in order to obtain the experimental conversion and conversion rate.

Table A2. Procedure to obtain experimental conversion and conversion rate from normalized mass and normalized DTG

1	A	B	C	D	E
2	T (°C)	W (-)	dW/dt (1/s)	α (-)	dα/dt (1/s)
3	150	0.900	-0.00090	=(B\$3-B3)/(B\$3-B\$877)	=(-C3)/(B\$3-B\$877)
4	151	0.880	-0.00095	=(B\$3-B4)/(B\$3-B\$877)	=(-C4)/(B\$3-B\$877)
5	152	0.860	-0.00100	=(B\$3-B5)/(B\$3-B\$877)	=(-C5)/(B\$3-B\$877)
⋮	⋮	⋮	⋮	⋮	⋮
437	450	0.300	-0.00110	=(B\$3-B437)/(B\$3-B\$437)	=(-C877)/(B\$3-B\$437)

APPENDIX C

Application of isoconversional methods

1. Selection of data (conversion, conversion rate, and temperature) for application of isoconversional methods.

Table C1 presents the experimental conversion, temperature and conversion rate exemplifying the application of isoconversional methods.

Table C1. Experimental conversion, temperature, and conversion rate

1	A	B	C
2	α (-)	T (°C)	da/dt (1/s)
3	0.00	150	0.00090
4	0.005	155	0.00095
5	0.0010	160	0.00100
⋮	⋮	⋮	⋮
437	1.00	450	0.00110

In Table C2 is presented the procedure used to select the data in the isoconversional methods, where 19 conversion levels were evaluated from 0.00 to 1.00 with step of 0.05. Then, the function LOOKUP was applied to obtain the temperature and conversion rate related to each conversion level. The function LOOKUP is equivalent to the functions *PROC* and *BUSCAR* in portuguese and spanish languages, respectively.

Table C2. Selection of data for application of isoconversional methods

1	E	F	G
2	α (-)	T (°C)	1/T (1/K)
3	0.00	=LOOKUP(E3,A3:A437,B3:B437)	=1/(F3+273.15)
4	0.05	=LOOKUP(E4,A3:A437,B3:B437)	=1/(F4+273.15)
5	0.10	=LOOKUP(E5,A3:A437,B3:B437)	=1/(F5+273.15)
⋮	⋮	⋮	⋮
23	1.00	=LOOKUP(E23,A3:A437,B3:B437)	=1/(F23+273.15)

In the Table C2 (continuation), the columns F and G are not represented in this step of procedure.

Table C2 (Continuation). Selection of data for application of isoconversional methods

1	E	...	H	I
2	α (-)	...	$d\alpha/dt$ (1/s)	$\ln[d\alpha/dt]$ (1/s)
3	0.00	...	=LOOKUP(E3,A3:A437,C3:C437)	=LN(H3)
4	0.05	...	=LOOKUP(E4,A3:A437,C3:C437)	=LN(H4)
5	0.10	...	=LOOKUP(E5,A3:A437,C3:C437)	=LN(H5)
⋮	⋮	...	⋮	⋮
23	1.00	...	=LOOKUP(E23,A3:A437,C3:C437)	=LN(H23)

2. Determination of activation energy from isoconversional methods

a) Method of Friedman

The method of Friedman is described by equation (3.8), in which the slope of the straight line obtained from $\ln(d\alpha/dt)$ vs $1/T$ multiplied by 8.314 provide the activation energy.

$$\ln\left(\frac{d\alpha}{dt}\right) = \ln A + \ln f(\alpha) - \left(\frac{E}{RT}\right) \quad (3.8)$$

Table C3 presents the experimental data used to obtain the activation energy and its procedure for each conversion level analyzed. The experimental data was separated by the different heating rates, β , considering three examples here. In order to obtain the slope was applied the tool SLOPE to set of experimental data. The function SLOPE is equivalent to the functions *INCLINAÇÃO* and *PENDIENTE* from portuguese and spanish languages, respectively.

Table C3. Experimental data applied in the Friedman method and procedure of determination of activation energy

1	A	B	C	D	E	F	G
2	α (-)	1/T (1/K)			$\ln[d\alpha/dt]$ (1/s)		
3		β_1	β_2	β_3	β_1	β_2	β_3
4	0.00	0.0025	0.0030	0.0035	-7.013	-8.013	-9.013
5	0.05	0.0020	0.0025	0.0030	-6.959	-7.959	-8.959
6	0.10	0.0015	0.0020	0.0025	-6.908	-7.908	-8.908
⋮	⋮	⋮	⋮	⋮	⋮	⋮	⋮
24	1.00	0.00125	0.00130	0.00135	-6.812	-7.812	-8.812

Table C3 (Continuation). Experimental data applied in the Friedman method and procedure of determination of activation energy

1	H	I
2	Slope	E (J/mol)
3		
4	=SLOPE(E4;F4;G4,B4;C4;D4)	=H4*8.314
5	=SLOPE(E5;F5;G5,B5;C5;D5)	=H5*8.314
6	=SLOPE(E6;F6;G6,B6;C6;D6)	=H6*8.314
⋮	⋮	⋮
24	=SLOPE(E24;F24;G24,B24;C24;D24)	=H24*8.314

b) Method of Ozawa-Flynn-Wall

The method of Ozawa-Flynn-Wall is described by equation (2.12), in which the slope of the straight line obtained from $\log(\beta)$ vs $1/T$ multiplied by $8.314/0.4567$ provide the activation energy for each conversion level.

$$\log(\beta) = \left[\log\left(\frac{AE}{R}\right) - \log[g(\alpha)] - 2.315 \right] - 0.4567 \left(\frac{E}{RT}\right) \quad (2.12)$$

Table C4 presents the experimental data used in the application of Ozawa-Flynn-Wall method for determination of the activation energy related to each conversion levels analyzed. The data were separated by heating rate, β , and also was calculated the logarithm of each β , as presented in the line 4 rows E, F, G, for β_1 , β_2 , and β_3 , respectively.

Table C4. Experimental data applied in the method of Ozawa-Flynn-Wall

1	A	B	C	D	E	F	G
2	α (-)	1/T (1/K)					$\ln \beta $ (°C/s)
3		β_1	β_2	β_3	β_1	β_2	β_3
4	0	0.0025	0.0030	0.0035	=LOG10(β_1)	=LOG10(β_2)	=LOG10(β_3)
5	0.05	0.0020	0.0025	0.0030			
6	0.10	0.0015	0.0020	0.0025			
⋮	⋮	⋮	⋮	⋮	⋮	⋮	⋮
24	1	0.00125	0.00130	0.00135			

Table C5 presents the procedure of the activation energy determination applying the data presented in Table C4. In the application of this method, the value of each logarithm of heating rate was fixed as constants in E4, F4, and G4 concerning to the y-axis values, and also the x-axis values correspond to inverse of absolute temperature ($1/T$), presented in the rows

B4, C4, and D4 for β_1 , β_2 , and β_3 , respectively, which decrease with the increasing of conversion.

Table C5. Procedure of determination of activation energy through the Ozawa-Flynn-Wall method

1	H	I
2	Slope	E (J/mol)
3		
4		
5	=SLOPE(E4;F4;G4,B5;C5;D5)	=(H5*8.314)/0.4567
6	=SLOPE(E4;F4;G4,B6;C6;D6)	=(H6*8.314)/0.4567
⋮	⋮	⋮
24	=SLOPE(E4;F4;G4,B24;C24;D24)	=(H24*8.314)/0.4567

c) Method of Vyazovkin

The activation energy of the method of Vyazovkin was obtained by minimization of equation (3.11). However, it is necessary to set a first activation energy for each conversion level, which will change after minimization. Then, as a first guess was used the activation energies obtained by Friedman method considering each conversion, which in this example were 155.1, 154.1, 154.6, and 153.5 for 0, 0.05, 0.10, and 1.00, respectively.

$$\begin{aligned} & \frac{[I(E_\alpha, T_\alpha)_{\beta_1}] \beta_2}{[I(E_\alpha, T_\alpha)_{\beta_2}] \beta_1} + \frac{[I(E_\alpha, T_\alpha)_{\beta_1}] \beta_3}{[I(E_\alpha, T_\alpha)_{\beta_3}] \beta_1} + \frac{[I(E_\alpha, T_\alpha)_{\beta_2}] \beta_1}{[I(E_\alpha, T_\alpha)_{\beta_1}] \beta_2} + \frac{[I(E_\alpha, T_\alpha)_{\beta_2}] \beta_3}{[I(E_\alpha, T_\alpha)_{\beta_3}] \beta_2} + \dots \\ & \dots + \frac{[I(E_\alpha, T_\alpha)_{\beta_3}] \beta_1}{[I(E_\alpha, T_\alpha)_{\beta_1}] \beta_3} + \frac{[I(E_\alpha, T_\alpha)_{\beta_3}] \beta_2}{[I(E_\alpha, T_\alpha)_{\beta_2}] \beta_3} = \min \end{aligned} \quad (3.11)$$

Table C6 presents the experimental data used in the method of Vyazovkin for determination of activation energy.

Table C6. Experimental data used in the Vyazovkin method

1	A	B	C	D
2	α (-)	1/T (1/K)		
3		β_1	β_2	β_3
4		0	0.0025	0.0030
5	0.05	0.0020	0.0025	0.0030
6	0.10	0.0015	0.0020	0.0025
⋮	⋮	⋮	⋮	⋮
24	1	0.00125	0.00130	0.00135

The function $I(E_\alpha, T_\alpha) = (E_\alpha/R)[p(x)]$ represents each conversion level and $x = E/RT$. The calculation of x is the first step, as presented in Table C7.

Table C7. Procedure of determination of $x = E/RT$

1	A	...	E	F	G
2	α (-)		$x = E/RT$ (-)		
3		...	β_1	β_2	β_3
4	0	...	$=(155.1*B4)/8.314$	$=(155.1*C4)/8.314$	$=(155.1*D4)/8.314$
5	0.05	...	$=(154.1*B5)/8.314$	$=(154.1*C5)/8.314$	$=(154.1*D5)/8.314$
6	0.10	...	$=(154.6*B6)/8.314$	$=(154.6*C6)/8.314$	$=(154.6*D6)/8.314$
⋮	⋮	⋮	⋮	⋮	⋮
24	1	...	$=(153*B24)/8.314$	$=(153*C24)/8.314$	$=(153*D24)/8.314$

The $p(x)$ approximate solution was solved through equation (3.10) according to Pérez-Maqueda and Criado (2000).

$$p(x) = \left(\frac{\exp(-x)}{x} \right) \left(\frac{x^7 + 70x^6 + 1886x^5 + 24920x^4 + \dots}{x^8 + 72x^7 + 2024x^6 + 28560x^5 + 216720x^4 + \dots} \right. \\ \left. \frac{\dots + 170136x^3 + 577584x^2 + 844560x + 357120}{\dots + 880320x^3 + 1794240x^2 + 1572480x + 403200} \right) = a \left(\frac{b}{c} \right) \quad (3.10)$$

However, in order to facilitate the explanation and presentation of the procedure, the equation 3.10 was divided into three parts, a, b, and c showed in equations (3.10a), (3.10b), and (3.10c), respectively.

$$a = \left(\frac{\exp(-x)}{x} \right) \quad (3.10a)$$

$$b = x^7 + 70x^6 + 1886x^5 + 24920x^4 + 170136x^3 + 577584x^2 + 844560x + 357120 \quad (3.10b)$$

$$c = x^8 + 72x^7 + 2024x^6 + 28560x^5 + 216720x^4 + 880320x^3 + 1794240x^2 + 1572480x + 403200 \quad (3.10c)$$

Table C8 presents the procedure of solution of equation (3.10a) related to the first part (a) of the equation (3.10).

Table C8. Procedure of solution of equation (3.10a)

1	H	I	J
2	Eq. (3.10a)	Eq. (3.10a)	Eq. (3.10a)
3	β_1	β_2	β_3
4	$=\text{EXP}(-E4)/E4$	$=\text{EXP}(-F4)/F4$	$=\text{EXP}(-G4)/G4$
5	$=\text{EXP}(-E5)/E5$	$=\text{EXP}(-F5)/F5$	$=\text{EXP}(-G5)/G5$
6	$=\text{EXP}(-E6)/E6$	$=\text{EXP}(-F6)/F6$	$=\text{EXP}(-G6)/G6$
⋮	⋮	⋮	⋮
24	$=\text{EXP}(-E24)/E24$	$=\text{EXP}(-F24)/F24$	$=\text{EXP}(-G24)/G24$

Table C9 presents the procedure of solution of equation (3.10b) corresponding to the numerator (part b) of the right side of equation (3.10). The following procedure must be done for all the heating rates as presented in Table C8. Here it was presented for only one heating rate, β_1 , in order to facilitate the procedure presentation.

Table C9. Procedure of solution of equation (3.10b)

1	K
2	Equation (3.10b)
3	β_1
4	$=E4^7+70*E4^6+1886*E4^5+24920*E4^4+170136*E4^3+577584*E4^2+844560*E4+357120$
⋮	⋮
24	$=E24^7+70*E24^6+1886*E24^5+24920*E24^4+170136*E24^3+577584*E24^2+844560*E24+357120$

In Table C10 is presented the procedure of solution of equation (3.10b) concerning the denominator (part c) of the right side of equation (3.10). This procedure must be done for all heating rates. Also, as aforementioned here was presented for only one heating rate, β_1 .

Table C10. Procedure of solution of equation (3.10b)

1	N
2	Equation (3.10c)
3	β_1
4	$=E4^8+72*E4^7+2024*E4^6+28560*E4^5+216720*E4^4+880320*E4^3+1794240*E4^2+1572480*E4+403200$
⋮	⋮
24	$=E24^8+72*E24^7+2024*E24^6+28560*E24^5+216720*E24^4+880320*E24^3+1794240*E24^2+1572480*E24+403200$

In Table C11 is presented the procedure of solution of the temperature integral $I(E_a, T_a) = (E_a/R)[p(x)]$ for all heating rates, related to each conversion level analyzed.

Table C11. Procedure of solution of the temperature integral $I(E_\alpha, T_\alpha)=(E_\alpha/R)[p(x)]$

1	Q	R	S
2	I(E,T)	I(E,T)	I(E,T)
3	β_1	β_2	β_3
4	$=(155.1/8.314)*(H4*(K4/N4))$	$=(155.1/8.314)*(I4*(L4/O4))$	$=(155.1/8.314)*(J4*(M4/P4))$
⋮	⋮	⋮	⋮
24	$=(153/8.314)*(H24*(K24/N24))$	$=(153/8.314)*(I24*(L24/O24))$	$=(153/8.314)*(J24*(M24/P24))$


Table C12 presents the procedure of solution of equation (3.11). The minimization of equation (3.11) was done modifying the activation energy, which initial values were obtained by the Friedman method, as aforementioned. Then, the activation energy which provides the lower value of equation (3.11) was considered to be the representative for the conversion level analyzed.

Table C12. Procedure of solution of the minimization correlation for determination of activation energy

1	A	...	T	U
2	α		Minimization	E (kJ/mol)
3	(-)	...	\emptyset	
4	0	...	$=(Q4*\beta_2/(R4*\beta_1))+(Q4*\beta_3/(S4*\beta_1))+(R4*\beta_1/(Q4*\beta_2))$ $+(R4*\beta_3/(S4*\beta_2))+(S4*\beta_1/(Q4*\beta_3))+(S4*\beta_2/(R4*\beta_3))$	155.1
⋮	⋮	⋮	⋮	
24	1	...	$=(Q24*\beta_2/(R24*\beta_1))+(Q24*\beta_3/(S24*\beta_1))+(R24*\beta_1/(Q24*\beta_2))$ $+(R24*\beta_3/(S24*\beta_2))+(S24*\beta_1/(Q24*\beta_3))+(S24*\beta_2/(R24*\beta_3))$	153.0

The variation of activation energy and consequently the determination of the lower value of equation (3.11) was carried out through the SOLVER tool. The first step was the selection of the cell in which is located the equation, which in this example was T4, as presented in Figure C1. Then, the varying cell was assumed to be U4, containing the initial values of activation energy, which changed in order to obtain the final activation energy for each conversion level. This procedure was done for all the conversions, i.e., line 4 to line 24 in this example.

Parámetros de Solver ×

Establecer objetivo: 

Para: Máx. Min. Valor de:

Cambiando las celdas de variables:




Figure C1. Configuration of SOLVER tool in excel for minimization of equation (3.11)

APPENDIX D

Application of the consecutive reactions scheme

The methodology applied to determine the final kinetic parameters in a consecutive reactions scheme is presented in Figure D1.

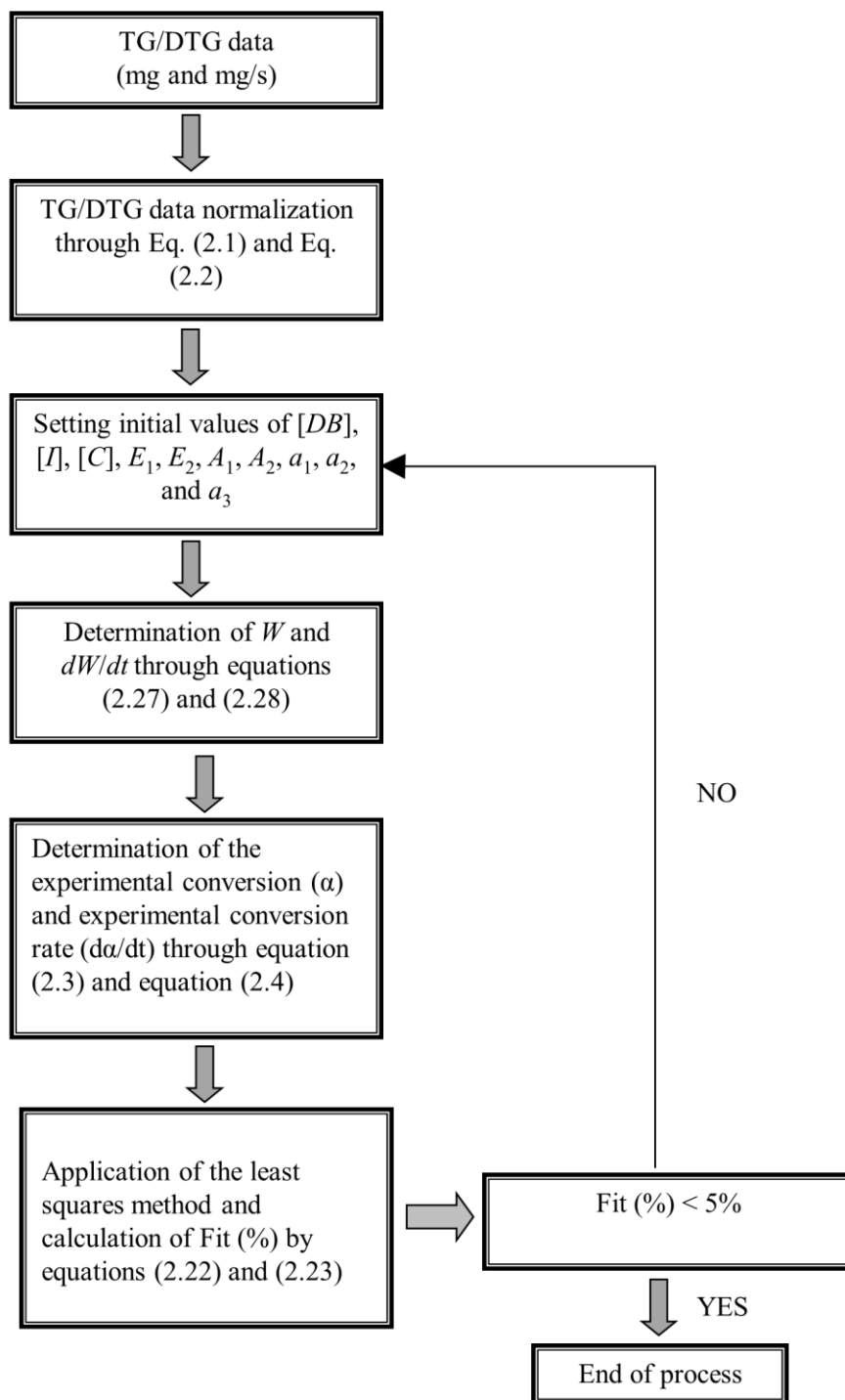


Figure D1. Flowchart of the application of the consecutive reactions scheme

The application of the consecutive reactions scheme was carried out according to equations (3.17) to (3.20), in which the first order reaction model was the same for all the reactions analyzed.

$$\frac{d[A]}{dt} = -(A_1) \left[\exp\left(\frac{-E_1}{RT}\right) \right] [A] \quad (3.17)$$

$$\frac{d[B]}{dt} = (A_1) \left[\exp\left(\frac{-E_1}{RT}\right) \right] [A] - (A_2) \left[\exp\left(\frac{-E_2}{RT}\right) \right] [B] \quad (3.18)$$

$$\frac{d[C]}{dt} = (A_2) \left[\exp\left(\frac{-E_2}{RT}\right) \right] [B] - (A_3) \left[\exp\left(\frac{-E_3}{RT}\right) \right] [C] \quad (3.19)$$

$$\frac{d[D]}{dt} = (A_3) \left[\exp\left(\frac{-E_3}{RT}\right) \right] [C] \quad (3.20)$$

The solution of the equations (3.17) to (3.20) was done through the application of the fourth order Runge-Kutta method given by equations (3.45) to (3.49) converted to concentration, in which the initial conditions were, step $h=5$ s, time $t_0=0$ s and $t=t_{i-1}+h$, temperature $T_0=150$ °C, and $[A]_0=1$, $[B]_0=0$, $[C]_0=0$, and $[D]_0=0$. The concentration $[X]$ is an example which could be applied for all the reactions analyzed, and used only to present the procedure of the Runge-Kutta method.

$$K_1 = h[X_i] \left\{ A \exp \left[\frac{-E}{R(T_0 + \beta t_i)} \right] \right\} \quad (3.45)$$

$$K_2 = h \left\{ [X_i] + \frac{h}{2} K_1 \right\} \left\{ A \exp \left[\frac{-E}{R \left(T_0 + \beta \left(t_i + \frac{h}{2} \right) \right)} \right] \right\} \quad (3.46)$$

$$K_3 = h \left\{ [X_i] + \frac{h}{2} K_2 \right\} \left\{ A \exp \left[\frac{-E}{R \left(T_0 + \beta \left(t_i + \frac{h}{2} \right) \right)} \right] \right\} \quad (3.47)$$

$$K_4 = h \{ [X_i] + hK_3 \} \left\{ A \exp \left[\frac{-E}{R(T_0 + \beta(t_i + h))} \right] \right\} \quad (3.48)$$

$$[X]_{i+1} = [X]_i + \left(\frac{K_1 + K_2 + K_3 + K_4}{6} \right) \quad (3.49)$$

Table D1 presents the initial kinetic parameters for the three reactions analyzed, which is the first step in the analysis. These values are the first guess, and are only examples.

Table D1. Initial kinetic parameters for the three reactions analyzed

1	A	B
2	Parameters	
3	E1 (kJ/mol)	150
4	A1 (1/s)	1.00E+10
5	a1 (-)	1.00
6		
7	E2 (kJ/mol)	200
8	A2 (1/s)	1.00E+15
9	a2 (-)	0.72
10		
11	E3 (kJ/mol)	100
12	A3 (1/s)	1.00E+5
13	a3 (-)	0.35
14		
15	a4 (-)	0.10

In Table D2 is presented the initial conditions $t_0=0$ s, $T_0=150$ °C, and $[A]_0=1$, $[B]_0=0$, $[C]_0=0$, and $[D]_0=0$, corresponding to time, temperature, and concentration, respectively. Also, in Table D2 the initial concentration was setted in 0 as example.

Table D2. Initial conditions of time, temperature, and concentration and their increasing

1	D	E	F
2	t (s)	T (°C)	[X] (-)
3	0	150	0
4	=D3+5	=E3+β*D4	=F3+((G3+H3+I3+J3)/6)
5	=D4+5	=E3+β*D5	=F4+((G4+H4+I4+J4)/6)
⋮	⋮	⋮	⋮
437	=D436+5	=E3+β*D437	=F436+((G436+H436+I436+J436)/6)

Then, in order to facilitate the presentation of the procedure, the solution of equations (3.45) to (3.49) showed here as example correspond only for one concentration, and was assumed that the solution of the other concentrations were carried out in different sheets.

In the application of the fourth order Runge-Kutta method the determination of the parameters K_1 , K_2 , K_3 , and K_4 was carried according to the procedure presented in Table D3, Table D4, Table D5 and Table D6, respectively.

Table D3. Procedure for solution of the parameter K_1 presented in equation (3.45)

1	G
2	K_1
3	$=5*(F3)*(\$B\$4*EXP(-\$B\$3/(8.314*(\$E\$3+\beta*D3))))$
⋮	⋮
437	$=5*(F437)*(\$B\$4*EXP(-\$B\$3/(8.314*(\$E\$3+\beta*D437))))$

Table D4. Procedure for solution of the parameter K_2 presented in equation (3.46)

1	H
2	K_2
3	$=5*(F3+5/2*G3)*(\$B\$4*EXP(-\$B\$3/(8.314*(\$E\$3+\beta*(D3+5/2))))$
⋮	⋮
437	$=5*(F437+5/2*G437)*(\$B\$4*EXP(-\$B\$3/(8.314*(\$E\$3+\beta*(D437+5/2))))$

Table D5. Procedure for solution of the parameter K_3 presented in equation (3.47)

1	I
2	K_3
3	$=5*(F3+5/2*H3)*(\$B\$4*EXP(-\$B\$3/(8.314*(\$E\$3+\beta*(D3+5/2))))$
⋮	⋮
437	$=5*(F437+5/2*H437)*(\$B\$4*EXP(-\$B\$3/(8.314*(\$E\$3+\beta*(D437+5/2))))$

Table D6. Procedure for solution of the parameter K_4 presented in equation (3.48)

1	J
2	K_4
3	$=5*(F3+5*I3)*(\$B\$4*EXP(-\$B\$3/(8.314*(\$E\$3+\beta*(D3+5))))$
⋮	⋮
437	$=5*(F437+5*I437)*(\$B\$4*EXP(-\$B\$3/(8.314*(\$E\$3+\beta*(D437+5))))$

The theoretical concentrations [A], [B], [C], and [D] were assumed as determined in sheet 1, sheet 2, sheet 3, and sheet 4, respectively. Then, it was proceeded to determine the concentration rate of [A], [B], [C], and [D], which procedures were presented in Tables D7, D8, D9, and D10, respectively.

Table D7. Procedure of determination of the concentration rate of [A] in equation (3.17)

1	K
2	$d[A]/dt$ (1/s)
3	$=-(F3)*(\$B\$4*EXP(-\$B\$3/(8.314*(\$E\$3+\beta*D3))))$
⋮	⋮
437	$=-(F437)*(\$B\$4*EXP(-\$B\$3/(8.314*(\$E\$3+\beta*D437))))$

Table D8. Procedure of determination of the concentration rate of [B] in equation (3.18)

1	L
2	$d[B]/dt$ (1/s)
3	$=(-F3)-('Sheet2'F3)*(\$B\$8*EXP(-\$B\$7/(8.314*(\$E\$3+\beta*D3))))$
⋮	⋮
437	$=(-F437)-('Sheet2'F437)*(\$B\$8*EXP(-\$B\$7/(8.314*(\$E\$3+\beta*D437))))$

Table D9. Procedure of determination of the concentration rate of [C] in equation (3.19)

1	M
2	$d[C]/dt$ (1/s)
3	$=('Sheet2'F3)*(\$B\$8*EXP(-\$B\$7/(8.314*(\$E\$3+\beta*D3))))-$ $(('Sheet3'F3)*(\$B\$12*EXP(-\$B\$11/(8.314*(\$E\$3+\beta*D3))))$
⋮	⋮
437	$=('Sheet2'F437)*(\$B\$8*EXP(-\$B\$7/(8.314*(\$E\$3+\beta*D437))))-$ $(('Sheet3'F437)*(\$B\$12*EXP(-\$B\$11/(8.314*(\$E\$3+\beta*D437))))$

Table D10. Procedure of determination of the concentration rate of [D] in equation (3.20)

1	N
2	$d[D]/dt$ (1/s)
3	$=('Sheet3'F3)*(\$B\$12*EXP(-\$B\$11/(8.314*(\$E\$3+\beta*D3))))$
⋮	⋮
437	$=('Sheet3'F437)*(\$B\$12*EXP(-\$B\$11/(8.314*(\$E\$3+\beta*D437))))$

The determination of the theoretical normalized mass and normalized DTG (dW/dt) was carried out through equations (3.23) and (3.24).

$$W = a_1[A] + a_2[B] + a_3[C] + a_4[D] \quad (3.23)$$

$$\frac{dW}{dt} = a_1 \frac{d[A]}{dt} + a_2 \frac{d[B]}{dt} + a_3 \frac{d[C]}{dt} + a_4 \frac{d[D]}{dt} \quad (3.24)$$

Table D11 presents the procedure of determination of the theoretical normalized mass, W , given in equation (3.23). As aforementioned, the theoretical concentrations [A], [B], [C], and [D] were assumed as determined in sheet 1, sheet 2, sheet 3, and sheet 4, respectively.

Table D11. Procedure of determination of the theoretical normalized mass, W

1	O
2	W theoretical (1/s)
3	=F3*\$B\$5+Sheet2!F3*Sheet1!\$B\$9+Sheet3!F3*Sheet1!\$B\$13 +Sheet4!F3*Sheet1!\$B\$15
⋮	⋮
437	=F437*\$B\$5+Sheet2!F437*Sheet1!\$B\$9+Sheet3!F437*Sheet1!\$B\$13 +Sheet4!F437*Sheet1!\$B\$15

In Table D12 is presented the procedure of determination of the normalized DTG, dW/dt , given in equation (3.24).

Table D12. Procedure of determination of the normalized DTG, dW/dt

1	P
2	dW/dt theoretical (1/s)
3	=K3*\$B\$5+L3*\$B\$9+M3*\$B\$13+N3*\$B\$15
⋮	⋮
437	=K437*\$B\$5+L437*\$B\$9+M437*\$B\$13+N437*\$B\$15

Once the theoretical normalized mass and normalized DTG (dW/dt) were determined, it is necessary to convert them to theoretical conversion and conversion rate, which is carried out through equations (3.4) and (3.5).

$$\alpha_e = \frac{w_i - w}{w_i - w_f} \quad (3.4)$$

$$\left(\frac{d\alpha}{dt}\right)_e = -\frac{dw}{dt} \left(\frac{1}{w_i - w_f}\right) \quad (3.5)$$

The procedure of determination of the theoretical conversion and conversion rate is presented in Table D13 and Table D14, respectively.

Table D13. Procedure of determination of theoretical conversion

1	Q
2	α theoretical (1/s)
3	=(O3-O3)/(O3-O437)
⋮	⋮
437	=(O3-O437)/(O3-O437)

Table D14. Procedure of determination of theoretical conversion rate

1	R
2	$\frac{d\alpha}{dt}$ theoretical (1/s)
3	$=(-P3)/(\$O\$3-\$O\$437)$
⋮	⋮
437	$=(-P437)/(\$O\$3-\$O\$437)$

The experimental conversion rate was defined in Appendix B, and to proceed with the comparison between experimental (exp) and theoretical (theo) data was applied the least squares method (RSS), defined by equation (3.21), and its procedure of application is presented in Table D15.

$$RSS = \sum_{i=0}^N \left[\left(\frac{d\alpha}{dt} \right)_{i,exp} - \left(\frac{d\alpha}{dt} \right)_{i,theo} \right]^2 \quad (3.21)$$

Table D15. Procedure of application of the least squares method

1	A	B	C	D
2	$(\frac{d\alpha}{dt})_{theo}$ (1/s)	$(\frac{d\alpha}{dt})_{exp}$ (1/s)	Least squares	
3	0.00090	0.00092	$=(B3-A3)^2$	$=SUM(C3:C437)$
4	0.00095	0.00098	$=(B4-A4)^2$	
5	0.00100	0.00130	$=(B5-A5)^2$	
⋮	⋮	⋮	⋮	
437	0.00110	0.00120	$=(B437-A437)^2$	

Once the experimental and theoretical conversion rate were compared the fit was evaluated through the average deviation (AD) given by equation (3.22), in which N is the number of data points analyzed, according to 435 in this example, and its procedure of determination is presented in Table D16.

$$AD(\%) = \left[\frac{\sqrt{\frac{RSS}{N}}}{\left(\frac{d\alpha}{dt} \right)_{e,max}} \right] 100 \quad (3.22)$$

Finally, after the determination of the average deviation the value obtained must be less than 3%, if this condition was not satisfied the activation energy, pre-exponential factor and the constant a_i must be changed. For this variation it is recommended the use of the SOLVER

minimization tool, varying each one of the parameters in order to obtain the minimum value of *AD*.

Table D16. Procedure of determination of the average deviation (*AD*)

1	C	D	E
2	Least squares		AD (%)
3	$= (B3 - A3)^2$	$= \text{SUM}(C3:C437)$	$= (((D3/435)^{(1/2)}) / 0.0123) * 100$
⋮	⋮		
437	$= (B437 - A437)^2$		

APPENDIX E

Application of the independent parallel reactions scheme

Figure E1 presents a flowchart of the methodology to determine the final kinetic parameters in an independent parallel reactions scheme.

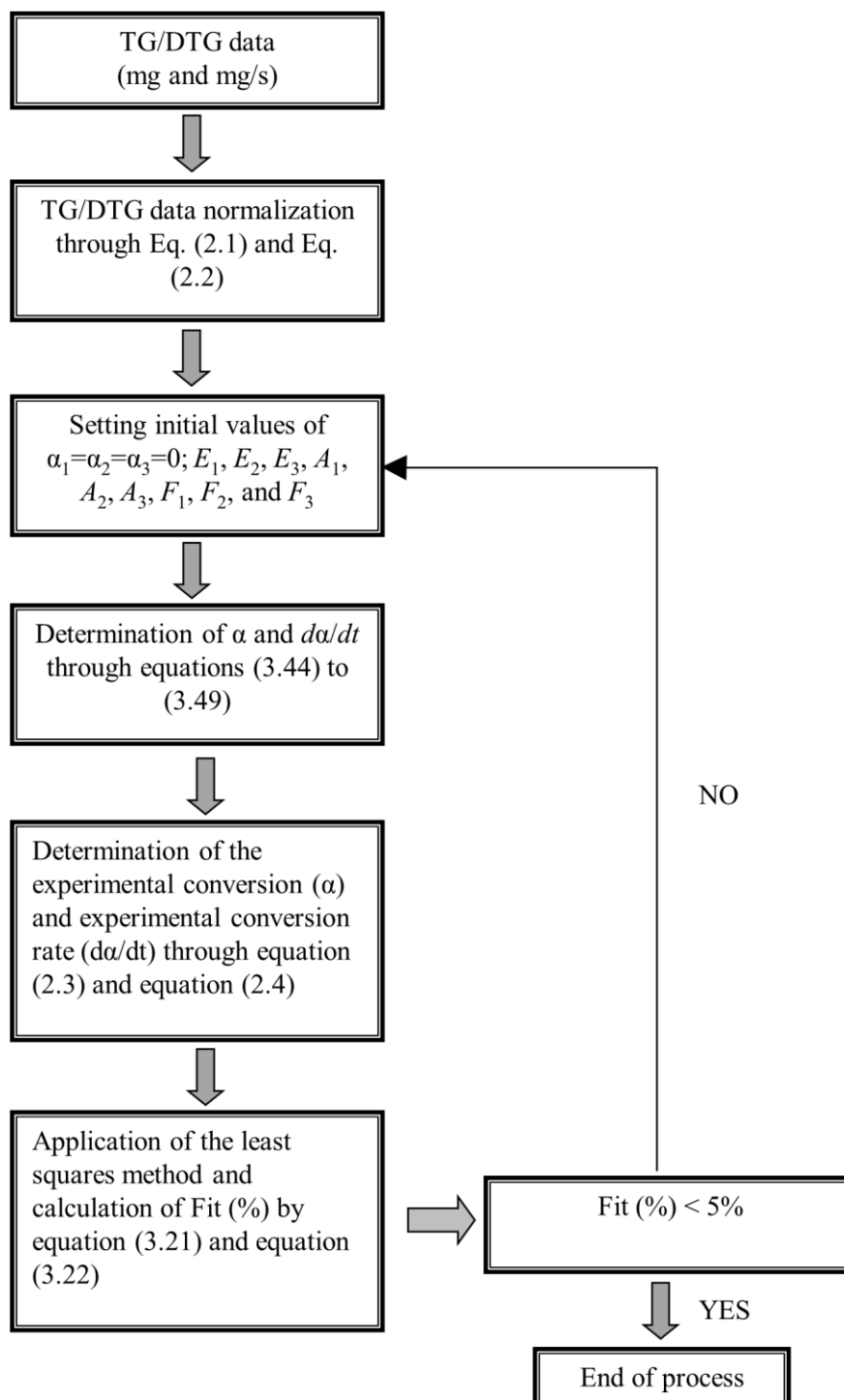


Figure E1. Flowchart of the application of the independent parallel reactions scheme

The application of the independent parallel reactions scheme was carried out according to equations (3.34) to (3.38), in which the reaction model $f(\alpha)=(1-\alpha)$, first order reaction, was the same for all the reactions analyzed.

$$\left(\frac{d\alpha}{dt}\right)_A = k_1[f(\alpha)]_1F_1 + k_2[f(\alpha)]_2F_2 + k_3[f(\alpha)]_3F_3 \quad (3.34)$$

$$\left(\frac{d\alpha}{dt}\right)_{HC} = k_1[f(\alpha)]_1F_1 \quad (3.35)$$

$$\left(\frac{d\alpha}{dt}\right)_c = k_2[f(\alpha)]_2F_2 \quad (3.36)$$

$$\left(\frac{d\alpha}{dt}\right)_L = k_3[f(\alpha)]_3F_3 \quad (3.37)$$

$$k_n = A_n \exp\left(\frac{E_n}{RT}\right) \quad (3.38)$$

The solution of the equations (3.35) to (3.37) was done through the application of the fourth order Runge-Kutta method given by equations (3.44) to (3.49), in which the initial conditions were, step $h=5$ s, time $t_0=0$ s and $t=t_{i-1}+h$, temperature $T_0=150$ °C, and $\alpha_0=0$.

$$f(x, y) = \frac{d\alpha}{dt} = (1 - \alpha_i)A \exp\left[\frac{-E}{R(T_0 + \beta t_i)}\right] \quad (3.44)$$

$$K_1 = h(1 - \alpha_i) \left\{ A \exp\left[\frac{-E}{R(T_0 + \beta t_i)}\right] \right\} \quad (3.45)$$

$$K_2 = h \left[1 - \left(\alpha_i + \frac{h}{2} K_1 \right) \right] \left\{ A \exp\left[\frac{-E}{R\left(T_0 + \beta\left(t_i + \frac{h}{2}\right)\right)}\right] \right\} \quad (3.46)$$

$$K_3 = h \left[1 - \left(\alpha_i + \frac{h}{2} K_2 \right) \right] \left\{ A \exp\left[\frac{-E}{R\left(T_0 + \beta\left(t_i + \frac{h}{2}\right)\right)}\right] \right\} \quad (3.47)$$

$$K_4 = h \left[1 - (\alpha_i + h K_3) \right] \left\{ A \exp\left[\frac{-E}{R(T_0 + \beta(t_i + h))}\right] \right\} \quad (3.48)$$

$$\alpha_{i+1} = \alpha_i + \left(\frac{K_1 + K_2 + K_3 + K_4}{6} \right) \quad (3.49)$$

The first step to apply the independent parallel reaction scheme is to select the initial kinetic parameters used as first guess, which are presented in Table E1, using as example three independent parallel reactions scheme.

Table E1. Initial kinetic parameters for an example of three independent parallel reactions scheme

1	A	B
2	Parameters	
3	E1 (kJ/mol)	150
4	A1 (1/s)	1.00E+08
5	F1 (-)	0.30
6		
7	E2 (kJ/mol)	200
8	A2 (1/s)	1.00E+14
9	F2 (-)	0.45
10		
11	E3 (kJ/mol)	100
12	A3 (1/s)	1.00E+05
13	F3 (-)	=1-\$B\$5-\$B\$9

Table E2 presents the procedure of setting the initial conditions: time, $t_0=0$ s, temperature, $T_0=150$ °C, and conversion $\alpha_0=0$, and the determination of the theoretical conversion:

Table E2. Initial conditions of time, temperature and conversion

1	D	E	F
2	t (s)	T (°C)	α (-)
3	0	150	0
4	=D3+5	=\$E\$3+ β *D4	=F3+((G3+H3+I3+J3)/6)
5	=D4+5	=\$E\$3+ β *D5	=F4+((G4+H4+I4+J4)/6)
⋮	⋮	⋮	⋮
437	=D436+5	=\$E\$3+ β *D437	=F436+((G436+H436+I436+J436)/6)

The fourth order Runge-Kutta method is based in the solution of the equations (3.45) to (3.48) concerning to the parameters K_1 , K_2 , K_3 , and K_4 . Tables E3, E4, E5, and E6 present the procedure for solution of the parameters K_1 , K_2 , K_3 , and K_4 , respectively.

Table E3. Procedure for solution of the parameter K_1 presented in equation (3.45)

1	G
2	K_1
3	$=5*(1-F3)*(\$B\$4*EXP(-\$B\$3/(8.314*(\$E\$3+\beta*D3))))$
⋮	⋮
437	$=5*(1-F437)*(\$B\$4*EXP(-\$B\$3/(8.314*(\$E\$3+\beta*D437))))$

Table E4. Procedure for solution of the parameter K_2 presented in equation (3.46)

1	H
2	K_2
3	$=5*(1-(F3+5/2*G3))*(\$B\$4*EXP(-\$B\$3/(8.314*(\$E\$3+\beta*(D3+5/2))))$
⋮	⋮
437	$=5*(1-(F437+5/2*G437))*(\$B\$4*EXP(-\$B\$3/(8.314*(\$E\$3+\beta*(D437+5/2))))$

Table E5. Procedure for solution of the parameter K_3 presented in equation (3.47)

1	I
2	K_3
3	$=5*(1-(F3+5/2*H3))*(\$B\$4*EXP(-\$B\$3/(8.314*(\$E\$3+\beta*(D3+5/2))))$
⋮	⋮
437	$=5*(1-(F437+5/2*H437))*(\$B\$4*EXP(-\$B\$3/(8.314*(\$E\$3+\beta*(D437+5/2))))$

Table E6. Procedure for solution of the parameter K_4 presented in equation (3.48)

1	J
2	K_4
3	$=5*(1-(F3+5*I3))*(\$B\$4*EXP(-\$B\$3/(8.314*(\$E\$3+\beta*(D3+5))))$
⋮	⋮
437	$=5*(1-(F437+5*I437))*(\$B\$4*EXP(-\$B\$3/(8.314*(\$E\$3+\beta*(D437+5))))$

Table E7 presents the procedure of determination of the conversion rate for each independent parallel reaction. Also, was assumed that in sheet 2 and sheet 3 are located the analysis of the other two independent parallel reactions.

Table E7. Procedure of determination of the conversion rate

1	K
2	$d\alpha/dt$ (1/s)
3	$=(1-F3)*(\$B\$4*EXP(-\$B\$3/(8.314*(\$E\$3+\beta*D3))))$
⋮	⋮
437	$=(1-F437)*(\$B\$4*EXP(-\$B\$3/(8.314*(\$E\$3+\beta*D437))))$

Table E8 presents in a new sheet the procedure of determination of the final conversion rate through the summation of all the conversion rates as presented in equation (3.34).

Table E8. Procedure of determination of the final conversion rate

1	A
2	dα/dt theoretical (1/s)
3	= 'Sheet1'!K3*'Sheet1'!\$B\$5+'Sheet2'!K3*'Sheet2'!\$B\$5+'Sheet3'!K3*'Sheet3'!\$B\$5
⋮	⋮
437	= 'Sheet1'!K437*'Sheet1'!\$B\$5+'Sheet2'!K437*'Sheet2'!\$B\$5 +'Sheet3'!K437*'Sheet3'!\$B\$5

The comparison of experimental (exp) and theoretical (theo) conversion rate through the least squares method, and the evaluation of the quality of fit were carried out applying equations (3.21) and (3.22), respectively. The procedure of application of these equations was presented in the *Appendix D – Application of the consecutive reactions scheme* in Table D15 and Table D16, respectively, which was the same applied here for the independent parallel reactions scheme.

$$RSS = \sum_{i=0}^N \left[\left(\frac{d\alpha}{dt} \right)_{i,exp} - \left(\frac{d\alpha}{dt} \right)_{i,theo} \right]^2 \quad (3.21)$$

$$AD(\%) = \left[\frac{\sqrt{\frac{RSS}{N}}}{\left(\frac{d\alpha}{dt} \right)_{e,max}} \right] 100 \quad (3.22)$$

APPENDIX F

Determination of the heat of reaction

The determination of the heat of reaction was carried out according to equations (3.50) to (3.54). However, to solve the equation (3.50) are necessary the heat capacity values given by equations (3.52) and (3.53).

$$Q_S = (1 - \alpha) \left(m_0 c_{p,s} \frac{dT}{dt} \right) + \alpha \left(m_c c_{p,c} \frac{dT}{dt} \right) \quad (3.50)$$

$$Q_R = Q_{DSC} - Q_S \quad (3.51)$$

$$Cp_s = 4.9700T + 1144.1638 \quad (3.52)$$

$$Cp_c = 1.400T + 688 \quad (3.53)$$

$$H_R = \frac{1}{m_0} \int_{t_1}^{t_2} Q_R dt \quad (3.54)$$

Table F1 presents the procedure for the determination of the heat capacity of sample and char, according to equations (3.52) and (3.53), respectively.

Table F1. Procedure for the determination of the heat capacity of sample and char

1	A	B	C	D
2	T (°C)	DSC (mW)	Cps (J kg ⁻¹ °C ⁻¹)	Cpc (J kg ⁻¹ °C ⁻¹)
3	150	0.00090	=4.97*A3+1144.1638	=1.4*A3+688
4	155	0.00095	=4.97*A4+1144.1638	=1.4*A4+688
5	160	0.00100	=4.97*A5+1144.1638	=1.4*A5+688
⋮	⋮	⋮	⋮	⋮
597	600	0.00110	=4.97*A597+1144.1638	=1.4*A597+688

In Table F2 is presented the procedure for the determination of heat flux required for heating the biomass sample (Q_S) according to equation (3.50).

Table F2. Procedure for the determination of heat flux required for heating the biomass sample (Q_s)

1	E	F	G	H
2	m_0 (mg)	m_c (mg)	α	Q_s (W)
3	2.9302	0.7962	0	$=(1-G3)*(\$E\$5*C3*(\beta/60))+G3*(\$F\$5*D3*(\beta/60))$
4	$=E3/1000$	$=F3/1000$	0.01	$=(1-G4)*(\$E\$5*C4*(\beta/60))+G4*(\$F\$5*D4*(\beta/60))$
5	$=E4/1000$	$=F4/1000$	0.03	$=(1-G5)*(\$E\$5*C5*(\beta/60))+G5*(\$F\$5*D5*(\beta/60))$
⋮			⋮	⋮
597			1	$=(1-G597)*(\$E\$5*C597*(\beta/60))+G597*(\$F\$5*D597*(\beta/60))$

Once determined Q_s and with the heat flux measured by the *DSC* was determined the heat flux of reaction, Q_R , which procedure of determination is presented in Table F3.

Table F3. Procedure of determination of the heat flux of reaction, Q_R

1	I
2	Q_R (W)
3	$=(B3/1000)-H3$
4	$=(B4/1000)-H4$
5	$=(B5/1000)-H5$
⋮	⋮
597	$=(B597/1000)-H597$

Once obtained the heat flux of reaction, it was proceeded to solve equation (3.54) with the numerical integration tool of the software *Origin 8* (analysis, mathematics, integrate). Finally, with the data obtained in equation (3.54) in kJ/kg and the temperature related to them was plotted the heat of reaction as a function of temperature presented in Figure 4.21.

ANNEXE A - Permission of the publisher IGI Global

8/2/13	APPROVED <i>By Jan Travers at 1:26 pm, Sep 03, 2015</i>	Submit by Email	Print Form		
<h3>Request from Author for Reuse of IGI Materials</h3>					
<p>IGI Global ("IGI") recognizes that some of its authors would benefit professionally from the ability to reuse a portion or all of some manuscripts that the author wrote and submitted to IGI for publication. Prior to the use of IGI copyrighted materials in any fashion contemplated by the IGI Fair Use Guidelines for Authors, the author must submit this form, completed in its entirety, and secure from IGI the written permission to use such materials. Further, as a condition of IGI providing its consent to the reuse of IGI materials, the author agrees to furnish such additional information or documentation that IGI, in its sole discretion, may reasonably request in order to evaluate the request for permission and extent of use of such materials.</p>					
<p>IGI will consider the special request of any author who:</p> <ul style="list-style-type: none"> • Completes, signs and returns this form agreeing to the terms; and • Agrees that unless notified to the contrary, only the final, typeset pdf supplied by IGI Global is authorized to be posted (no pre-prints or author's own file.) 					
<p>Title of article/chapter you are requesting: <u>Modelling the kinetics of Lignocellulosic Biomass pyrolysis</u></p> <p>Book Title and author/editor where this IGI material appears: <u>Innovative Solutions in Fluid-Particle Systems and Renewable Energy Management. Editor: Katia Tannous</u></p>					
<p>Purpose of request (where this material will appear):</p> <p><input type="checkbox"/> Posted on a secure university website for your students to access in support of a class. (Posted paper must carry the IGI Global copyright information as outlined above.)</p> <p><input type="checkbox"/> Posted in a university archive. The Website address is: <u>http://</u> _____</p> <p><input type="checkbox"/> Posted on a personal Website: The Website address is: <u>http://</u> _____</p> <p><input type="checkbox"/> Republished in a book of which I am the editor/author. Book title of proposed book: _____</p> <p style="margin-left: 40px;">Publisher of proposed book: _____</p> <p><input checked="" type="checkbox"/> Other purpose (please explain): <u>Request permission for inclusion of the chapter in the author's doctoral thesis</u></p> <p style="margin-left: 40px;">_____</p>					
<p>With your signature below, you agree to the terms stated in the IGI Global Fair Use Guidelines. This permission is granted only when IGI returns a copy of the signed form for your files and the manuscript pdf.</p>					
<p>Your name: <u>Yesid Javier Rueda Ordóñez</u></p> <p>Your signature: <u>Yesid Javier Rueda Ordóñez</u> <small>Digitally signed by Yesid Javier Rueda Ordóñez DN: cn=Yesid Javier Rueda Ordóñez, o=University of Campinas, ou=Faculty of Chemical Engineering, email=yesid@feq.unicamp.br, c=BR</small></p> <p>Organization: <u>University of Campinas</u></p> <p>Address: <u>500 Albert Einstein Avenue, Campinas, SP, Brazil</u></p> <p style="margin-left: 40px;">ZIP code: <u>13083-852</u></p> <p>Fax: <u>+55 19 35213910</u></p> <p>E-mail: <u>+55 19 35213927 yesid@feq.unicamp.br</u></p>					
<table border="1" style="width: 100%; border-collapse: collapse;"> <tr> <td style="width: 40%; padding: 5px;"> For IGI Use Request accepted by IGI Global: _____ Date: _____ </td> <td style="width: 60%; text-align: center; padding: 5px;"> <div style="font-size: 2em; font-weight: bold; margin: 0;">Jan Travers</div> <div style="font-size: 0.8em; margin-top: 5px;"> Digitally signed by Jan Travers DN: cn=Jan Travers, o=IGI Global, ou=Director of Intellectual Property & Contracts, email=jtravers@igi- global.com, c=US Date: 2015.09.03 13:28:03 -04'00' </div> </td> </tr> </table>				For IGI Use Request accepted by IGI Global: _____ Date: _____	<div style="font-size: 2em; font-weight: bold; margin: 0;">Jan Travers</div> <div style="font-size: 0.8em; margin-top: 5px;"> Digitally signed by Jan Travers DN: cn=Jan Travers, o=IGI Global, ou=Director of Intellectual Property & Contracts, email=jtravers@igi- global.com, c=US Date: 2015.09.03 13:28:03 -04'00' </div>
For IGI Use Request accepted by IGI Global: _____ Date: _____	<div style="font-size: 2em; font-weight: bold; margin: 0;">Jan Travers</div> <div style="font-size: 0.8em; margin-top: 5px;"> Digitally signed by Jan Travers DN: cn=Jan Travers, o=IGI Global, ou=Director of Intellectual Property & Contracts, email=jtravers@igi- global.com, c=US Date: 2015.09.03 13:28:03 -04'00' </div>				
<p>Please complete and mail or fax this request form to:</p> <p>Jan Travers • IGI Global, 701 E Chocolate Avenue • Hershey PA 17033 • Fax: 717/533-8661 • jtravers@igi-global.com</p>					

ANNEXE B - Permissions of the publisher Elsevier B.V.

This is a License Agreement between Yesid Javier Rueda ("You") and Elsevier ("Elsevier") provided by Copyright Clearance Center ("CCC"). The license consists of your order details, the terms and conditions provided by Elsevier, and the payment terms and conditions.

Supplier	Elsevier Limited The Boulevard,Langford Lane Kidlington,Oxford,OX5 1GB,UK 1982084
Registered Company Number	
Customer name	Yesid Javier Rueda-Ordóñez
Customer address	School of Chemical Engineering Campinas, São Paulo 13083-852
License number	3701350583096
License date	Sep 02, 2015
Licensed content publisher	Elsevier
Licensed content publication	Bioresource Technology
Licensed content title	Isoconversional kinetic study of the thermal decomposition of sugarcane straw for thermal conversion processes
Licensed content author	Yesid Javier Rueda-Ordóñez,Katia Tannous
Licensed content date	November 2015
Licensed content volume number	196
Licensed content issue number	n/a
Number of pages	9
Start Page	136
End Page	144
Type of Use	reuse in a thesis/dissertation
Portion	full article
Format	both print and electronic
Are you the author of this Elsevier article?	Yes
Will you be translating?	No
Title of your thesis/dissertation	THERMAL DECOMPOSITION ANALYSIS OF SUGARCANE STRAW UNDER INERT AND OXIDATIVE ATHMOSPHERES BY TG AND DSC FOR THERMAL CONVERSION PROCESSES
Expected completion date	Feb 2016
Estimated size (number of pages)	120
Elsevier VAT number	GB 494 6272 12
Permissions price	0.00 USD
VAT/Local Sales Tax	0.00 USD / 0.00 GBP
Total	0.00 USD

Supplier	Elsevier Limited The Boulevard,Langford Lane Kidlington,Oxford,OX5 1GB,UK 1982084
Registered Company Number	
Customer name	Yesid Javier Rueda-Ordóñez
Customer address	School of Chemical Engineering Campinas, São Paulo 13083-852
License number	3715921012277
License date	Sep 25, 2015
Licensed content publisher	Elsevier
Licensed content publication	Fuel Processing Technology
Licensed content title	An empirical model to obtain the kinetic parameters of lignocellulosic biomass pyrolysis in an independent parallel reactions scheme
Licensed content author	Yesid Javier Rueda-Ordóñez,Katia Tannous,Edgardo Olivares-Gómez
Licensed content date	December 2015
Licensed content volume number	140
Licensed content issue number	n/a
Number of pages	9
Start Page	222
End Page	230
Type of Use	reuse in a thesis/dissertation
Portion	full article
Format	both print and electronic
Are you the author of this Elsevier article?	Yes
Will you be translating?	No
Title of your thesis/dissertation	THERMAL DECOMPOSITION ANALYSIS OF SUGARCANE STRAW UNDER INERT AND OXIDATIVE ATHMOSPHERES BY TG AND DSC FOR THERMAL CONVERSION PROCESSES
Expected completion date	Feb 2016
Estimated size (number of pages)	120
Elsevier VAT number	GB 494 6272 12
Permissions price	0.00 USD
VAT/Local Sales Tax	0.00 USD / 0.00 GBP
Total	0.00 USD

Supplier	Elsevier Limited The Boulevard,Langford Lane Kidlington,Oxford,OX5 1GB,UK 1982084
Registered Company Number	
Customer name	Yesid Javier Rueda-Ordóñez
Customer address	School of Chemical Engineering Campinas, São Paulo 13083-852
License number	3858210596407
License date	Apr 28, 2016
Licensed content publisher	Elsevier
Licensed content publication	Bioresource Technology
Licensed content title	Thermal decomposition of sugarcane straw, kinetics and heat of reaction in synthetic air
Licensed content author	Yesid Javier Rueda-Ordóñez,Katia Tannous
Licensed content date	July 2016
Licensed content volume number	211
Licensed content issue number	n/a
Number of pages	9
Start Page	231
End Page	239
Type of Use	reuse in a thesis/dissertation
Portion	full article
Format	both print and electronic
Are you the author of this Elsevier article?	Yes
Will you be translating?	No
Title of your thesis/dissertation	THERMAL DECOMPOSITION ANALYSIS OF SUGARCANE STRAW UNDER INERT AND OXIDATIVE ATHMOSPHERES BY TG AND DSC FOR THERMAL CONVERSION PROCESSES
Expected completion date	Feb 2016
Estimated size (number of pages)	120
Elsevier VAT number	GB 494 6272 12
Permissions price	0.00 USD
VAT/Local Sales Tax	0.00 USD / 0.00 GBP
Total	0.00 USD